Experiments and Models of Carbon Black-based Nanofluids for Photothermal and Electrical Applications

Shihao Wei

Thesis for the degree of Philosophiae Doctor (PhD)
University of Bergen, Norway
2023

UNIVERSITY OF BERGEN

Experiments and Models of Carbon Black-based Nanofluids for Photothermal and Electrical Applications

Shihao Wei

Thesis for the degree of Philosophiae Doctor (PhD)
at the University of Bergen

Date of defense: 26.06.2023

Year: 2023

Title: Experiments and Models of Carbon Black-based Nanofluids for Photothermal and Electrical Applications

Name: Shihao Wei

Print: Skipnes Kommunikasjon / University of Bergen

Scientific Environment

The research presented in this thesis was conducted at the Department of Physics and Technology, University of Bergen, and at the Department of Mechanical and Marine Engineering, Western Norway University of Applied Sciences.

This work was funded by the Chongqing University and China Scholarship Council through its Ph.D. program.

Acknowledgements

I wish to thank the China Scholarship Council for financial support and Chongqing University for giving me the opportunity to study abroad.

I would like to express my gratitude to my supervisors Professor Pawel Kosinski at the Department of Physics and Technology, University of Bergen, and Professor Boris V. Balakin at the Department of Mechanical and Marine Engineering, Western Norway University of Applied Sciences. I am grateful for the excellent guidance, patient discussions, and encouragement I received throughout my doctoral training. The insightful and constructive feedback on my work was invaluable to me, and I appreciate the effort taken to provide it. In particular, I would like to express my gratitude to Pawel, whose concern for my well-being during my stay in Norway helped me to feel less isolated while living in a foreign country.

I would like to express my appreciation to my colleagues at IFT and HVL for their assistance and feedback regarding both my research work and personal life.

I would like to acknowledge Dr. M. Pisarevsky from MEPhI for supporting the photos related to the sedimentation of nanofluids.

I would like to extend a special thanks to my dear friends Dr. Wantong Sun and Przemek Machul, as well as the friends I made while living in Haukelandsbakken Studenthjem. Their support and kindness were indispensable in helping me swiftly adjust to academic and social life at UiB and successfully integrate into the Norwegian way of life.

Finally, I would like to express my warm and heartfelt appreciation to my family, who provided me with immense sources of love, patience, support, and hopes throughout these years. I am especially grateful for my father and mother, who have always encouraged and supported my efforts to improve my professional and academic development.

Abstract in English

Nanofluids are a type of fluid that contains dispersed nanoparticles, which can enhance their thermal and electrical properties compared to base fluids. This has led to their widespread use in applications such as solar energy storage. One specific application of nanofluids is in direct absorption solar collectors (DASCs), where they are used as working fluids to convert solar energy into thermal energy. Additionally, their enhanced electrical properties make them suitable for use in cooling systems for electrical devices, as dielectric materials, in photovoltaic systems, etc. Furthermore, nanofluids have the potential for use in hydrogen production via water electrolysis, which can store solar energy as hydrogen. Therefore, investigating the performance of nanofluids in various energy industry applications can be valuable.

The properties of nanofluids are influenced by various factors, such as the material of nanoparticles, their size and shape, and their concentration. Therefore, it is crucial to measure their optical, electrochemical, and thermal properties, including the extinction coefficient, zeta potential, and electrical conductivity.

In this study, a rectangular DASC with internal baffles and rectangular cross-section pipes was designed and tested. Carbon black (CB) nanofluids were utilized as working fluids, and a halogen lamp was used to simulate the concentrated solar radiation. The photothermal properties and enhancements of the system were evaluated by monitoring the temperature of the working fluids at the inlet and outlet, as well as the DASC's efficiency.

To study the behavior of nanoparticles and other important parameters that are difficult to observe during experiments, such as the distribution of temperature and velocity vectors of working fluids, this thesis developed a numerical model for analyzing the flow pattern and distribution of CB nanoparticles in DASCs using a volumetric heat transfer model based on Beer-Lambert's law. The extinction coefficient of CB nanofluids, which was determined by measuring the reduction in heat flux when light passed through the nanofluids, was an important parameter in the model. The

simulation results can be used to analyze the behavior and deposition of nanoparticles, as well as the heat transfer and flow characteristics of nanofluids at a micro level.

The electrochemical performance of CB nanofluids was evaluated through an experiment on electrolyte nanofluids electrolysis. The hydrogen production rate of the water split reaction and the efficiency of electrolysis are important indicators to determine the enhancement of the electrolyte nanofluids. In this study, two types of electrolyte nanofluids, sodium sulfate and sodium hydroxide, were tested.

A semi-empirical correlation based on Faraday's law of electrolysis and the Maxwell model of electrical conductivity was developed to evaluate the effect of CB nanofluids. Some simplifications were made regarding the concentration of nanofluids, making it possible to evaluate them using experimental results. This correlation can be used to assess the total hydrogen production for alkaline electrolyte nanofluids at low concentrations.

In addition to the aforementioned studies, stability tests were conducted to evaluate the stability of different types and concentrations of CB nanofluids. The factors that contribute to the destabilization of nanofluids were also discussed in this study.

Abstract in Norwegian

Nanofluid er en type væske som inneholder spredte nanopartikler, som kan forbedre deres termiske og elektriske egenskaper sammenlignet med basevæsker. Dette har ført til omfattende bruksområder, som for eksempel solenergilagring. En type anvendelse av nanofluid er i direct absorption solar collectors (DASCs), der de brukes som arbeidsvæsker for å konvertere solenergi til termisk energi. I tillegg gjør deres forbedrede elektriske egenskaper dem egnet for bruk i kjølesystemer for elektriske enheter, som dielektriske materialer, i fotovoltaiske systemer, etc. Videre har nanofluid potensiale for bruk i hydrogenproduksjon via vannelektrolyse, som kan lagre solenergi som hydrogen. Grunnet dette kan det være verdifullt å undersøke ytelsen til nanofluid i ulike energiindustriapplikasjoner.

Egenskapene til nanofluid påvirkes av ulike faktorer, som materialet til nanopartikler, deres størrelse og form og konsentrasjonen. Det er derfor avgjørende å måle deres optiske, elektrokjemiske og termiske egenskaper, inkludert utryddelseskoeffisient, zetapotensial og elektrisk ledningsevne.

I denne studien ble en rektangulær DASC med interne baffler og rektangulære rør med tverrsnitt designet og testet. Karbon sot (CB) nanofluid ble brukt som arbeidsvæske, og en halogenlampe ble brukt til å simulere konsentrert solstråling. De fototermiske egenskapene og forbedringene av systemet ble evaluert ved å overvåke temperaturen til arbeidsvæskene ved innløpet og utløpet, samt effektiviteten til DASC.

For å studere oppførselen til nanopartikler og andre viktige parametere som er vanskelige å observere under eksperimenter, for eksempel distribusjonen av temperatur og hastighetsvektorer til arbeidsvæsker, utviklet denne avhandlingen en numerisk modell for å analysere strømningsmønsteret og distribusjonen av CB-nanopartikler i DASCs ved hjelp av en volumetrisk varmeoverføringsmodell basert på Beer-Lamberts lov. Utryddelseskoeffisienten til CB-nanofluider, som ble bestemt ved å måle reduksjonen i varmefluks når lys passerte gjennom nanofluidene, var en viktig parameter i modellen. Simuleringsresultatene kan brukes til å analysere oppførselen og

avleiringen av nanopartikler, samt varmeoverføring og strømningskarakteristikker av nanofluider på mikronivå.

Den elektrokjemiske ytelsen til CB-nanofluider ble evaluert gjennom en eksperimentell elektrolyse av nanofluidelektrolytter. Hydrogenproduksjonsraten fra vannsplittelsesreaksjonen og effektiviteten av elektrolysen er viktige indikatorer for å bestemme forbedringen av nanofluidelektrolytter. I denne studien ble to typer nanofluidelektrolytter, natriumsulfat og natriumhydroksid, testet.

En semi-empirisk korrelasjon basert på Faradays elektrolyselov og Maxwells modell for elektrisk ledningsevne ble utviklet for å evaluere effekten av CB-nanofluider. Noen forenklinger ble gjort med hensyn til konsentrasjonen av nanofluider, slik at de kunne evalueres ved hjelp av eksperimentelle resultater. Denne korrelasjonen kan brukes til å vurdere den totale hydrogenproduksjonen for alkaliske nanofluidelektrolytter ved lave konsentrasjoner.

I tillegg til de nevnte studiene, ble stabilitetstester utført for å evaluere stabiliteten til forskjellige typer og konsentrasjoner av CB-nanofluider. Faktorene som bidrar til destabilisering av nanofluider ble også diskutert i denne studien.

List of Publications

Wei, S., Hikmati, J., Balakin, B. V., & Kosinski, P. (2022). Experimental study of hydrogen production using electrolyte nanofluids with a simulated light source. International Journal of Hydrogen Energy, 47(12), 7522-7534.

Wei, S., Espedal, L., Balakin, B. V., & Kosinski, P. (2023). Experimental and Numerical Investigation of Direct Absorption Solar Collectors (DASCs) Based on Carbon Black Nanofluids (accepted by Experimental Heat Transfer)

Wei, S., Balakin, B. V., & Kosinski, P. (2023). Investigation of nanofluids in alkaline electrolytes: stability, electrical properties, and hydrogen production (submitted to Journal of Cleaner Production)

Additional Scientific Contributions

Wei, S., Balakin, B. V., & Kosinski, P. (2021). Numerical investigation of direct absorption solar collectors based on carbon black nanofluids, ICNAAM 2021 Conference, Rhodes, Greece, 20-26 September 2021

Contents

1. General Introduction

The extensive use of fossil fuels has led to the emission of greenhouse gases, which is currently the most pressing environmental issue. One of the most urgent goals is to reduce the concentration of carbon dioxide in the atmosphere. In 2021, the European Commission announced the 2030 Climate Target Plan, which aims to reduce greenhouse gas emissions by a minimum of 55% by 2030, with the ultimate objective of achieving climate neutrality by 2050 [1]. In a similar vein, China has set a target of achieving carbon neutrality by 2060, with the aim of reaching peak carbon emissions before 2030 [2].

To achieve these climate targets, the most critical factor is to find a clean energy source with zero greenhouse footprint that can replace fossil fuels. One of the most promising renewable energy sources is solar energy, which has tremendous potential in the field of energy resources because it is a practically infinite source of energy [3]. However, solar energy is weather- and time-dependent, making energy storage a vital aspect of its use. One common method for utilizing solar energy is through the use of solar collectors, which can convert solar energy into thermal energy.

Solar collectors are thermal systems that harness solar radiation by employing various working fluids, such as water, thermal oil, ethylene glycol, and others [4]. However, low energy efficiency remains a significant challenge for engineers seeking to utilize solar energy. To address this issue, some researchers have proposed using nanofluids as working fluids due to their superior thermal conductivity [5].

Nanofluids refer to suspensions of nanoparticles in base fluids that exhibit exceptional thermal conductivity, leading to higher heat transfer coefficients compared to conventional working fluids. Nanofluids can be classified into four types based on the type of nanoparticles they contain, including (1) metal-based nanofluids, (2) metal oxide-based nanofluids, (3) carbon-based nanofluids, (4) hybrid metal-based nanofluids [6]. The thermal properties of nanofluids are mainly affected by the dispersed nanoparticles. Therefore, there has been growing research interest in investigating carbon-based nanofluids, as they exhibit outstanding thermophysical

properties when compared to other types of nanofluids [7]. As an example, graphene offers considerably enhanced thermal conductivity in nanofluids, owing to its high aspect ratio, low density, reduced surface effects of erosion and corrosion, superior stability, and lower requirements for pressure drop and pumping power, when compared to other types of nanomaterials [9-11]. Given these advantages, investigating the properties of nanofluids is critical for their potential applications in various fields. Therefore, in this study, carbon black (CB), which is a commonly used carbon-based nanoparticle, was chosen to investigate its properties.

This chapter provides a brief overview of the fundamental concepts and properties of nanofluids. Additionally, the purpose of this study and the main works are also presented.

1.1 Nanofluids

Nanoparticles in nanofluids exhibit a larger relative surface area, which facilitates heat transfer [12]. Furthermore, the small size of the particles promotes micro-convection within the fluids, enhancing their mobility [13]. To gain a comprehensive understanding of the heat transfer processes in nanofluids, it is crucial to investigate the dynamic forces of nanoparticles in the base fluid. Therefore, further research is needed to explore the detailed motion of nanoparticles at the nanoscale.

1.1.1 Forces in nanofluids

The enhancement of nanofluids' thermal properties can be attributed to two factors: the intrinsic properties of nanoparticles and their motion within the fluid. Nanoparticle motion plays a predominant role in determining the behavior of nanofluids, including aggregation, convective heat and mass transfer, and enhancement of electrical conductivity.

When suspended in base fluids, nanoparticles experience a variety of forces, as illustrated in Figure 1.1 [12]. These forces can be categorized into four groups based on their origins: interparticle forces, forces between nanoparticles and the base fluid, external forces, and other forces.

Nanofluids experience interparticle forces such as van der Waals forces, electrostatic double-layer forces, as well as other forces like steric, capillary, and depletion forces, which have a relatively minor impact on the stability of nanofluids [14]. Said et al. [12] classified nanofluids into two categories based on their concentrations: diluted and dense nanofluids. Dilute nanofluids are those with a volume concentration below 0.1 vol.%, whereas those above this limit are classified as dense nanofluids. In diluted nanofluids, interparticle forces can be neglected due to the absence of adhesive forces. The Derjaguin-Landau-Verwey-Overbeek (DLVO) theory is a classical theory that describes the interactions and deposition kinetics of colloidal particles. The total potential energy that supports colloidal stability is composed of van der Waals and electrostatic potentials. When the attraction force dominates, it leads to aggregation and unstable suspensions. Conversely, higher repulsion forces can make the suspension stable.

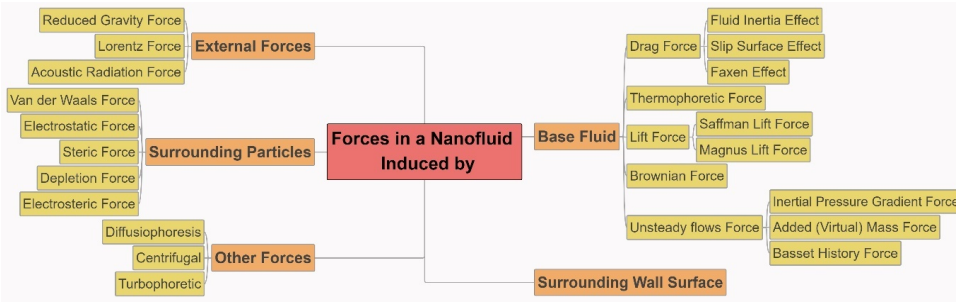

Fig. 1.1 Forces in a nanofluid according to Said et al. [12]

The dispersion of nanoparticles in a base fluid induces several forces on the particles, including those from the liquid, solid surfaces, surrounding walls, and external fields. However, only a small number of these forces have a significant impact on the stability of nanofluids, while others have a relatively minor effect due to their smaller magnitude [15]. These forces play crucial roles in the thermal processes within nanofluids, such as drag force, lift force, Brownian force, thermophoretic force, and some forces related to unsteady flow.

External forces, as the name suggests, are forces created by external fields. Gravity is the most common external force. Some special nanofluids require the use of a magnetic field or sound waves during manufacturing, resulting in the existence of the Lorentz force or acoustic radiation force [16-17].

1.1.2 Stability

The forces present in nanofluids facilitate the motion of nanoparticles, which can enhance convective mass and heat transfer, but also increase the likelihood of nanoparticle collisions. Similarly, during the fabrication of nanofluids, nanoparticles tend to agglomerate and form sediment due to gravity, leading to the instability of nanofluids. This instability can increase the viscosity of the nanofluid [18], reduce thermal conductivity [19], and affect light scattering and absorption [20]. Therefore, it is essential to understand the stability of nanofluids and prevent it from occurring.

The stability of a colloidal system can be categorized into dispersion stability, kinetic stability, and chemical stability [21]. Dispersion stability in nanofluids refers to the propensity of nanoparticles to aggregate. Kinetic stability primarily represents the Brownian motion of nanoparticles and their aggregation in the nanofluids. Chemical stability refers to the possibility of chemical reactions between nanoparticles and the base fluid, although such reactions are rare in nanofluids due to the need for additional conditions such as high temperature, high pressure, and catalysts [22]. Therefore, clustering and sedimentation are the primary factors that affect the stability of nanofluids.

Physical instability in nanofluids can result in sedimentation, which can exhibit different types of performance, namely dispersed sedimentation, flocculated sedimentation, and mixed sedimentation, as illustrated in Fig. 1.2 [23]. Flocculated sedimentation involves the agglomeration of particles to form clusters that settle down, typically taking place in environments with high concentrations of solids. In contrast, dispersed sedimentation occurs in scenarios where solid concentrations are minimal, with each particle settling on its own. In mixed sedimentation, particles exhibit both flocculated and dispersed sedimentation tendencies simultaneously [8]. Dr. M.

Pisarevsky investigated the formation of sedimentation in aluminum nanofluids, as shown in Fig. 1.3. According to the speed of sediment forms and settles in an unstable nanofluid, the whole process can be classified into two regions, rapid settling region and slow settling stage [24].

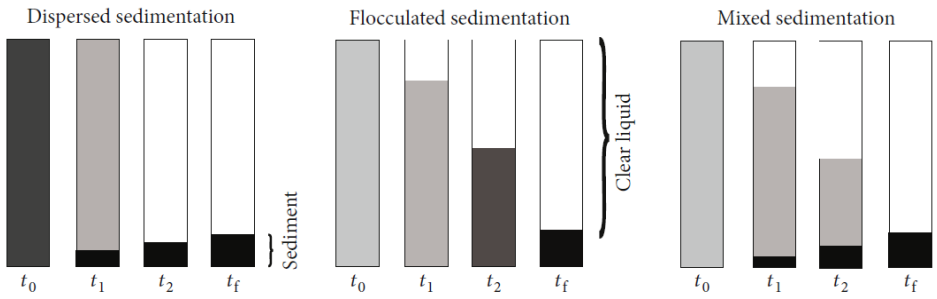

Fig. 1.2 Schematic of different sedimentation from Ali et al [23] (license CC BY 4.0)

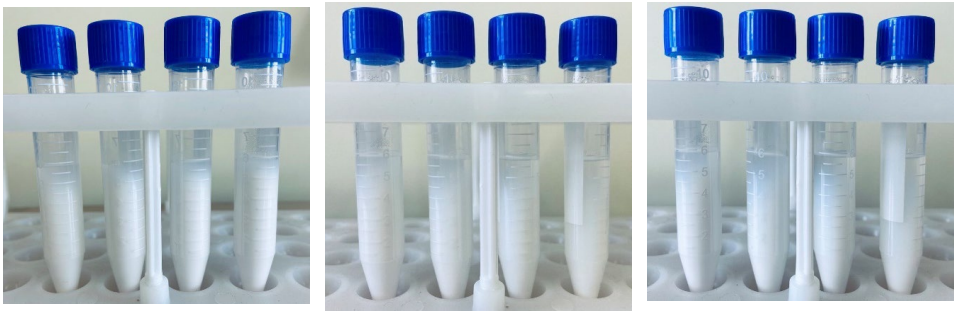

(a) 39 days (b) 42 days (c) 44 days

Fig. 1.3 The forming of sedimentation (private communication with Dr. M. Pisarevsky from MEPhI)

Nowadays, there are several methods available to evaluate the stability of nanofluids. Some of the most widely used methods are 1) sedimentation observation, 2) Zeta potential measurement, 3) 3-ω method, 4) dynamic light scattering (DLS) approach, 5) scanning electron microscopy (SEM) analysis, and 6) spectral analysis [25-31].

In the manufacturing and storage of nanofluids, destabilization is an inevitable occurrence. Factors such as temperature, concentration, solution chemistry, and storage

time can all impact the stability of nanofluids [32-34]. The concentration of nanofluids plays a crucial role in determining their essential optical and thermophysical properties, and sedimentation can reduce this concentration, thereby affecting these properties.

Various technologies have been developed to enhance the stability of nanofluids, which can be divided into two types: mechanical stabilization and chemical stabilization [12]. Four commonly used mechanical stabilization methods include ultrasonic bath sonication, magnetic stirring, homogenizer/probe sonication, and ball milling [35]. These methods are employed during the preparation of nanofluids to prevent clustering beforehand. In contrast, chemical stabilization techniques can prevent clustering after nanofluids are prepared and maintain long-term stability. Adding a surfactant is a typical chemical stabilization technique, as ionic surfactants can assist in covalent surface functionalization [36].

Surfactants play a crucial role in stabilizing colloids by attaching to particle surfaces and forming micelles that hinder the agglomeration of the dispersed phase. Furthermore, certain surfactants can also adjust the pH of nanofluids to cause the suspension to stabilize or destabilize [37]. However, some surfactants can be harmful to the environment by producing sulfates and persulfates at high concentrations [38]. Therefore, researchers have begun investigating the environmental impact and biodegradability of surfactant-nanoparticle mixtures. Non-ionic surfactants, such as alkyl polyglucosides, have been considered for use [39]. The most widely used surfactant, sodium dodecyl sulfate (SDS), has shown excellent performance in stabilizing carbon-based nanofluids [40], and stabilization by surfactants is the main technique employed to ensure the long-term stability of carbon-based nanofluids in this study.

1.1.3 Thermophysical properties

For the effective utilization of nanofluids in various applications, it is necessary to evaluate the thermophysical properties of nanofluids, such as thermal conductivity, density, specific heat, and dynamic viscosity. These properties can be determined using either experimental methods or models [41-44]. Of these properties, thermal

conductivity is particularly crucial since it significantly impacts the performance of the working fluid. Therefore, researchers investigating nanofluids have made thermal conductivity enhancement their primary focus [45-46]. The enhancement in the effective thermal conductivity of nanofluids is attributed to the incorporation of solid particles in the liquid, which possess considerably higher thermal conductivity compared to the base fluid.

Estimating the effective thermal conductivity of nanofluids is a complex task, owing to its reliance on several crucial factors. These factors include the type and morphology of particles, particle concentration, base fluid type, temperature, the presence of surfactants, and dispersion stability [47-48]. In the current literature, there are several equations available to estimate the thermal conductivity of nanofluids [49]. One well-known and widely used equation is Maxwell's general formula, which employs the volumetric concentration of nanoparticles as well as the thermal conductivities of the base fluid and nanoparticles [50]:

$$\frac{k_{nf}}{k_f} = \frac{k_p + 2k_f + 2(k_p - k_f)\varphi}{k_p + 2k_f - (k_p - k_f)\varphi}, \tag{1-1}$$

where k_{nf}, k_f and k_p are the thermal conductivity of the nanofluid, base fluid and nanoparticles, φ is the concentration of nanofluids.

In 1962, Hamilton and Crosser modified this equation to incorporate parameters that account for the morphology of nanoparticles, using an empirical shape factor [51], but it is more appropriate for use in scenarios with low concentrations. Yu and Choi used the ratio of nanolayer thickness to particle radius to determine thermal conductivity through the Maxwell model. A nanolayer refers to the layered structure formed by liquid molecules adhering to the surface of a nanoparticle. The equation can be expressed as follows [52]:

$$\frac{k_{nf}}{k_f} = \frac{k_p + 2k_f + 2(k_p - k_f)\varphi(1+\beta)^3}{k_p + 2k_f - (k_p - k_f)\varphi(1+\beta)^3}, \tag{1-2}$$

where β is the ratio of the nanolayer thickness to the particle radius.

In addition, several researchers have proposed various theoretical models to anticipate the thermal conductivity of nanofluids [7]. However, many of these equations suffer from conceptual limitations due to their experimental origin. This is because the primary factors that significantly affect the thermal conductivity of nanofluids are the aggregation or agglomeration of nanoparticles, nanoparticle size, thickness of the nanolayer, temperature, and concentration of nanoparticles [12].

Apart from theoretical models, there are different methods available to measure the thermal conductivity of nanofluids. These methods include the parallel plate steady-state technique, the laser flash method, the transient hot wire approach, and the transient plane source method [53]. It should be noted that the presence of air and the limitations of the measuring instrument can result in significantly lower values when measuring thermal conductivity [54-55].

1.1.4 Electrical properties

Nanofluids are not limited to use in solar collectors but can also be applied in other energy fields, such as mineral processing systems, fuel cells, and electric field heat transfer applications [56]. Several studies have reported an enhancement in the heat transfer of nanofluids when subjected to electric or magnetic fields [57-58]. As these fields are often utilized in such applications, investigating the electrical properties of nanofluids is crucial.

Electrical conductivity is considered the most important electrical property of a nanofluid. However, research in this area is still in its early stages, and the mechanisms behind the enhancement are not entirely understood [59]. Nevertheless, unlike thermal conductivity, electrical conductivity can be directly measured with less error, making it suitable for experimental investigation.

The electrical conductivity of nanofluids can be affected by several factors, including concentration, temperature, presence or absence of surfactants, nanoparticle size, and preparation method. However, many of these factors have not been fully explored, except for concentration and temperature [60-61]. Experimental studies have indicated

that higher temperatures generally result in an increase in electrical conductivity, but the impact of temperature is typically less pronounced than that of concentration [62-63].

An increase in electrical conductivity is observed as the concentration of nanoparticles increases within a certain range. However, there is no accurate explanation for this phenomenon. The factors responsible for the rise in electrical conductivity can be mainly attributed to the impact of the electric double layer and the increased conductance of the particles [59]. Several mechanisms have been proposed by researchers to explain this phenomenon [64-69]:

- interaction between the solid nanoparticles and the electrical double layer,
- electrophoretic mobility of the nanoparticles,
- agglomeration of nanoparticles,
- the polarity of the base liquid,
- the ionic concentrations of the base fluid.

In addition to experimental measurements, there are also several theoretical models available for estimating the electrical conductivity of nanofluids [70]. Among them, the Maxwell model is considered most suitable for low concentrations of spherical nanoparticles. This model takes into account the electrical conductivity of both the nanoparticles and the base fluid to predict the electrical conductivity of the nanofluid, and it writes [50]:

$$\sigma_{nf} = \sigma_f \left[1 + \frac{3\left(\frac{\sigma_p}{\sigma_f} - 1\right)\varphi}{\frac{\sigma_p}{\sigma_f} + 2 - \left(\frac{\sigma_p}{\sigma_f} - 1\right)\varphi} \right], \tag{1-3}$$

where σ_{nf}, σ_f and σ_p are the electrical conductivity of the nanofluid, base fluid and nanoparticles.

1.2 Aim of the current study

The main aim of this study is to examine the performance of carbon black-based nanofluids in photothermal and electrochemical applications and gain a thorough understanding of the properties of nanofluids through a series of numerical models and empirical correlations.

To investigate the use of nanofluids in photothermal applications, a set of indoor experiments will be conducted in a direct absorption solar collector (DASC) employing carbon black (CB) nanofluids. The effectiveness of the DASC will allow for the evaluation of photothermal properties and enhanced thermal-physical properties.

To investigate the behavior of CB nanoparticles, a numerical model should be developed, including volumetric heat transfer for nanofluids and the ability to predict nanoparticle sedimentation. The simulation results will be validated through experimental results.

To investigate the use of nanofluids in electrochemical applications, electrolyte nanofluids will be synthesized. The performance of the nanofluid will be evaluated based on the total hydrogen production and the efficiency of the electrolysis system.

2. Experiments and Modeling of Direct Absorption Solar Collectors: Review

Low-to-medium temperature solar collector technology can be categorized into four main types [71]: flat plate solar collector (FPSC), parabolic trough solar collector (PTSC), evacuated tube solar collector (ETSC), and direct absorption solar collector (DASC). DASC differs from other types of solar collectors as it allows working fluids to directly absorb solar radiation through a transparent cover, without an absorber surface, resulting in reduced heat loss. Consequently, traditional heat transfer fluids are not the best choice for DASC, leading researchers to explore the use of nanofluids to improve their thermal performance. Several studies have demonstrated that adding less than 1% volume fraction of nanoparticles can significantly enhance the absorption of solar radiation in the working fluid [72-74].

This chapter provides a brief review of the experimental and numerical studies conducted on DASC. A description of the volumetric heat transfer model and extinction coefficient is introduced since they are crucial components in DASC modeling.

2.1 Direct absorption solar collectors

The aim of the researchers studying DASC is to improve its thermal efficiency. The efficiency of the DASC is influenced by various factors, including the design of the collector, flow properties, and properties of the working fluid [71]. However, due to the small size of nanoparticles and low translucency of nanofluids, it is difficult to observe some phenomena of nanoparticles during experiments. Therefore, a combination of experiments and simulations is the best approach.

The thermal performance of a Direct Absorption Solar Collector (DASC) is affected by the design of the collector, which influences the absorption behavior of the working fluid. Bhalla et al. [75] conducted a study using the Taguchi method to investigate the impact of collector length on the performance of nanofluid-based solar collectors. The

results indicated that a smaller height of the collector, indicating a thinner layer of nanofluids, can achieve higher outlet temperatures. They also analyzed the effect of collector length on the temperature rise and thermal efficiency, and found that increasing the length of the collector can result in an increase in the outlet temperature rise of the nanofluid due to the extended exposure time to irradiation. However, increasing the length of the collector can lead to higher heat losses through the sides and bottom, which decreases the overall thermal efficiency of the system.

Sharaf et al. [76] conducted a computational study to examine how various design parameters, such as collector length and flow velocity, impact the energy and exergy efficiency of a DASC that uses CuO nanofluids. Their findings indicated that the exergy efficiency of the collector increases as the collector length increases. After reaching an optimal collector length, the exergy efficiency sharply decreases until it reaches a constant value.

While the two aforementioned studies primarily investigate the geometry of the DASC, such as its length and depth, an equally important factor to consider is the configuration of the cross-section. When using nanofluids as working fluids, the pipes' cross-section may come in various configurations, such as rectangular. Rectangular tubes have a larger optical contact area for radiation and working fluids compared to circular tubes. However, due to their shape, rectangular tubes are more prone to inducing turbulent flow at pipe bends, which can lead to the sedimentation of nanoparticles at corners. Other factors affecting the thermal efficiency of DASC have also been studied. In an article by Otanicar et al. [77], the performance of various nanofluids (carbon nanotube, Ag, graphite) in a DASC was examined. The research concluded that the addition of nanoparticles to the fluid mixture can considerably improve the efficiency of the collector. The most effective nanoparticles were found to be 20 nm silver nanoparticles. However, the author only tested different types and sizes of nanoparticles and did not investigate the effect of nanofluid concentration.

Ladjevardi et al. [78] conducted a numerical and experimental study to examine the impact of altering the diameters and volume fraction of graphite nanoparticles in a

DASC. The findings of the study revealed that increasing the concentration of graphite nanoparticles led to a rise in the collector output temperature. Furthermore, using graphite nanoparticles with a volume fraction of approximately 0.00025% resulted in a considerable increase in the outlet dimensionless temperature compared to pure water while incurring only a minimal increase in cost. However, the simulation results did not account for the behavior of the nanoparticles.

Several researchers have attempted to develop empirical correlations to evaluate heat transfer in DASC, such as convection internal heat transfer and heat loss. Karami et al. [79] have devised highly accurate empirical correlations for the Nusselt number to evaluate the heat loss of a DASC. The authors employed a general formula for the Nusselt number that is dependent on the non-dimensional numbers of Reynolds and Prandtl, with other parameters being determined through experiments. They used a PVP-stabilized silver nanofluid as the working fluid in DASC. However, the correlation can only be utilized to calculate the heat transfer coefficient for the range of $20 < Re < 200$ and $3 < Pr < 6$. The agglomeration of nanoparticles is an essential factor that should be considered when evaluating heat transfer.

Several studies have investigated factors affecting the thermal efficiency of a DASC, such as types of nanofluids, concentrations and sizes of nanoparticles, and tilt angles of the DASC. These studies have yielded similar results to those discussed above. However, only a few studies have focused on the impact of nanoparticle agglomeration, despite its negative influence on the thermal properties of nanofluids [18-20], as discussed in Section 1.1.2. While a small amount of aggregation can enhance the thermal conductivity of a nanofluid by facilitating heat transfer through physical chains [12], it is still necessary to investigate the effects of agglomeration. Simulation is the best method for investigating these effects.

2.2 Simulation models

In order to simulate the behavior of nanoparticles and investigate the thermal properties of nanofluids, a precise simulation model is required. The model should have the ability to predict heat transfer and flow characteristics in the DASC.

2.2.1 Model of nanofluids

There are two models commonly used to investigate the behavior of nanofluids, single-phase and two-phase models [80].

The single-phase model assumes that both the fluid phase and nanoparticles move at the same velocity while maintaining thermal equilibrium. In this approach, nanofluids are assumed to be homogeneous solutions consisting of the host fluid and nanoparticles, with minimal slip occurring between them. Consequently, the exchange of momentum and interphase forces between the fluid and nanoparticles are assumed to be infinite [81-84]. One advantage of this model is low computational costs and simplicity [85]. Nonetheless, its accuracy is limited. Beg et al. [86] reported that the single-phase model exhibited approximately 28% discrepancies in comparison to experimental findings, whereas the two-phase model demonstrated only 2% discrepancies.

The two-phase model, as its name suggests, considers the nanoparticles and the base fluids separately. Depending on the treatment of these two phases, the two-phase model can be divided into the Eulerian-Lagrangian method and the Eulerian-Eulerian method.

For low particle volume fractions, the Eulerian-Lagrangian method is applicable and utilizes the Lagrangian assumption to model the particle phase and the Eulerian approach to model the base liquid. Continuum equations are used to solve the governing equations for the base fluid [87-90]. This model is useful for studying the effects of thermophoretic and Brownian motion of the nanoparticles [91-93]. According to the investigation of various literature conducted by Habeen et al. [80], the Eulerian-Lagrangian method demonstrated a deviation range of 2% to 11.29%, while the Eulerian-Eulerian method exhibited a deviation range of 3% to 11.78%. However, despite the superiority of the Eulerian-Lagrangian method, it requires a significant amount of computational time, memory, and CPU power due to the presence of numerous nanofluid particles in the computational domain.

The Eulerian-Eulerian method considers base fluids and nanoparticles as two continuous phases and is a more suitable technique for modeling particles with high-volume fractions. It is based on the assumption that the liquid and nanoparticle phases continue to interpenetrate [94-96]. This technique includes mixture and segregated Eulerian models. The mixture model takes into account both the base fluids and nanoparticles, with each having their respective volume fraction and velocity vector, enabling the interpretation of the interaction between the two phases. The Eulerian model is more complex and requires solving continuity, momentum, and energy equations for both fluid and nanoparticle phases. This model allows each phase to have its own velocity vector while sharing the same pressure. These methods possess comparable precision and computational running time. According to the literature review of Habeen et al. [80], the mixture model exhibited a deviation range of 3% to 11.78%. In contrast, the Eulerian model had a deviation range of 7% to 12.61%. Nevertheless, several studies have reported an overprediction of the convective heat transfer coefficient, which becomes more pronounced with increasing nanofluid concentration [97-98].

2.2.2 Volumetric heat transfer

DASCs differ from conventional solar collectors by absorbing solar energy through working fluids, specifically through the use of nanoparticles. As a result, volumetric heat transfer is critical for accurately simulating DASC performance. To account for this, thermal conductivity, density, specific heat capacity, and other thermal properties that affect the heat transfer process must be considered in a volumetric model [99-101]. This model includes the energy balance equation for the entire volume, accounting for heat transfer by conduction, convection, and radiation, to accurately predict DASC performance.

In a simplified model, the volumetric heat generation can be treated as the energy change in the *z*-direction [99]:

$$q_v = -\frac{dI(z)}{dz}, \tag{2-1}$$

where, z is the length of the light path in the z-direction, $I(z)$ is the radiative intensity from the upper surface of the incident light, when z = 0, $I(0)$ represents the intensity of the incident radiation at the upper surface. $I(z)$ can be determined by Beer-Lambert's law [102]:

$$-\frac{dI(z)}{dz} = k_{nf} z, \tag{2-2}$$

where k is the extinction coefficient, subscript *nf* represents the nanofluid. It is an important photothermal property of nanofluids, and it will be discussed in the next section. Bohren and Huffman [103] suggested that, for a given wavelength, it can be calculated by:

$$k_{nf} = k_{sca} + k_{abs} \tag{2-3}$$

$$k_{sca} = \frac{8}{3}\beta^4 \left| \frac{m^2 - 1}{m^2 + 2} \right| \tag{2-4}$$

$$k_{abs} = 4\beta I(0) m \left\{ \frac{m^2 - 1}{m^2 + 2} \left[1 + \frac{\beta^2}{15} \left(\frac{m^2 - 1}{m^2 + 2} \right) \frac{m^4 + 27m^2 + 38}{2m^2 + 3} \right] \right\} \tag{2-5}$$

where k_{sca} is the scattering coefficient, k_{abs} is the absorption coefficient. β is defined as $\beta = \frac{\pi d}{\lambda}$, m is the relative complex refractive index of the nanofluid：

$$m = \frac{n_p + ik_p}{n_f} \tag{2-6}$$

where n is the refractive index. It is defined as the ratio of the speed of light in vacuum to the speed of light in a medium, so the refractive index of vacuum is $n \equiv 1$. $n_p + ik_p$ is the complex refractive index of the nanoparticle, where n_p represents the refraction in the medium and ik_p is the attenuation term in the medium that represents the energy loss.

According to Eqs. (2-4) and (2-5), scattering is proportional to the d^4, and absorption is proportional to the d^3, so scattering can be neglected for nanosized particles. Taylor et al. [104] conducted a simplified correlation for the extinction coefficient for nanofluids, written as:

$$k_{nf} = k_f + k_p \approx \frac{4\pi n_f}{\lambda} + \frac{3}{2}\frac{\alpha_p k_{abs}}{d} \tag{2-7}$$

In the experiments, some chemicals, such as SDS (surfactant), antifoam, etc. are added into nanofluids for stabilization. The chemicals altered the optical properties of the base and the particles. Therefore, the extinction coefficient of the base fluid and nanofluids should be determined experimentally.

Under a constant radiation resource condition, the average extinction coefficient of nanofluid at different concentrations can be fit as:

$$k_{nf} = k_f + \alpha_p \mathcal{A}\left(1 + \frac{d^2}{\mathcal{B}}\right) \tag{2-8}$$

where $\mathcal{A}$ and $\mathcal{B}$ are the fitting constants. Combining Eqs. (2-2) and (2-8) and substituting them into Eq. (2-1), the volumetric heat generation term reads:

$$q_v = I(0)ke^{-k_{nf}z} \tag{2-9}$$

2.2.3 Extinction coefficient

The extinction coefficient is an important photothermal property of nanofluids, as demonstrated in Eq. (2-9). This property measures how strongly a nanofluid absorbs light at a specific wavelength. The extinction coefficient is calculated as the product of the absorption coefficient, the path length of light through the nanofluids, and the concentration of the nanofluids [105].

Ladjevardi et al. [78] discovered that increasing the diameter of nanoparticles resulted in a significant increase in extinction coefficients for wavelengths below 1.25 μm, resulting in greater energy absorption. However, increasing nanoparticle diameter also

affects sedimentation, the effective fluid viscosity, thermal properties, and pumping cost. Notably, this study did not address the impact of nanofluid concentration on the extinction coefficient.

Choi et al. [106] conducted an experiment to measure the extinction coefficient of water-based paraffin-filled MWCNT (multi-wall carbon nanotube) nanofluids under a radiation wavelength of 632.8 nm. Their results indicate that the extinction coefficient increases linearly with the volume fraction when the carbon nanotube volume fraction is less than 0.05%. However, when the volume fraction exceeds 0.05%, the rate of increase is less pronounced.

Ahmad et al. [107] reported similar findings, showing that the extinction coefficient is directly proportional to the volume fraction and increases with the concentration of nanoparticles. Additionally, they investigated the effect of different base fluids on the extinction coefficient of carbon-based nanofluids and found that as the wavelength increased, the extinction coefficients of all nanofluids increased.

The studies mentioned above indicate that the extinction coefficient of nanofluids is a sensitive parameter that depends on the concentration of nanoparticles and the wavelength of the incident light. It should be noted that the wavelength may differ if a different radiation source is used. Therefore, an important parameter for developing an accurate model is the wavelength-averaged extinction coefficient, which must be determined experimentally to ensure precision.

3. Experiments of Electrolyte Nanofluids Electrolysis: Review

Typically, carbon-based nanofluids are in an acidic solution with a pH value of approximately 4 [108]. This is because, to maintain stability in the nanofluids, an electric double layer (EDL) is formed on the surface of the nanoparticles. If the pH value approaches 7, the electrochemical charges on the surface of the nanoparticles become neutralized, leading to the destabilization of the nanofluids [109]. However, due to their low electron concentration, nanofluids are not easily electrolyzed. Therefore, electrolyte nanofluids must be synthesized to conduct electrolysis.

3.1 Electrolyte nanofluids

Electrolyte nanofluids, as the name suggests, are nanofluids in which small amounts of nanoparticles are suspended in an electrolyte solution. These nanofluids exhibit enhanced thermal conductivity and electrical conductivity, which can be several times higher than that of the base electrolyte solution. Due to this property, they are promising candidates for a wide range of heat transfer applications, such as cooling of electronic devices, thermal management of batteries, and solar thermal energy conversion. The presence of electrolyte solutions in nanofluids can have an impact on the pH environment and destabilize the electrolyte nanofluids, making the long-term stabilization of electrolyte nanofluids a challenging task. Therefore, it is imperative to prioritize the development of long-term stabilized electrolyte nanofluids.

Wang et al. [110] investigated the use of Al_2O_3 nanoparticles as electrolytes in batteries for marine applications to enhance their micro-generation and heat-transfer capabilities, comparing them with tap water, mineral water, and seawater. The study's findings demonstrated that the Al_2O_3 nanofluid had the highest thermoelectric performance, with an optimal concentration of 0.1 wt%. The authors concluded that the electrochemical reaction of alumina nanofluid was able to improve the battery output and heat-transfer rate across various electrolytes, operating temperatures, and electrode areas. However, the study also revealed several issues that require attention,

such as the concentration change of the electrolyte nanofluids over time, which could impact the redox electrode reaction. Additionally, the Zeta potential of alumina nanofluids at a pH of 5.516 was not strong enough to counteract the repulsion between nanoparticles, which resulted in the formation of an unstable suspension that eventually caused precipitation.

Liu et al. [111] conducted a study to investigate the electrical conductivity and diffusion behavior of an electrolyte-based alumina nanofluid. The researchers prepared a water-based alumina nanofluid with a high-ionic-strength potassium ferro/ferricyanide electrolyte and sodium dodecyl sulfate, and analyzed its electrical conductivity and diffusion behavior. The results showed that the electrical conductivity of the nanofluids increased with an increasing concentration of alumina nanoparticles. Additionally, the Levich equation was used to determine the diffusion coefficient of the electrolyte nanofluids, and the diffusion behavior of the electrolyte was found to depend on the concentration of alumina nanoparticles. Furthermore, the authors explored the potential use of this electrolyte-based alumina nanofluid in thermogalvanic applications aimed at improving the performance of an electrolyte in thermal energy harvesting.

Beiki et al. [112] investigated the turbulent mass transfer of Al_2O_3 and TiO_2 electrolyte nanofluids in a circular tube with a diameter of 19 mm and a length of 1.5 m. The study revealed that the mass transfer coefficient, calculated by current and transfer rate of ions between the electrodes, increased with the concentration of nanoparticles, reaching an optimal concentration (0.01% in Al_2O_3/electrolyte nanofluid and 0.015% in TiO_2/electrolyte nanofluid) before decreasing with further increases in concentration. The enhancement ratio, which is the ratio of the mass transfer coefficient of the nanofluid to that of the base fluid, was found to be dependent on nanoparticle concentration and independent of the Reynolds number. The study also found that the Brownian motion and clustering mechanisms of nanoparticles could describe the enhancement ratio behavior in ENF. Additionally, TiO_2 nanofluids exhibited a higher mass transfer coefficient than Al_2O_3 nanofluids. This can be attributed to the smaller

size and higher Brownian velocity of TiO_2 particles, which increase micro-convection within the nanofluid.

The existing studies have primarily focused on the thermal enhancement of electrolyte nanofluids, while the exploration of their application in solar energy storage remains limited. The investigation of the electrical enhancements of electrolyte nanofluids is a crucial area that requires further investigation. The electrical properties of electrolyte nanofluids play a crucial role in the performance of electrochemical systems, and their potential applications are not limited to such systems. A hybrid system that can effectively utilize both the electrical and thermal-optical properties of nanofluids is highly valuable for the energy industry.

3.2 Electrolyte nanofluids electrolysis

Hiraki et al. [113] investigated the use of waste aluminum sources for hydrogen production by utilizing an aqueous solution of sodium hydroxide at various temperatures. The authors aimed to explore the efficiency of alkaline solutions in generating pressurized hydrogen from aluminum. The results showed a significant increase in the rate of hydrogen production with the concentration of sodium hydroxide and the temperature of the aqueous solution. The study presents a promising new technology for hydrogen production that has a significantly reduced environmental impact compared to conventional methods.

According to the study, the use of electrolyte nanofluids in water electrolysis and solar light irradiation was possible to increase total hydrogen production. The improved electrolysis efficiency was attributed to the enhanced thermal properties of the nanofluids under solar irradiation, which results in higher temperatures. The study also suggests that the nanoparticle motion in the electrolyte promotes electrolysis through the electrical double layer (EDL), while the applied electric field enhances the convective heat transfer within the nanofluids.

Choi et al. [114] observed an increase in hydrogen production during water electrolysis using cellulose nanofluid. The study found that the optimal hydrogen generation

efficiency was achieved with an electrolyte concentration of 1.8 wt%, resulting in both high efficiency and near-neutral pH values after the experiment. Additionally, the use of cellulose nanofluid as an electrolyte resulted in high stability and low causticity. It should be noted, however, that the enhancement was due to the nanostructure of cellulose rather than its thermoelectric properties, which warrants further investigation.

Furthermore, the electrolysis of electrolyte nanofluids poses a significant challenge to their stability. The increased temperature and electrical field during electrolysis can facilitate the collision of nanoparticles, leading to agglomeration and sedimentation. This factor has not been fully addressed in the literature.

4. Summary of Papers Included in the Thesis

This chapter summarizes the work and findings presented in Papers 1-3, which investigate the performance of nanofluids in a DASC and in water electrolysis, as well as the preparation and stability analysis of these nanofluids.

4.1 Paper 1

Wei, S., Hikmati, J., Balakin, B. V., & Kosinski, P. (2022). Experimental study of hydrogen production using electrolyte nanofluids with a simulated light source. International Journal of Hydrogen Energy, 47(12), 7522-7534.

This work presents an experimental study that investigates the viability of using nanofluids in the electrolyte of water electrolysis. The performance of the nanofluids was evaluated based on the total hydrogen production and production rate.

In this study, water electrolysis experiments using a Hoffman voltameter with CB-based sodium sulfate (SS) electrolyte nanofluids were conducted to analyze the effects of light irradiation on such systems. The main objective was to investigate the impact of different irradiation areas on the performance of the nanofluid-based systems using a halogen lamp as a radiation source.

The study revealed that the addition of CB and light irradiation could increase the hydrogen production rate when using a salt electrolyte, as shown in Fig. 4.1. The CB enhanced the electrical conductivity of the electrolyte, while light irradiation increased its temperature. Moreover, the effect of different CB concentrations on hydrogen production was investigated. The results demonstrated that the highest production rate was achieved at CB concentrations of 0.1 wt.% and 0.05 wt.% when a screen was used to block light, as illustrated in Fig. 4.2.

The experimental results also revealed that nanoparticles might have both positive and negative effects on electrolysis, as the average hydrogen production rates did not consistently increase or decrease every two minutes. Hence, the overall electrolysis process can be regarded as a dynamic balance.

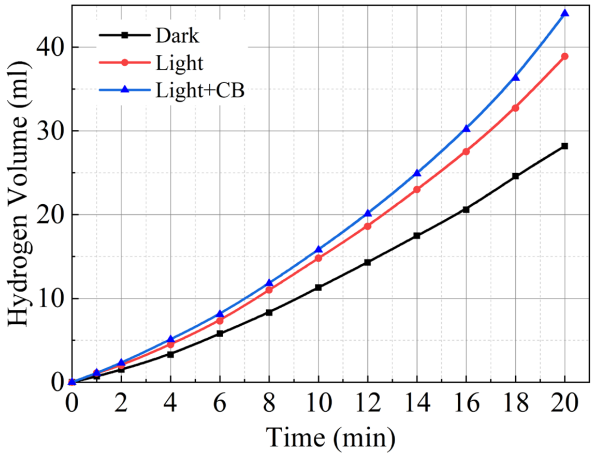

Fig. 4.1 Hydrogen volume variation with time for tests in different environments (The intensity of light was 1000 W/m^2, and the concentration of CB and SS was 0.05 wt.% and 10 wt.%, respectively.)

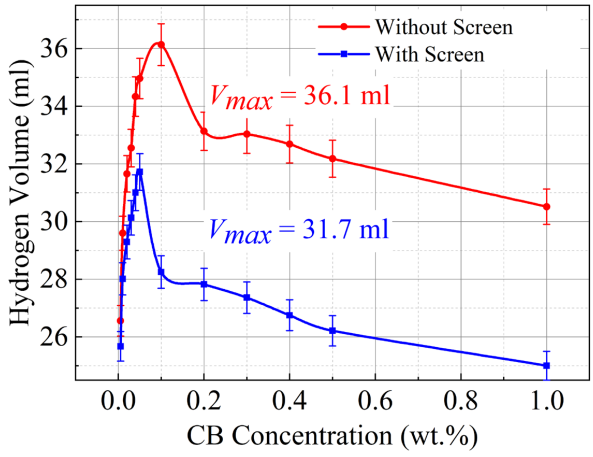

Fig. 4.2 Hydrogen production vs. different CB concentration (The intensity of light was 1000 W/m^2, and the concentration of SS was 10 wt.%)

4.2 Paper 2

Wei, S., Espedal, L., Balakin, B. V., & Kosinski, P. (2023). Experimental and Numerical Investigation of Direct Absorption Solar Collectors (DASCs) Based on Carbon Black Nanofluids (accepted by Experimental Heat Transfer)

The aim of this work is to investigate the performance of CB nanofluids in a rectangular DASC. The experimental results were used to build and validate the simulation model.

The experiments were conducted with both water and nanofluids containing 0.05 wt.% nanoparticle concentration at various flow rates and tilt angles under a concentrated simulated solar power source. The results indicated that the thermal efficiency of the DASC increased with an increasing flow rate and reached 0.57 at a flow rate of 4 l/min. Compared to the surface collector, the DASC exhibited a 10% higher thermal efficiency at a flow rate of 2.0 l/min, as shown in Fig. 4.3. The total thermal efficiency of the DASC depended on its orientation relative to the light source, as demonstrated in Fig. 4.4. The efficiency decreased as the incline angle of the DASC increased up to a tilt angle of 90° and then increased. Additionally, the results revealed that the down-faced (0° tilt angle) DASC outperformed the 180° tilt angle, with an efficiency approximately 35% higher due to reduced heat loss and stronger macroscopic convection.

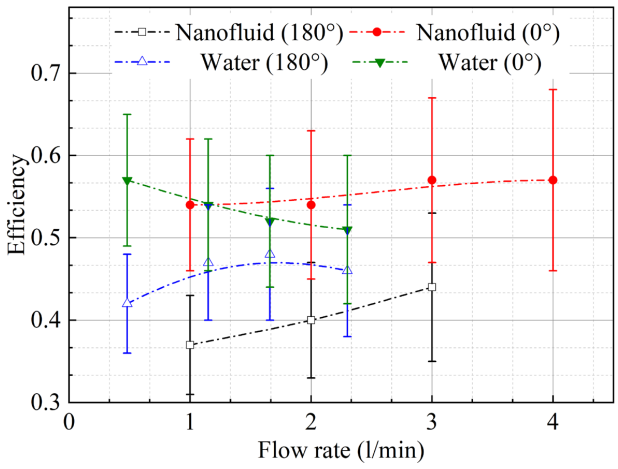

Fig. 4.3 Thermal efficiency at different flow rates and tile angles for nanofluids and water (C_{CB}=0.05 wt.%)

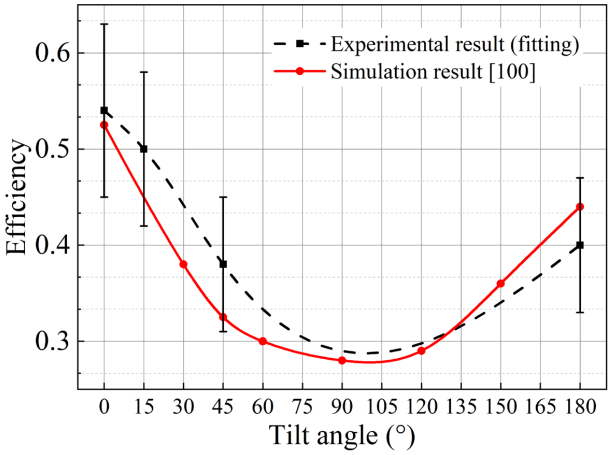

Fig. 4.4 Prediction of the change tendency between efficiency of nanofluid and tilt angles (C_{CB}=0.05 wt.%, Q=2 l/min). Compared with Balakin et al. [100]

A volumetric heat transfer model based on Beer-Lambert's law was developed to analyze the flow pattern and distribution of CB nanoparticles in the DASC in this study. The key parameter of the model was the extinction coefficient of CB nanofluids, as discussed in Sections 2.2.2 and 2.2.3, which was determined by measuring the reduction in heat flux when light passed through the nanofluids. The results are shown in Fig. 4.5. The simulation results indicated that the highest efficiency occurred at a concentration of 0.05 wt.%. The results also revealed the presence of a high-temperature zone with low fluid velocity, which may result in heat loss. Additionally, the CB nanoparticles could deposit in certain areas near the internal surface edges, affecting the inward heat flow, as shown in Fig. 4.6.

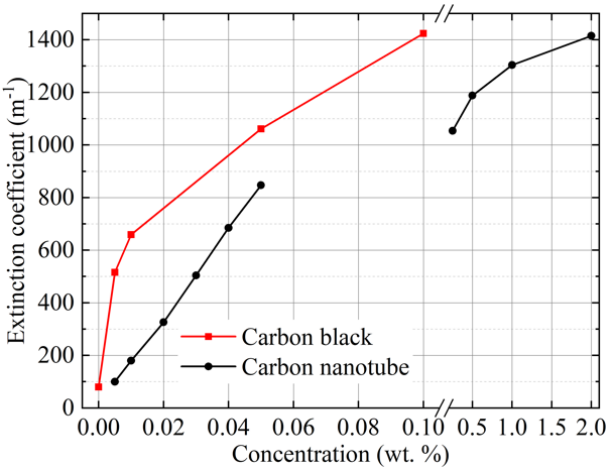

Fig. 4.5 Extinction coefficient of CB nanofluids (red line). The results are compared to the literature results [106] that focused on carbon nanotubes.

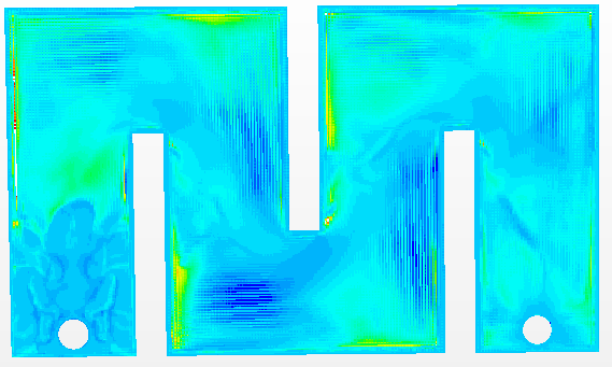

Fig. 4.6 CB volume fraction distribution on internal surface (C_{CB}=0.05 wt.%, Q=2 l/min)

4.3 Paper 3

Wei, S., Balakin, B. V., & Kosinski, P. (2023). Investigation of nanofluids in alkaline electrolytes: stability, electrical properties, and hydrogen production (submitted to Journal of Cleaner Production)

This work is a continuation of Paper 1 and aims to investigate the performance of CB nanofluids in the electrolysis of alkaline electrolytes.

In this paper, a mixture of CB nanoparticles and sodium hydroxide (SH) solution was used to prepare an electrolyte nanofluid (ENF) for hydrogen production through electrolysis in a Hoffman voltameter. The stability of CB nanofluids and sodium sulfate electrolyte nanofluids (SSENF) were compared with SHENF. The results showed that the stability of nanofluids could be weakened by the presence of salt or alkaline solutions, leading to the complete sedimentation of nanoparticles within seven days

The electrolysis experiments results indicated that CB nanoparticles could enhance the electrical conductivity, mass transfer, and heat absorption of electrolysis, resulting in improved hydrogen production rates. The hydrogen production rate increased by 23.62% when the concentration of SHENF was 10 wt.%, and CB concentration was 0.1 wt.%. As the concentration of CB increased, the hydrogen production rate also increased before eventually decreasing. The optimal CB concentration was found to be 0.2 wt.% when a screen was used, as shown in Fig. 4.7.

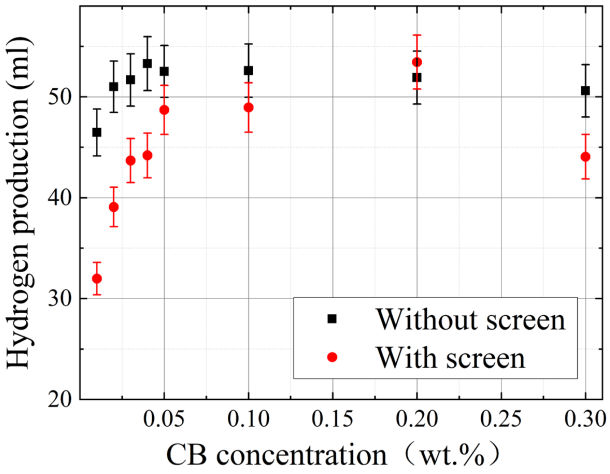

Figure 4.7 Total hydrogen production vs. different CB concentrations with and without the screen (C_{SH} = 5 wt.%)

A semi-empirical correlation was developed to evaluate the total hydrogen production based on Faraday's law of electrolysis and the Maxwell model, as described in Section 1.1.4. However, due to certain assumptions and simplifications, this correlation demonstrated good agreement with experimental results only for CB concentrations

below 0.1 wt.%, and can solely be utilized for predicting hydrogen production from the electrolysis of SHENF.

5. Concluding Remarks and Further Work

In the dissertation, it was demonstrated that the performance analysis of nanofluids could be achieved through both experiments and simulations. The study presented in Paper 2 demonstrates that simulations can replicate experimentally observed flow patterns, energy transfer, mass transfer, and various other parameters that have a significant impact on the performance of nanofluids, as well as the behavior of nanoparticles. However, the behavior of nanoparticles is difficult to observe in experiments, and thus simulations provide a better tool for investigating it. Additionally, simulations require more precision in the model, particularly in considering the forces acting on nanofluids due to the small size of nanoparticles.

Papers 1 and 2 have demonstrated that using ENF for hydrogen production through electrolysis is feasible, as it involves physical and chemical phenomena. The motion of nanoparticles in the electrolyte enhances electrolysis through the electrical double layer (EDL), and the applied electric field enhances convective heat transfer within the nanofluids, leading to an increase in the system's temperature and facilitating the chemical reaction. This application of nanofluids in water electrolysis holds significant potential in the energy sector, establishing a new connection between solar energy and hydrogen.

Theoretical models can also be used to predict hydrogen production. In Paper 3, a semi-empirical correlation was proposed to predict the hydrogen production in the electrolysis of low concentrations of SHENF. However, as the concentration of nanofluids increases, the likelihood of collisions and agglomeration of nanoparticles also increases. To predict hydrogen production at higher concentrations, a more precise theoretical model is required to describe the agglomeration and sedimentation of nanoparticles, which has not been fully investigated. This highlights the importance of nanofluid stability at the microscale.

Future research on the performance of nanofluids in DASCs should aim to optimize the numerical model and develop a more precise volumetric heat transfer model that considers all the important forces affecting nanoparticle motion, as discussed in Section

1.1.1. Additionally, research should explore the efficiencies of various nanofluids and evaluate the performance of different DASC geometries.

As for the electrochemical performance of CB nanofluids, two critical issues require further exploration. The first is to identify an improved method for enhancing the stability of electrolyte nanofluids, while the second entails the development of a model that accurately depicts the impact of electrical fields on nanoparticle aggregation and sedimentation. In addition, exploring the use of different nanofluids, not limited to CB, such as investigating the potential of biodegradable fluids, which have recently gained popularity.

References

[1] European Commission. (2020). Communication on the 2030 Climate Target Plan. (COM(2020) 562 final). https://eur-lex.europa.eu/legal-content/EN/TXT/?uri=CELEX:52020DC0562

[2] The state council of the People's Republic of China. (2021). Action Plan for Carbon Dioxide Peaking Before 2030. (State Council (2021) No. 23) http://english.www.gov.cn/policies/latestreleases/202110/27/content_WS6178a47ec6d0df57f98e3dfb.html

[3] Mekhilef, S., Saidur, R., & Safari, A. (2011). A review on solar energy use in industries. Renewable and sustainable energy reviews, 15(4), 1777-1790.

[4] Hayat, M. B., Ali, D., Monyake, K. C., Alagha, L., & Ahmed, N. (2019). Solar energy—A look into power generation, challenges, and a solar‐powered future. International Journal of Energy Research, 43(3), 1049-1067.Bellos, E., Tzivanidis, C., & Antonopoulos, K. A. (2017). A detailed working fluid investigation for solar parabolic trough collectors. Applied Thermal Engineering, 114, 374-386. Borton, J. & Clay, E. (1986): "The African Food Crisis of 1982-1986", Disasters, Vol. 10: 258-72.

[5] Kumar, V., Tiwari, A. K., & Ghosh, S. K. (2015). Application of nanofluids in plate heat exchanger: a review. Energy conversion and management, 105, 1017-1036. Bhalla, V., Khullar, V., & Tyagi, H. (2019). Investigation of factors influencing the performance of nanofluid-based direct absorption solar collector using Taguchi method. Journal of Thermal Analysis and Calorimetry, 135, 1493-1505.

[6] Sezer, N., Atieh, M. A., & Koç, M. (2019). A comprehensive review on synthesis, stability, thermophysical properties, and characterization of nanofluids. Powder technology, 344, 404-431.

[7] Ali, N., Bahman, A. M., Aljuwayhel, N. F., Ebrahim, S. A., Mukherjee, S., & Alsayegh, A. (2021). Carbon-based nanofluids and their advances towards heat transfer applications—a review. Nanomaterials, 11(6), 1628.

[8] Ilyas, S. U., Pendyala, R., & Marneni, N. (2013). Settling characteristics of alumina nanoparticles in ethanol-water mixtures. In Applied Mechanics and Materials (Vol. 372, pp. 143-148). Trans Tech Publications Ltd.

[9] Hong, P. N., Minh, D. N., Van Hung, N., Minh, P. N., & Khoi, P. H. (2017). Carbon nanotube and graphene aerogels—The world's 3D lightest materials for environment applications: A review. Int. J. Mater. Sci. Appl, 6, 277.

[10] Askari, S., Lotfi, R., Seifkordi, A., Rashidi, A. M., & Koolivand, H. (2016). A novel approach for energy and water conservation in wet cooling towers by using MWNTs and nanoporous graphene nanofluids. Energy conversion and

management, 109, 10-18.

[11] Neuberger, N., Adidharma, H., & Fan, M. (2018). Graphene: A review of applications in the petroleum industry. Journal of Petroleum Science and Engineering, 167, 152-159.

[12] Said, Z., Sundar, L. S., Tiwari, A. K., Ali, H. M., Sheikholeslami, M., Bellos, E., & Babar, H. (2022). Recent advances on the fundamental physical phenomena behind stability, dynamic motion, thermophysical properties, heat transport, applications, and challenges of nanofluids. Physics Reports, 946, 1-94.

[13] Das, S. K., Putra, N., Thiesen, P., & Roetzel, W. (2003). Temperature dependence of thermal conductivity enhancement for nanofluids. J. Heat Transfer, 125(4), 567-574.

[14] Verwey, E. J. W., & Overbeek, J. T. G. (1955). Theory of the stability of lyophobic colloids. Journal of Colloid Science, 10(2), 224-225.

[15] Al-Farhany, K., Alomari, M. A., Saleem, K. B., Al-Kouz, W., & Biswas, N. (2021). Numerical investigation of double-diffusive natural convection in a staggered cavity with two triangular obstacles. The European Physical Journal Plus, 136(8), 814.

[16] Daniel, Y. S., Aziz, Z. A., Ismail, Z., & Salah, F. (2018). Impact of thermal radiation on electrical MHD flow of nanofluid over nonlinear stretching sheet with variable thickness. Alexandria Engineering Journal, 57(3), 2187-2197.

[17] Zhao, D., Hedayat, M., Barzinjy, A. A., Dara, R. N., Shafee, A., & Tlili, I. (2019). Numerical investigation of Fe3O4 nanoparticles transportation due to electric field in a porous cavity with lid walls. Journal of Molecular Liquids, 293, 111537.

[18] Suganthi, K. S., & Rajan, K. S. (2017). Metal oxide nanofluids: Review of formulation, thermo-physical properties, mechanisms, and heat transfer performance. Renewable and Sustainable Energy Reviews, 76, 226-255.

[19] Angayarkanni, S. A., & Philip, J. (2014). Effect of nanoparticles aggregation on thermal and electrical conductivities of nanofluids. Journal of Nanofluids, 3(1), 17-25.

[20] Duan, H. (2020). Analysis on the extinction properties of nanofluids for direct solar absorption. Physica E: Low-dimensional Systems and Nanostructures, 120, 114046.

[21] Bakthavatchalam, B., Habib, K., Saidur, R., Saha, B. B., & Irshad, K. (2020). Comprehensive study on nanofluid and ionanofluid for heat transfer enhancement: A review on current and future perspective. Journal of Molecular Liquids, 305, 112787.

[22] Qiu, L., Zhu, N., Feng, Y., Michaelides, E. E., Żyła, G., Jing, D., ... & Mahian,

O. (2020). A review of recent advances in thermophysical properties at the nanoscale: From solid state to colloids. Physics Reports, 843, 1-81.

[23] Ali, N., Teixeira, J. A., & Addali, A. (2019). Aluminium nanofluids stability: A comparison between the conventional two-step fabrication approach and the controlled sonication bath temperature method. Journal of Nanomaterials, 2019, 1-9.

[24] Witharana, S., Hodges, C., Xu, D., Lai, X., & Ding, Y. (2012). Aggregation and settling in aqueous polydisperse alumina nanoparticle suspensions. Journal of Nanoparticle Research, 14, 1-11.

[25] Bakthavatchalam, B., Habib, K., Saidur, R., Saha, B. B., & Irshad, K. (2020). Comprehensive study on nanofluid and ionanofluid for heat transfer enhancement: A review on current and future perspective. Journal of Molecular Liquids, 305, 112787.

[26] Oh, D. W., Kwon, O., & Lee, J. S. (2008). Transient Thermal Conductivity and Colloidal Stability Measurements of Nanofluids by Usingthe 3ω method. Journal of Nanoscience and nanotechnology, 8(10), 4923-4929.

[27] Kong, L., Sun, J., & Bao, Y. (2017). Preparation, characterization and tribological mechanism of nanofluids. Rsc Advances, 7(21), 12599-12609.

[28] Chang, H., Jwo, C. S., Fan, P. S., & Pai, S. H. (2007). Process optimization and material properties for nanofluid manufacturing. The International Journal of Advanced Manufacturing Technology, 34, 300-306.

[29] Chamsa-Ard, W., Brundavanam, S., Fung, C. C., Fawcett, D., & Poinern, G. (2017). Nanofluid types, their synthesis, properties and incorporation in direct solar thermal collectors: A review. Nanomaterials, 7(6), 131.

[30] Zhang, H., Qing, S., Zhai, Y., Zhang, X., & Zhang, A. (2021). The changes induced by pH in TiO2/water nanofluids: Stability, thermophysical properties and thermal performance. Powder Technology, 377, 748-759.

[31] Colla, L., Fedele, L., Scattolini, M., & Bobbo, S. (2012). Water-based Fe2O3 nanofluid characterization: thermal conductivity and viscosity measurements and correlation. Advances in Mechanical Engineering, 4, 674947.

[32] Kumar, D. D., & Arasu, A. V. (2018). A comprehensive review of preparation, characterization, properties and stability of hybrid nanofluids. Renewable and Sustainable Energy Reviews, 81, 1669-1689.

[33] Kovalchuk, N. M., Johnson, D., Sobolev, V., Hilal, N., & Starov, V. (2019). Interactions between nanoparticles in nanosuspension. Advances in Colloid and Interface Science, 272, 102020.

[34] Wijenayaka, L. A., Ivanov, M. R., Cheatum, C. M., & Haes, A. J. (2015).

Improved parametrization for extended Derjaguin, Landau, Verwey, and Overbeek predictions of functionalized gold nanosphere stability. The Journal of Physical Chemistry C, 119(18), 10064-10075.

[35] Chakraborty, S., & Panigrahi, P. K. (2020). Stability of nanofluid: A review. Applied Thermal Engineering, 174, 115259.

[36] Okonkwo, E. C., Wole-Osho, I., Almanassra, I. W., Abdullatif, Y. M., & Al-Ansari, T. (2021). An updated review of nanofluids in various heat transfer devices. Journal of Thermal Analysis and Calorimetry, 145, 2817-2872.

[37] Xian-Ju, W., & Xin-Fang, L. (2009). Influence of pH on nanofluids' viscosity and thermal conductivity. Chinese Physics Letters, 26(5), 056601.

[38] Romanelli, M. F., Moraes, M. C. F., Villavicencio, A. L. C. H., & Borrely, S. I. (2004). Evaluation of toxicity reduction of sodium dodecyl sulfate submitted to electron beam radiation. Radiation Physics and Chemistry, 71(1-2), 411-413.

[39] Lechuga, M., Fernández-Serrano, M., Ríos, F., Fernández-Arteaga, A., & Jiménez-Robles, R. (2022). Environmental impact assessment of nanofluids containing mixtures of surfactants and silica nanoparticles. Environmental Science and Pollution Research, 29(56), 84125-84136.

[40] Ulset, E. T., Kosinski, P., & Balakin, B. V. (2018). Solar steam in an aqueous carbon black nanofluid. Applied Thermal Engineering, 137, 62-65.

[41] Sundar, L. S., Ramana, E. V., Said, Z., Punnaiah, V., Mouli, K. V. C., & Sousa, A. C. (2020). Properties, heat transfer, energy efficiency and environmental emissions analysis of flat plate solar collector using nanodiamond nanofluids. Diamond and Related Materials, 110, 108115.

[42] Hachicha, A. A., Said, Z., Rahman, S. M. A., & Al-Sarairah, E. (2020). On the thermal and thermodynamic analysis of parabolic trough collector technology using industrial-grade MWCNT based nanofluid. Renewable Energy, 161, 1303-1317.

[43] Said, Z., Sundar, L. S., Rezk, H., Nassef, A. M., Chakraborty, S., & Li, C. (2021). Thermophysical properties using ND/water nanofluids: An experimental study, ANFIS-based model and optimization. Journal of Molecular Liquids, 330, 115659.

[44] Tiwari, A. K., Pandya, N. S., Said, Z., Öztop, H. F., & Abu-Hamdeh, N. (2021). 4S consideration (synthesis, sonication, surfactant, stability) for the thermal conductivity of CeO2 with MWCNT and water based hybrid nanofluid: An experimental assessment. Colloids and Surfaces A: Physicochemical and Engineering Aspects, 610, 125918.

[45] Cakmak, N. K., Said, Z., Sundar, L. S., Ali, Z. M., & Tiwari, A. K. (2020).

Preparation, characterization, stability, and thermal conductivity of rGO-Fe3O4-TiO2 hybrid nanofluid: An experimental study. Powder technology, 372, 235-245.

[46] Said, Z., & Saidur, R. (2017). Thermophysical properties of metal oxides nanofluids. Nanofluid heat and mass transfer in engineering problems, 39.

[47] Barai, D. P., Bhanvase, B. A., & Sonawane, S. H. (2020). A review on graphene derivatives-based nanofluids: investigation on properties and heat transfer characteristics. Industrial & Engineering Chemistry Research, 59(22), 10231-10277.

[48] Ambreen, T., & Kim, M. H. (2020). Influence of particle size on the effective thermal conductivity of nanofluids: A critical review. Applied Energy, 264, 114684.

[49] Syam Sundar, L., Venkata Ramana, E., Said, Z., Pereira, A. M., & Sousa, A. C. (2021). Heat transfer of rGO/CO3O4 hybrid nanomaterial-based nanofluids and twisted tape configurations in a tube. Journal of Thermal Science and Engineering Applications, 13(3), 031004.

[50] Maxwell, J. C. (1873). A treatise on electricity and magnetism (Vol. 1). Oxford: Clarendon Press.

[51] Hamilton, R. L., & Crosser, O. K. (1962). Thermal conductivity of heterogeneous two-component systems. Industrial & Engineering chemistry fundamentals, 1(3), 187-191.

[52] Yu, W., & Choi, S. U. S. (2003). The role of interfacial layers in the enhanced thermal conductivity of nanofluids: a renovated Maxwell model. Journal of nanoparticle research, 5, 167-171.

[53] Qiu, L., Zhu, N., Feng, Y., Michaelides, E. E., Żyła, G., Jing, D., ... & Mahian, O. (2020). A review of recent advances in thermophysical properties at the nanoscale: From solid state to colloids. Physics Reports, 843, 1-81.

[54] Pradhan, N. R., Duan, H., Liang, J., & Iannacchione, G. S. (2009). The specific heat and effective thermal conductivity of composites containing single-wall and multi-wall carbon nanotubes. Nanotechnology, 20(24), 245705.

[55] Che, J., Cagin, T., & Goddard III, W. A. (2000). Thermal conductivity of carbon nanotubes. Nanotechnology, 11(2), 65.

[56] Pordanjani, A. H., Aghakhani, S., Afrand, M., Mahmoudi, B., Mahian, O., & Wongwises, S. (2019). An updated review on application of nanofluids in heat exchangers for saving energy. Energy Conversion and Management, 198, 111886.

[57] Wang, G., Zhang, Z., Wang, R., & Zhu, Z. (2020). A review on heat transfer of

nanofluids by applied electric field or magnetic field. Nanomaterials, 10(12), 2386.

[58] Narankhishig, Z., Ham, J., Lee, H., & Cho, H. (2021). Convective heat transfer characteristics of nanofluids including the magnetic effect on heat transfer enhancement-a review. Applied Thermal Engineering, 193, 116987.

[59] Minea, A. A. (2019). A review on electrical conductivity of nanoparticle-enhanced fluids. Nanomaterials, 9(11), 1592.

[60] Shoghl, S. N., Jamali, J., & Moraveji, M. K. (2016). Electrical conductivity, viscosity, and density of different nanofluids: An experimental study. Experimental Thermal and Fluid Science, 74, 339-346.

[61] Sarojini, K. K., Manoj, S. V., Singh, P. K., Pradeep, T., & Das, S. K. (2013). Electrical conductivity of ceramic and metallic nanofluids. Colloids and Surfaces A: Physicochemical and Engineering Aspects, 417, 39-46.

[62] Shirazi, S. F. S., Gharehkhani, S., Yarmand, H., Badarudin, A., Metselaar, H. S. C., & Kazi, S. N. (2015). Nitrogen doped activated carbon/graphene with high nitrogen level: green synthesis and thermo-electrical properties of its nanofluid. Materials Letters, 152, 192-195.

[63] Akilu, S., Baheta, A. T., Kadirgama, K., Padmanabhan, E., & Sharma, K. V. (2019). Viscosity, electrical and thermal conductivities of ethylene and propylene glycol-based β-SiC nanofluids. Journal of Molecular Liquids, 284, 780-792.

[64] Zawrah, M. F., Khattab, R. M., Girgis, L. G., El Daidamony, H., & Abdel Aziz, R. E. (2016). Stability and electrical conductivity of water-base Al2O3 nanofluids for different applications. HBRC journal, 12(3), 227-234.

[65] Bagheli, S., Fadafan, H. K., Orimi, R. L., & Ghaemi, M. (2015). Synthesis and experimental investigation of the electrical conductivity of water based magnetite nanofluids. Powder Technology, 274, 426-430.

[66] Anu, K., & Hemalatha, J. (2019). Magnetic and electrical conductivity studies of zinc doped cobalt ferrite nanofluids. Journal of Molecular Liquids, 284, 445-453.

[67] Heyhat, M. M., & Irannezhad, A. (2018). Experimental investigation on the competition between enhancement of electrical and thermal conductivities in water-based nanofluids. Journal of Molecular Liquids, 268, 169-175.

[68] Mashali, F., Languri, E., Mirshekari, G., Davidson, J., & Kerns, D. (2019). Nanodiamond nanofluid microstructural and thermo-electrical characterization. International Communications in Heat and Mass Transfer, 101, 82-88.

[69] Zakaria, I., Mohamed, W. A. N. W., Azmi, W. H., Mamat, A. M. I., Mamat, R., & Daud, W. R. W. (2018). Thermo-electrical performance of PEM fuel cell using

Al2O3 nanofluids. International Journal of Heat and Mass Transfer, 119, 460-471.

[70] Banisi, S., Finch, J. A., & Laplante, A. R. (1993). Electrical conductivity of dispersions: A review. Minerals engineering, 6(4), 369-385.

[71] Karami, M., Bozorgi, M., & Delfani, S. (2021). Effect of design and operating parameters on thermal performance of low-temperature direct absorption solar collectors: a review. Journal of Thermal Analysis and Calorimetry, 146, 993-1013.

[72] Bertocchi, R., Kribus, A., & Karni, J. (2004). Experimentally determined optical properties of a polydisperse carbon black cloud for a solar particle receiver. J. Sol. Energy Eng., 126(3), 833-841.

[73] Sani, E., Barison, S., Pagura, C., Mercatelli, L., Sansoni, P., Fontani, D., ... & Francini, F. (2010). Carbon nanohorns-based nanofluids as direct sunlight absorbers. Optics Express, 18(5), 5179-5187.

[74] Otanicar, T., Hoyt, J., Fahar, M., Jiang, X., & Taylor, R. A. (2013). Experimental and numerical study on the optical properties and agglomeration of nanoparticle suspensions. Journal of nanoparticle research, 15, 1-11.

[75] Bhalla, V., Khullar, V., & Tyagi, H. (2019). Investigation of factors influencing the performance of nanofluid-based direct absorption solar collector using Taguchi method. Journal of Thermal Analysis and Calorimetry, 135, 1493-1505.

[76] Sharaf, O. Z., Al-Khateeb, A. N., Kyritsis, D. C., & Abu-Nada, E. (2019). Energy and exergy analysis and optimization of low-flux direct absorption solar collectors (DASCs): Balancing power-and temperature-gain. Renewable Energy, 133, 861-872.

[77] Otanicar, T. P., Phelan, P. E., Prasher, R. S., Rosengarten, G., & Taylor, R. A. (2010). Nanofluid-based direct absorption solar collector. Journal of renewable and sustainable energy, 2(3), 033102.

[78] Ladjevardi, S. M., Asnaghi, A., Izadkhast, P. S., & Kashani, A. H. (2013). Applicability of graphite nanofluids in direct solar energy absorption. Solar Energy, 94, 327-334.

[79] Karami, M., Bozorgi, M., Delfani, S., & Akhavan-Behabadi, M. A. (2018). Empirical correlations for heat transfer in a silver nanofluid-based direct absorption solar collector. Sustainable Energy Technologies and Assessments, 28, 14-21.

[80] Habeeb, A. S., Karamallah, A. A., & Aljabair, S. (2022). Review of computational multi-phase approaches of nanofluids filled systems. Thermal Science and Engineering Progress, 28, 101175.

[81] Huminic, G., & Huminic, A. (2019). The influence of hybrid nanofluids on the performances of elliptical tube: Recent research and numerical study. International Journal of Heat and Mass Transfer, 129, 132-143.

[82] Alshare, A., Al-Kouz, W., & Khan, W. (2020). Cu-Al2O3 water hybrid nanofluid transport in a periodic structure. Processes, 8(3), 285.

[83] Jedsadaratanachai, W., & Boonloi, A. (2017). Performance analysis and flow visualization in a round tube heat exchanger inserted with wavy V-ribs. Advances in Mechanical Engineering, 9(9), 1687814017724091.

[84] Mehdi, S. M., Akhtar, M., Hussain, A., Alothmany, D. S., & Aziz, S. (2016). CFD study of liquid sodium inside a wavy tube for laminar convectors: effect of reynolds number, wave pitch, and wave amplitude. Mathematical Problems in Engineering, 2016.

[85] Ambreen, T., Saleem, A., & Park, C. W. (2021). Homogeneous and multiphase analysis of nanofluids containing nonspherical mwcnt and gnp nanoparticles considering the influence of interfacial layering. Nanomaterials, 11(2), 277.

[86] Beg, O. A., Rashidi, M. M., Akbari, M., & Hosseini, A. (2014). Comparative numerical study of single-phase and two-phase models for bio-nanofluid transport phenomena. Journal of Mechanics in Medicine and Biology, 14(01), 1450011.

[87] Kumar, N., & Puranik, B. P. (2017). Numerical study of convective heat transfer with nanofluids in turbulent flow using a Lagrangian-Eulerian approach. Applied Thermal Engineering, 111, 1674-1681.

[88] Ravnik, J., Skerget, L., Tibaut, J., & Yeigh, B. W. (2017). Solution of energy transport equation with variable material properties by BEM. International Journal of Computational Methods and Experimental Measurements, 5(3), 337-347.

[89] Sharaf, O. Z., Al-Khateeb, A. N., Kyritsis, D. C., & Abu-Nada, E. (2019). Numerical investigation of nanofluid particle migration and convective heat transfer in microchannels using an Eulerian–Lagrangian approach. Journal of Fluid Mechanics, 878, 62-97.

[90] Ambreen, T., & Kim, M. H. (2017). Comparative assessment of numerical models for nanofluids' laminar forced convection in micro and mini channels. International Journal of Heat and Mass Transfer, 115, 513-523.

[91] Aminfar, H., Motallebzadeh, R., & Farzadi, A. (2010). The study of the effects of thermophoretic and Brownian forces on nanofluid thermal conductivity using Lagrangian and Eulerian approach. Nanoscale and Microscale Thermophysical Engineering, 14(4), 187-208.

[92] Aminfar, H., & Motallebzadeh, R. (2011). Numerical investigation of the effects of nanoparticle diameter on velocity field and nanoparticle distribution of nanofluid using Lagrangian-Eulerian approach. Journal of Dispersion Science and Technology, 32(9), 1311-1317.

[93] Aminfar, H., & Motallebzadeh, R. (2012). Investigation of the velocity field and nanoparticle concentration distribution of nanofluid using Lagrangian-Eulerian approach. Journal of dispersion science and technology, 33(1), 155-163.

[94] Aghanajafi, A., Toghraie, D., & Mehmandoust, B. (2017). Numerical simulation of laminar forced convection of water-CuO nanofluid inside a triangular duct. Physica E: Low-dimensional Systems and Nanostructures, 85, 103-108.

[95] Sekrani, G., & Poncet, S. (2016). Further investigation on laminar forced convection of nanofluid flows in a uniformly heated pipe using direct numerical simulations. Applied Sciences, 6(11), 332.

[96] Kalteh, M., Abbassi, A., Saffar-Avval, M., & Harting, J. (2011). Eulerian–Eulerian two-phase numerical simulation of nanofluid laminar forced convection in a microchannel. International journal of heat and fluid flow, 32(1), 107-116.

[97] Akbari, M., Galanis, N., & Behzadmehr, A. (2012). Comparative assessment of single and two-phase models for numerical studies of nanofluid turbulent forced convection. International Journal of Heat and Fluid Flow, 37, 136-146.

[98] Akbari, M., Galanis, N., & Behzadmehr, A. (2011). Comparative analysis of single and two-phase models for CFD studies of nanofluid heat transfer. International Journal of Thermal Sciences, 50(8), 1343-1354.

[99] Struchalin, P. G., Yunin, V. S., Kutsenko, K. V., Nikolaev, O. V., Vologzhannikova, A. A., Shevelyova, M. P., ... & Balakin, B. V. (2021). Performance of a tubular direct absorption solar collector with a carbon-based nanofluid. International Journal of Heat and Mass Transfer, 179, 121717.

[100] Balakin, B. V., Zhdaneev, O. V., Kosinska, A., & Kutsenko, K. V. (2019). Direct absorption solar collector with magnetic nanofluid: CFD model and parametric analysis. Renewable Energy, 136, 23-32.

[101] Bårdsgård, R., Kuzmenkov, D. M., Kosinski, P., & Balakin, B. V. (2020). Eulerian CFD model of direct absorption solar collector with nanofluid. Journal of renewable and sustainable energy, 12(3), 033701.

[102] Modest, M. F., & Mazumder, S. (2021). Radiative heat transfer. Academic press.

[103] Bohren, C. F., & Huffman, D. R. (2008). Absorption and scattering of light by small particles. John Wiley & Sons.

[104] Taylor, R. A., Phelan, P. E., Otanicar, T. P., Adrian, R., & Prasher, R. (2011). Nanofluid optical property characterization: towards efficient direct absorption

solar collectors. Nanoscale research letters, 6, 1-11.

[105]Wei, S., Hikmati, J., Balakin, B. V., & Kosinski, P. (2022). Experimental study of hydrogen production using electrolyte nanofluids with a simulated light source. international journal of hydrogen energy, 47(12), 7522-7534.

[106]Choi, T. J., Kim, S. H., Jang, S. P., Lin, L., & Kedzierski, M. A. (2020). Aqueous nanofluids containing paraffin-filled MWCNTs for improving effective specific heat and extinction coefficient. Energy, 210, 118523.

[107]Ahmad, S. H. A., Saidur, R., Mahbubul, I. M., & Al-Sulaiman, F. A. (2017). Optical properties of various nanofluids used in solar collector: A review. Renewable and Sustainable Energy Reviews, 73, 1014-1030.

[108]Kessler, J. C., Padoin, N., Hotza, D., & Soares, C. (2019). Rheological behavior of a silver aqueous nanofluid stabilized with aminosilane-based surfactant under confined flow. Brazilian Journal of Chemical Engineering, 36, 229-237.

[109]Zuccaro, L., Krieg, J., Desideri, A., Kern, K., & Balasubramanian, K. (2015). Tuning the isoelectric point of graphene by electrochemical functionalization. Scientific reports, 5(1), 1-13.

[110]Wang, R. T., & Wang, J. C. (2016). Alumina nanofluids as electrolytes comparisons to various neutral aqueous solutions inside battery. Journal of Mechanics, 32(3), 369-379.

[111]Liu, C., Lee, H., Chang, Y. H., & Feng, S. P. (2016). The study of electrical conductivity and diffusion behavior of water-based and ferro/ferricyanide-electrolyte-based alumina nanofluids. Journal of colloid and interface science, 469, 17-24.

[112]Beiki, H., Esfahany, M. N., & Etesami, N. (2013). Turbulent mass transfer of Al 2 O 3 and TiO 2 electrolyte nanofluids in circular tube. Microfluidics and nanofluidics, 15, 501-508.

[113]Hiraki, T., Takeuchi, M., Hisa, M., & Akiyama, T. (2005). Hydrogen production from waste aluminum at different temperatures, with LCA. Materials transactions, 46(5), 1052-1057.

[114]Choi, D., & Lee, K. Y. (2020). Experimental study on water electrolysis using cellulose nanofluid. Fluids, 5(4), 166.

Scientific Papers

INTERNATIONAL JOURNAL OF HYDROGEN ENERGY 47 (2022) 7522–7534

Available online at www.sciencedirect.com

ScienceDirect

journal homepage: www.elsevier.com/locate/he

Experimental study of hydrogen production using electrolyte nanofluids with a simulated light source

Shihao Wei [a], *Javad Hikmati* [a], *Boris V. Balakin* [b,c], *Pawel Kosinski* [a,*]

[a] *University of Bergen, Department of Physics and Technology, Bergen, Norway*
[b] *Western Norway University of Applied Sciences, Department of Mechanical and Marine Engineering, Bergen, Norway*
[c] *Department of Thermal Physics, National Research Nuclear University MEPhI, Russia*

HIGHLIGHTS

- Successfully prepared a stabilized sodium sulfate electrolyte with carbon black nanoparticles.
- Hydrogen production increases with the increasing of the concentration of nanofluids then decrease.
- Carbon black nanoparticles have both positive and negative impacts on electrolysis.
- Using nanofluids can increase the efficiency of electrolysis.

ARTICLE INFO

Article history:
Received 21 June 2021
Received in revised form
2 December 2021
Accepted 13 December 2021
Available online 3 January 2022

Keywords:
Electrolysis
Carbon black
Nanofluids
Hydrogen production rate
Electrical properties

ABSTRACT

In this research, we conducted water electrolysis experiments of a carbon black (CB) based sodium sulfate electrolyte using a Hoffman voltameter. The main objective was to investigate hydrogen production in such systems, as well as analyse the electrical properties and thermal properties of nanofluids. A halogen lamp, mimicking solar energy, was used as a radiation source, and a group of comparative tests were also conducted with different irradiation areas. The results showed that by using CB and light, it was possible to increase the hydrogen production rate. The optimal CB concentration was 0.1 wt %. At this concentration, the hydrogen production rate increased by 30.37% after 20 min of electrolysis. Hence, we show that using CB in electrolytes irradiated by solar energy could save the electrical energy necessary for electrolysis processes.

Introduction

Because of the depletion of traditional energy reserves and their detrimental emissions into our ecosystem, hydrogen is recognized as the global future energy. So far hydrogen has been widely produced from hydrocarbon sources, initiating an enormous output of carbon dioxide and contaminants [1]. With renewable energy consumption on the rise as well as the global energy demand [2], electrolytic hydrogen production technologies offer a sustainable alternative to conventional hydrogen production methods [3]. Water electrolyser can utilize solar energy to generate hydrogen of high purity with

* *Corresponding author*. Universitetet i Bergen, Postboks 7803, N-5020 Bergen, Norway.
E-mail address: Pawel.Kosinski@uib.no (P. Kosinski).
https://doi.org/10.1016/j.ijhydene.2021.12.130

zero adverse emissions, at any location around the world with access to sunlight, due to its simplicity and flexibility [4].

The most important parameter of electrolysis is efficiency. A low efficiency can make the energy cost larger than the energy produced. There are many factors that can affect the efficiency of electrolysis. The most investigated, and also the most important, factor is the use of catalysts. Some researchers reported outstanding catalytic performance of chemical compounds at different electrolytes [5,6]. Furthermore, some nanocomposites can also be used as high-efficiency electrocatalysts in the water-splitting reaction [7–9]. Moreover, nanosized materials or nanostructures have good optical and electrochemical properties that can increase the thermal stability of electrolytes and electrolysis devices [10–15]. Finally, the excellent electrochemical performance also makes some nanocomposites be a potential hydrogen storage material [16].

It is also recognized that the main parameters influencing the heat transfer efficiencies of fluids are their thermal properties such as viscosity, density, heat capacity, and thermal conductivity, with the latter being the most influential factor [17]. Since base fluids (water, oil, and ethylene) possess low thermal conductivity, their solar absorption efficiency is also usually low [18]. Nevertheless, Maxwell [19] in 1873 proposed a mechanism that involves adding micro-sized particles into a base fluid to improve the heat absorption capability of the base fluid, and Choi and Tran [20] identified that adding even smaller particles to a base liquid could improve the heat transfer characteristics of the base fluid. They stated that the addition of nanoparticles (NPs) (solid particles with a diameter in the range of 1~100 nm) into conventional fluids raised thermal conductivity and defined these innovative classes of heat transfer fluids as nanofluids (NF) [21]. Compared to the absorption efficiency of water (13%) [22], carbon-based NF may absorb 96% of solar radiation [23].

Carbon black (CB) is one of several substances with analogous absorption characteristics as the ideal concept of a black body, which in theory absorbs all incident radiation [24]. Similarly, CB is a kind of material that has good absorption throughout the whole wavelength range of sunlight and has thus high potential for solar energy applications.

Sani et al. [25] experimented with carbon black nanoparticles (CB NPs) in distilled water (DW) and reported that the photothermal efficiency of CB was 85%. Another advantage of nanometre-sized particles is that they can pass through small passages, unlike micrometre-sized particles that cause severe clogging problems in heat transfer equipment [20]. Also, Han et al. [26] stated that 90% of incoming radiation can be absorbed by a thick layer of CB.

Multiple researchers agree that hydrogen production by electrolysis depends vastly on the temperature of the electrolyte. For instance, Galney et al. [27] designed a high-temperature alkaline electrolysis cell and tested it at a temperature between 35 °C and 400 °C. The electrolyte showed a significant performance enhancement at the higher temperature. Also, Brett et al. [28] investigated the enhancement in the hydrogen production rate via raising the temperature of the electrolyte. The accumulated heat of the sun through a heat absorber material can thus be coupled with electrical energy in a conventional water electrolyser to improve production efficiency.

Electrolyzing NF-based electrolytes is a new research field. Some investigation has been carried out to describe the electrical properties of NFs according to different NPs, size, volume fraction, etc. Lobato et al. [29] discovered that nanofluids with a 0.04 wt% of carbon nanoparticles attained higher charge capacities and energy efficiencies at higher current densities. Bose et al. [30] reported that the ionanofluid (ionic liquid-based nanofluid) electrolyte delivered a higher discharge capacity than a conventional electrolyte. Moreover, Yen et al. [31] utilized the dimensional analysis method to investigate the Al_2O_3 water-based nanofluid. The results showed the Al_2O_3 nanofluid with the emulsifying agent had the highest electric charge density at 40 °C and 2.5 wt%.

The studies mentioned above were focused on the thermal or electrical properties of nanofluid-based electrolytes. At present, there is no report in the literature concerning both properties. Similarly, no study focuses on the hydrogen production of electrolyzing nanofluid-based electrolytes. Therefore, the main purpose of this work is to investigate these issues.

Experimental method

Nanofluid preparation

The experimental procedure of nanofluid preparation is shown in Fig. 1. Firstly, the suitable weight fractions of CB nanoparticles (Ensaco 350G Carbon Black, Timcal) and surfactants (sodium dodecyl sulfate, SDS) were weighed and blended with distilled water. Each component was using a Sartorius CPA 324 S balance. To acquire a more uniform mixture, the suspension was stirred for 5 min using a ceramic magnet stirrer plate with a magnetic stirrer bar. Meanwhile, the tank of a Branson 3510 ultrasonic cleaner (a bath sonicator) was filled with tap water to the operating level line (3 cm from the top) and degassed for 10 min to eliminate bubbles formed in the water. The cleaner had a frequency of 40 kHz and a maximum power of 335 V with a maximum capacity equal to 6 L. Secondly, the stopwatch was set to 60 min before

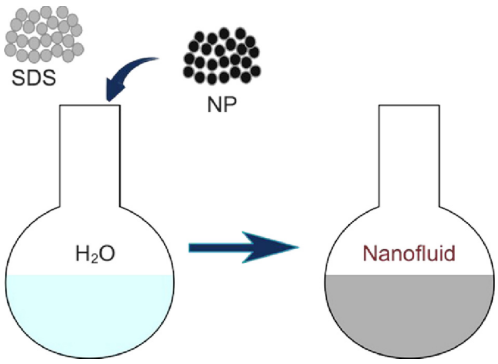

Fig. 1 – Two steps of NF preparation.

carefully locating the beaker containing the solution within the tank. As waves are transferred and distributed throughout the water, the beaker must therefore not touch the tank bottom (beaker floats). The beaker was submerged in the water bath, and the level of the water tank was higher than the level of the solution inside the beaker.

Several authors emphasize the duration of sonication as a crucial step for NF preparation. Asadi et al. [32] investigated the impact of sonication time on various NPs and emphasized that for most NPs the optimum sonication time was between 20 to 40 min. For comparison, samples with a varied sonication time of 10, 20, 30 and 60 min were prepared in this work. The samples that were sonicated for 20 min showed greater improved stability than those that were sonicated for 10 min. When the concentration of NF was larger than 0.1 wt%, 30 min of sonication was not sufficient to acquire a stable NF. Therefore, all the samples were sonicated for 60 min in this work, as mentioned previously.

Following the chemical and physical treatments of NFs, a sodium sulfate (SS) electrolyte was subsequently added and stirred for a minimum of 5 min with a magnet stirrer before discharging the electrolyte solution from the upper opening of the electrolysis apparatus into the bubble-shaped reservoir of a Hofmann voltameter (see Fig. 2). The anode and cathode compartments were filled by stirring the valves at the upper end of the two cylindrical tubes. Given that the adsorption of SDS decreases with temperature, one drop of Antifoam B Emulsion was added to the solution to minimize the risk of foam formation.

SS is a neutral salt, so the pH of its aqueous solution is around 7. As it has been tested by many researchers, pH has a significant impact on the stability of nanofluids. When pH value is below 7, nanofluids show a significant enhancement on stability with the increasing of pH value until 7. However, when pH is above 7, sedimentation occurs [33]. Therefore, we chose SS solution as the electrolyte as it has less impact on the stability of nanofluids.

In this study, nanofluids with different weight percent concentrations (0.005 wt %~1 wt %) were manufactured. Hwang et al. [34] suggest that using 1 wt % SDS improves the stability of carbon-based nanofluids. Therefore, the same amount of this surfactant was added to all the samples.

Surfactant is an important compound to stabilize the colloid because surfactants can attach to the particle surfaces to form micelles. This hinders the agglomeration of the dispersed phase. According to our study, SDS has excellent performance on stabilizing CB-based nanofluid [35,36]. On the other hand, SDS can be harmful to the environment as it can produce sulfates and persulfates at high concentrations [37]. Therefore, many researchers have started to study the environmental impact and biodegradability of the mixture of surfactants and nanoparticles. Here, alkyl polyglucoside, a non-ionic surfactant, has been considered [38]. Therefore, we are planning to investigate the feasibility to use this surfactant to prepare CB nanofluid in our future work.

Experimental procedure

Hydrogen production was investigated by using a Hoffman voltameter, where the volume of hydrogen produced by

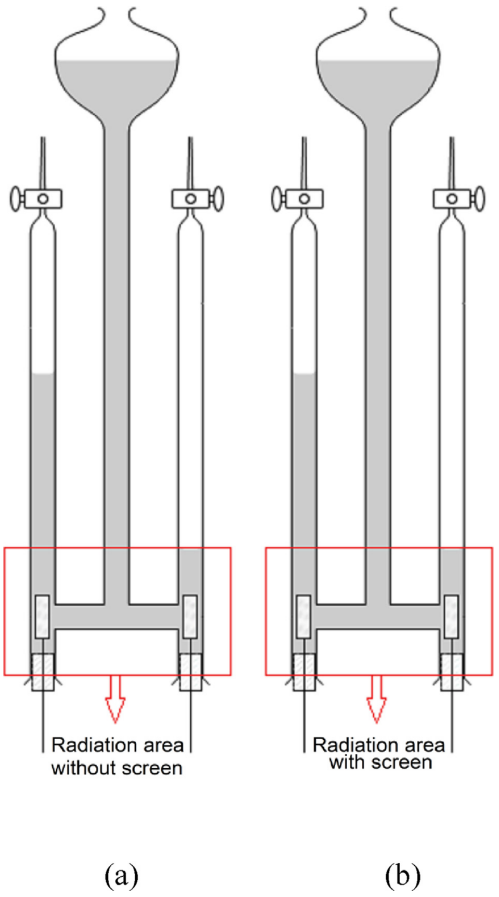

Fig. 2 – The scheme of Hoffmann voltameter irradiated by the artificial light: (a) without the protective screen/collimator; (b) with a protective screen/collimator (irradiation occurs only in the marked area).

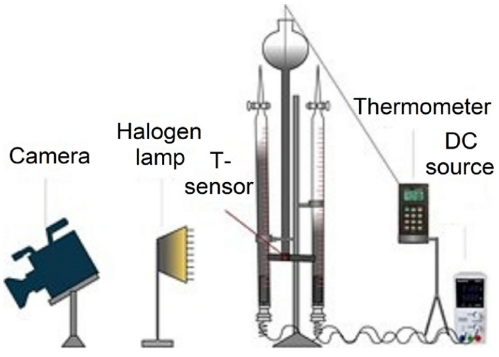

Fig. 3 – Schematic representation of experimental apparatus.

electrolysis can be read directly from the scale on the pipe. Fig. 3 shows the framework of nanofluid-based electrolysis experiments. The DC source from Peakteck, and its maximum output current and voltage, are 2 A and 30 V with the measurement accuracy within ±1% + 5 digits, respectively. The temperature was measured by thermocouples and recorded through an Omega HH506RA thermometer with an error range of ±0.05%. A Cotech 400 W/230 V flood-light halogen lamp with an Osram 400 W/230 V R7S light bulb was used to simulate the solar irradiation. The meter from Linshang Technology with an accuracy of ±0.10% measured the irradiance intensity. After preparing the nanofluids as described in Section Nanofluid preparation, we let the nanofluids stay still to cool down. The 1-h sonification made the temperature of the nanofluid higher than the room temperature. When the temperature of the nanofluid reached 30 °C, the camera, the lamp and the DC source were simultaneously turned on. The lamp directly illuminated the area near the electrodes, which is denoted as the rectangle in Fig. 2. The temperature, electric current and hydrogen volume were recorded every 2 min.

The reactions for SS in this work were as follows:

$$\text{Anode: } 4OH^- - 4e^- = 2H_2O + O_2 \quad (1)$$

$$\text{Cathode: } 4H^+ + 4e^- = 2H_2 \quad (2)$$

$$\text{Overall Reaction: } 2H_2O = 2H_2 + O_2 \quad (3)$$

In this work, we focused on three issues influencing hydrogen production. First, to investigate the electrolyte effect on hydrogen production, the electrolysis was performed at ambient temperature in the range of 20~26 °C. All tests excluding NF and light are conducted in the darkroom for a particular amount of time with SS concentration in the range of 1~12 wt%, while keeping a constant applied voltage (30 V). The darkroom means there were only natural light sources in the room, and the light intensity was below 100 W/m^2.

Subsequently, the experiments were performed under the presence of the halogen lamp, while holding other parameters constant (voltage and SS wt.%). The centre of the halogen lamp and the electrolytic plates were fixed on the same level to ensure the core zone of electrolysis could be illuminated by the maximum radiation, see Fig. 2 (a). The radiated heat flux coming from the halogen lamp resulted in the temperature increase of the electrolyte. The elevated temperature gave rise to a higher current density in the electrolyser. The highest current density for the maximum voltage and electrolyte concentration was 0.3 A/cm ^{2}.

Afterwards, the experiments were conducted with CB coupled with the halogen lamp. The effect of CB on hydrogen production was studied as follows: (i) the effect of light intensity was investigated by changing the distance between the electrolyser and the radiation source, thus influencing the irradiance intensity, while keeping the other parameters constant; (ii) the experiments were performed with CB concentrations in the range of (0.005–1.0) wt.%, while SS concentration and the distance to the radiation source were kept constant. Considering that some metal elements (the wires and electrodes) could absorb heat, which has a negative impact on experimental results, i.e., those mental elements could absorb heat and cause the temperature to increase faster, a set of comparative tests was conducted. For comparative tests, a 5 mm thick screen with a small hole (20 mm × 30 mm) was set between the halogen lamp and Hoffman voltameter. The radiation area is shown in Fig. 2 (b), where the red rectangle has the same size as the small hole in the screen. Therefore, only this area was irradiated by the light. It could ensure that the core zone of electrolysis was illuminated by the light, but it also eliminated the heat absorption by the metal elements.

Results and discussion

Experimental results for single variables

The effect of CB-based nanofluids on water electrolysis has not been done in the research literature yet. Therefore, many factors may affect experimental results. Generally, the optical properties of nanofluids are one of them. Thus, experimental results of water electrolysis using salt electrolyte and CB nanofluids conducted in dark and light environments are presented in this section.

(1) *The dark and light environments*

Fig. 4 shows the results of electrolyzing the SS solution with different concentrations. These experiments were conducted in the dark environment and light environment, respectively. The irradiance of light was 1000 W/m^2 (i.e., 1 sun), and the processing time was 20 min. We observed a similar linear trend that the hydrogen production rate increased with the increase of SS concentration for both dark and light environments. According to the results, the rate of hydrogen production for the environment with light (1.88 ml/min) was higher than for the dark room (1.5 ml/min), as

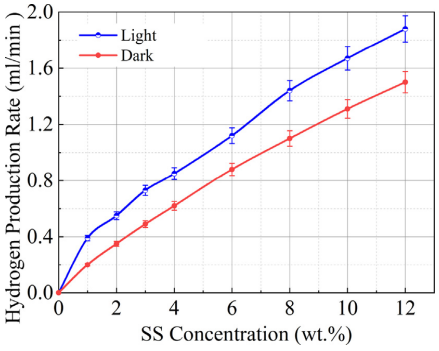

Fig. 4 – Hydrogen production rate for light and dark environments, for different SS concentrations.

expected. This occurred for SS concentration equal to 12 wt%. Thus, the light radiated the nanofluid and increased the temperature. The higher temperature accelerated the movement of ions in the electrolyte that facilitates the dissociation of water. As a consequence, a higher temperature decreases the voltage needed for electrolysis, i.e., the consumption of electricity.

This can also be explained by analysing the fundamental relation for Gibbs energy of water electrolysis in standard conditions [39]:

$$\Delta G_d^\circ(H_2O(l)) = \Delta H_d^\circ(H_2O(l)) - T\cdot\Delta S_d^\circ(H_2O(l)) \quad (4)$$

where ΔG is Gibbs energy, ΔH is enthalpy and ΔS is entropy.

The process of a water splitting reaction requires energy input, and this energy is almost constant within the experimental environment. That means the variation of ΔH with temperature can be omitted. For electrolysis, the Gibbs energy is the required electrical energy. Therefore, from Eq. (4), when ΔH remains constant, increasing T means decreasing ΔG. Thus, Gibbs energy decreases with the increase of the operating temperature.

(2) *Carbon black*

In our next experiments, 0.05 wt% of CB was added to the electrolyte. The reaction time was again 20 min. All the samples were added SDS, and the concentration of SS was the only variable in the experiments. It must be noted that SDS could not only stabilize the nanofluids, it also increased the electrical conductivity of the electrolyte [40,41]. The results of the experiments are collected in Fig. 5.

Adding CB into an SS solution can increase the hydrogen production rate, as mentioned previously, because NPs could increase the electrical conductivity of the electrolyte. Some researchers indicated that carbon-based nanoparticles could increase the conductivity of the solutions, and the maximum values were obtained for the concentrations about 0.2 wt% [42,43]. In electrolytes, electrical conduction occurred by motion of ions. Therefore, higher electrical conductivity means the faster movement of ions can facilitate electrolysis. Maxwell [44] showed a model that was considered applicable, mostly for estimating the electrical conductivity of a nanofluid. This model is a function of the electrical conductivity of nanoparticles and the base fluid:

$$\frac{\sigma_{nf}}{\sigma_{bf}} = 1 + \frac{3\left(\frac{\sigma_p}{\sigma_{bf}} - 1\right)\varphi}{\frac{\sigma_p}{\sigma_{bf}} + 2 - \left(\frac{\sigma_p}{\sigma_{bf}} - 1\right)\varphi}, \quad (5)$$

where σ_{nf} is the electrical conductivity of the nanofluid; σ_{bf} is the electrical conductivity of the base fluid; σ_p is the electrical conductivity of the particles and φ is the concentration of the solution.

In our experiments, Brownian motion and electrophoretic mobility are also vital factors that could affect the electrical conductivity of the nanofluid. Shen et al. [45] combined these two factors and the updated Maxwell model. The model for electrophoretic mobility can be written:

$$\sigma_E = \frac{2\varphi\varepsilon_r^2\varepsilon_0^2 U_0^2}{\eta r^2}, \quad (6)$$

where σ_E is the electrical conductivity due to electrophoretic mobility; ε_r is the dielectric constant of base fluid; ε_0 is the dielectric constant of vacuum; U_0 is the zeta potential of nanoparticles; η is the viscosity of the nanofluid and r is the radius of nanoparticles.

Also, the model for Brownian motion is as follows:

$$\sigma_B = \frac{3\varphi\varepsilon_r\varepsilon_0 U_0\left(\frac{RT}{L}\cdot\frac{1}{3\pi\eta}\right)}{r^{\frac{3}{2}}} \quad (7)$$

where σ_B is the electrical conductivity caused by Brownian motion, R is the thermodynamic constant, T is temperature and L is the Avogadro constant.

Therefore, the total electrical conductivity for nanofluid becomes:

$$\sigma = \sigma_{nf} + \sigma_E + \sigma_B. \quad (8)$$

(3) *Light and carbon black*

Fig. 6 and Fig. 7 show histories of hydrogen volume and temperature during the experiments. The curves represent

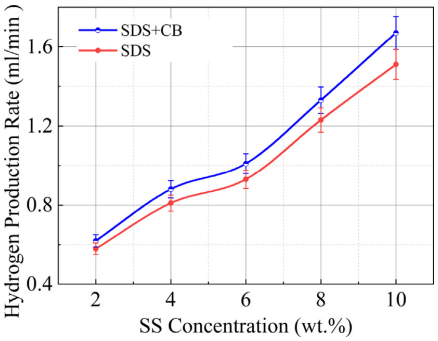

Fig. 5 – Hydrogen production rate for different SS concentration.

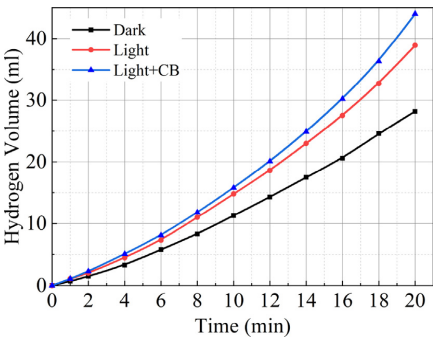

Fig. 6 – Hydrogen volume variation with time for tests in different environments.

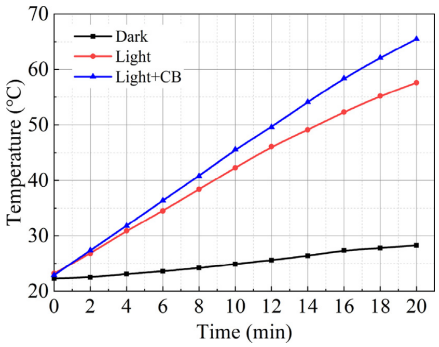

Fig. 7 – Temperature variation with the time in different environments.

the results of the experiments carried out for three cases: (i) in a dark environment, (ii) with light, and (iii) for CB based solutions. The intensity of light was 1000 W/m^2, and the concentration of CB and SS was 0.05 wt% and 10 wt%, respectively. SDS was added to all the electrolytes. The general conclusion from the results is that using a nanofluid-based electrolyte has a positive impact on electrolysis as an increased temperature can speed up the reaction rate. From Figs. 6 and 7, the temperatures after 20 min were 65.5 °C, 57.6 °C and 28.3 °C, from the top to the bottom. The maximum temperature (Fig. 7) increased 103.53% and 131.45% for the case with only light, and light with CB, respectively.

Lavasani et al. [46] used graphene-based nanofluids to investigate the thermal conductivity enhancement for different weight fractions, and their results showed that the increase in thermal conductivity at high temperatures becomes more prominent by increasing weight percentage. The increase of the fluid temperature is also associated with the increase in hydrogen production. The maximum volume of hydrogen increased by 37.94% and 56.03% for light and light and CB, respectively (Fig. 6). It is easy to see the direct effect of temperature on hydrogen production from Fig. 7. Although both electrical conductivity and temperature could increase the hydrogen production, when comparing the three initial conditions, the temperature had a more obvious effect on it. In addition, the electrical conductivity increases with temperature due to the enhanced Brownian motion, see Eq. (7).

Heyhat et al. [47] found that the electrical conductivity of carbon-based nanofluids increased with the increase of temperature and nanofluid concentration. The maximum augmentation was for temperature 25 °C and the minimum occurred in the temperature 55 °C. Also, the effect of increasing the nanofluid concentration was stronger than temperature. This observation does not directly correspond to our experimental results. Comparing Figs. 4 and 5, the temperature effect (using light) is more significant than that of CB concentration because the hydrogen production rates increased more.

In our research, the impact of different irradiance of light was also studied for the electrolyte with CB and without CB. The values of irradiance were 1000 W/m^2, 1500 W/m^2 and 2000 W/m^2 and are denoted respectively as black, red, and blue lines in Fig. 8. The results showed the higher irradiance induced higher temperature, and CB intensified the process. It is worth noting that the temperature can still be rather high even without CB. The maximum temperatures in Fig. 8 (a) were 67.3 °C, 61.7 °C and 57.6 °C. Also, according to Fig. 7 (b), the values were 82 °C, 70.7 °C and 65.5 °C. Thus, the presence of CB increased the temperature by a factor of 21.84%, 14.59% and 13.72%, respectively.

Effect of CB concentration

In Section Experimental results for single variables, the optical properties of electrolyte were investigated. In this section, however, we focus on the photothermal properties and electrical properties as they have a vital role in the process of energy transformation. The objective of this part of the study is to investigate how the concentration of CB affects the hydrogen production rate. To minimize the influence of temperature on the results, the ideal gas law was used to modify the hydrogen volume measured during the experiments. The modified hydrogen volume is the volume of hydrogen at room temperature, i.e., we eliminate the volume expansion of hydrogen volume at high temperatures. This can be calculated from the following:

$$V_1 = V_0 \frac{T_1}{T_0} \tag{9}$$

where V_1 is the modified hydrogen volume; V_0 is the hydrogen volume measured in the experiments; T_1 is the room temperature and T_0 is the temperature measured in the experiments.

The findings from the previous sections revealed an improvement in hydrogen production rate, which was attributed to the higher temperature stimulated by the CB NPs. To examine the consequence of NF density, viscosity, and the applicability of higher NF concentrations for hydrogen production, several experiments were accomplished with CB concentrations in the range of 0.005~1 wt% together with comparative experiments. Each experiment was performed using constant SS concentration (10 wt%), constant radiation intensity (1000 W/m^2), and the same reaction time (20 min).

The maximum hydrogen volume that was calculated as the volume at room temperature for each experiment and conducted without the screen is depicted by a red line in Fig. 9. The modified generated hydrogen volumes (i.e., calculated from Eq. (9)) with the increase of CB weight percentage were 26.56 ml, 29.59 ml, 31.65 ml, 32.55 ml, 34.33 ml, 34.96 ml, 36.13 ml, 33.13 ml, 33.03 ml, 32.68 ml, 32.18 ml, 30.52 ml, respectively. As seen, the highest hydrogen volume obtained was 36.1 ml with a CB concentration of 0.1 wt%, whereas the lowest hydrogen volume (26.56 ml) resulted from the lowest CB concentration (0.005 wt%). According to Fig. 9, hydrogen production increased first and then decreased with the rising of the CB concentration. When the CB concentration was lower than 0.1 wt%, the hydrogen production increased rapidly with concentration. However, for higher concentrations, the influence of the concentration was less significant. The experimental results illustrate that the optimum hydrogen volume was produced for lower CB concentrations.

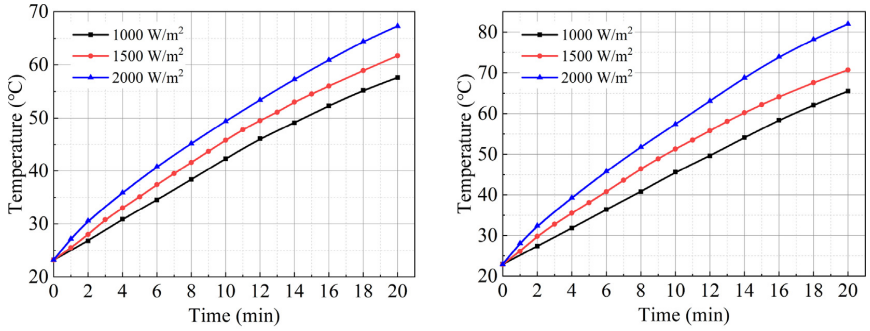

Fig. 8 – Temperature vs. time for different values of light irradiance: (a) no CB was used in the electrolyte; (b) the electrolyte contained 0.05 wt.% CB.

As the fraction of CB particles exceeds 0.1 wt%, the hydrogen volume declines. This is due to the fact that, apart from the influence of temperature, electrical conductivity increases with the rising of nanoparticle concentration as it strengthens Brownian motion and electrophoresis, see Eqs. (6) and (7) [48]. Zawrah et al. [49] also demonstrated this behaviour and noticed a following decrease of electrical conductivity when concentration increases. They explained this phenomenon as the complex processes related to the electrical double layer (EDL). The interaction between the nanoparticles and the EDL is the reason for the augmentation of electrical conductivity. However, with the increasing of the particle numbers, the charges available for the formation of EDL are insufficient and the electrostatic attraction force becomes a repulsion force among nanoparticles [49].

In addition to electrical conductivity, temperature is also a vital factor that affects the hydrogen production rate. An increase in particle concentration should increase the temperature of the nanofluid because more particles absorb heat. However, when the concentration reaches a certain range, nanoparticles form a "shield" in the outer nanofluids that blocks light from penetrating the nanofluids. In other words, for high particle concentrations, radiation cannot penetrate the system so that the heat transfer is dominated by conduction and convection. In addition, the rising of concentration induces higher viscosity [43], which hinders convection in the nanofluids. As a result, the heating process in the bulk of the fluid decreases.

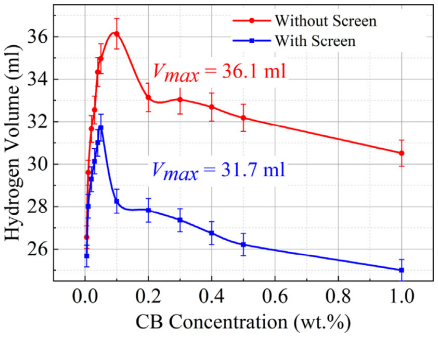

Fig. 9 – Hydrogen production vs. different CB concentration.

The blue line in Fig. 9 shows the results when the screen was used. The modified generated hydrogen volume with the increase of CB weight percent was 25.67 ml, 28.01 ml, 29.29 ml, 30.13 ml, 31 ml, 31.72 ml, 28.25 ml, 27.82 ml, 27.36 ml, 26.75 ml, 26.21 ml, 25 ml, respectively. This curve has the same trend as the red line, but the values are significantly lower. Moreover, it is worth noting that the maximum volume of hydrogen production occurred for concentration 0.05 wt %. In these experiments, only a small part of the nanofluids was illuminated by light. Under the same heat flux on the front face of a Hoffman voltameter, the radiation area was smaller than the experiments without the screen. As a result, the total energy that could be absorbed was also smaller. Although the radiation area was smaller here, the heat dissipation area was the same, i.e., the part of the Hoffman voltameter filled by the electrolyte. Thus, lower energy and nearly the same heat loss led to lower temperature increasing, and then less hydrogen production. When the temperature increased, the heat loss still increased so that a maximum total temperature occurred. This could be the potential reason that induces the maximum value for the concentration of 0.05%.

Fig. 10 (a) shows the modified hydrogen production rate for every 2 min for different CB concentrations. Five selected concentrations (0.02 wt %, 0.04 wt %, 0.05 wt %, 0.1 wt %, 0.2 wt %) are depicted in the figures. During the first 4~6 min, the hydrogen production rate was similar for all the studied concentrations. After 6 min, the rates still kept a rising tendency on average, but it was rather low except for a concentration of 0.1 wt %. During this time, all the rate curves show oscillations, and the amplitudes for the concentrations greater than 0.1% are higher than for the lowest concentrations. After 16 min, the hydrogen production rate showed a rising trend again. It also easily seen from Fig. 10 (a) that the average rates for different concentrations have a significant

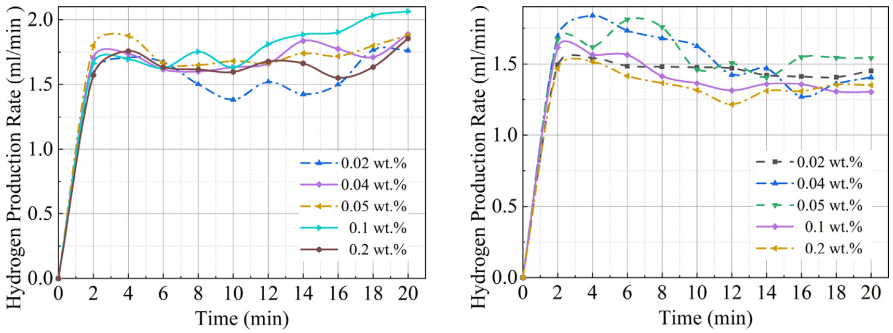

Fig. 10 – Hydrogen production rate variation vs. time for different CB concentrations: (a) no protective screen was used; (b) the voltameter was irradiatied by using a protective screen/collimator.

difference. The rates increased first and then decreased with the rising concentration, and the maximum showed a 0.1 wt %. A suitable concentration of nanofluids can increase the conductivity of the electrolyte, but too high concentrations of nanofluids might hinder the movement of electrons and decrease the hydrogen production rate. The hydrogen production rates during the whole processes of electrolysis can be treated as unstable oscillatory rising processes. Apart from the aforementioned effects of the heat transfer process and the variation of electrical conductivity, there are some possible explanations for this phenomenon.

On the one hand, the concentration of nanofluids increased as the electrolysis progressed because the water was electrolyzed. Similarly, the concentration of sodium sulfate solution also increased. Both have critical concentrations that led to some optimal hydrogen production, and a higher concentration of nanoparticles results in agglomerations and coat formations at the anodes, which has deteriorating effects on electrolysis [50]. Furthermore, the temperature kept increasing during the whole process, which could facilitate the electrolysis. This is discussed in the next section. Two different phenomena induced the oscillation in the curves. When the concentration was greater than 0.1 wt %, the nanofluids were more prone to be unstable and non-uniform and more disorder in the electrolyte induced greater oscillation amplitudes. From Figs. 4–6 temperature has a stronger effect on the electrolysis, which is reflected in the production of more hydrogen. Therefore, combining with the results in Fig. 10 (a), the whole trend should be increasing.

Fig. 10 (b) shows the results of the experiments with the collimator. The difference from the experiments without the screen is that the whole trend for these curves is falling. As stated before, the smaller energy source did not allow the system to reach the optimal temperature for the reaction, which means it is difficult to allow the positive to impact greater than the negative. Almost all the positive impacts are related to the temperature, including the reaction rate, electrical conductivity and some thermal properties of the electrolyte. They will change in a positive direction with the temperature rising. However, all the negative impacts are connected to the concentrations, like CB concentration, SS concentration, etc. Given that the essence of electrolyzing the SS solution was electrolyzing water, the concentrations can only increase. In other words, negative impacts will augment with time. In that case, negative impacts are much easier to show at lower temperatures than higher temperatures with the rising of concentrations. In this study, only the small radiation area could absorb heat, see Fig. 2 (b), and this part transfers the heat to the rest of the system. Furthermore, the two vertical pipes of the Hoffman voltameter had a larger surface area than the horizontal pipe within the radiation area, which means the high-temperature zone had a small dissipation area (the horizontal pipe) and the cold zone had a greater dissipation area (the two vertical pipes). This results in a large temperature gradient in the system, and the higher the temperature in the irradiated zone, the greater the gradient. On one hand, the temperature gradient could destabilize the nanofluid, and make nanoparticles easier to aggregate. The heat flow invokes convective currents in the system that could push the nanoparticles to move from the high temperature zone to the low-temperature zone. This increases the probability of contact and collision. More specifically, there were more particles near the electrodes than the area near the screen. In a colloidal system, charged ions adsorbed onto the surface of particles. As a result, the increasing number of nanoparticles in some areas made the charges available for the formation of an electrical double layer insufficient [49]. The electrostatic attraction becomes more than a repulsion force that destroys the stability of nanofluids. On the other hand, the temperature gradient could inhibit the electrolysis, and the larger the gradient, the stronger the inhibition. The mass flow caused by a temperature gradient, as well as electrophoresis, led charges to move to the electrodes (followed by the nanoparticles), which was inconsistent with electrolysis. Hence, this imbalance of potential in the electrolyte affected the progress of the water splitting reaction. Therefore, these two reasons may have caused the whole production rate to develop a falling trend.

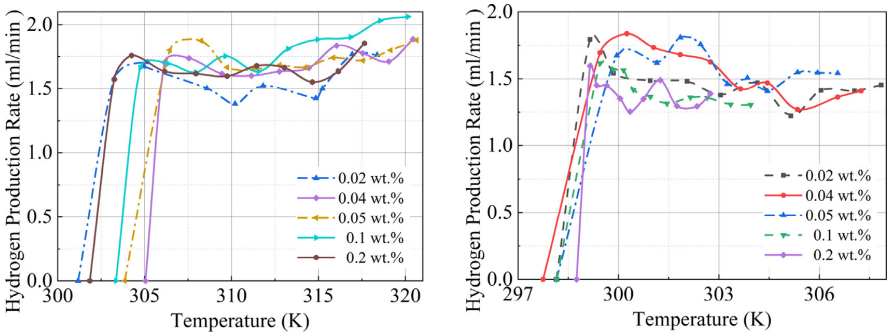

Fig. 11 – Hydrogen production rate for different CB concentrations vs. temperature: (a) no protective screen was used; (b) the voltameter was irradiatied by using a protective screen/collimator.

Effect of temperature

According to the discussion in Section Effect of CB concentration, the temperature plays an important role during the process. It was shown that the presence of CB nanoparticles increases the fluid temperature. In this section, however, we focus on how the temperature increase affects electrolysis and hydrogen production. Fig. 11 (a) shows the relationship between the modified hydrogen production rate and temperature without a screen. The graph makes it easier to conclude that the hydrogen production rate increased as the temperature increased. Also, the graphs in Fig. 11 (a) clearly show three stages: hydrogen production rate rapid rise stage, steady stage, slow rise stage. In the first stage, the hydrogen production rate increased very fast and reached the first extreme value (about 1.7 ml/min), while the temperature was below 305 K. When the temperature reached 305 K, the increase of hydrogen production rate seems to be paused until the temperature was greater than 315 K. In the third stage, the temperature increased again. However, the increase rate at this stage was less than the rate at the first stage. The maximum temperature occurred when the concentration was 0.1 wt %.

As we mentioned before, the higher CB concentration can increase the heat absorption ability of the electrolyte, and it can cause the temperature of the electrolyte to increase quickly when illuminated by light. Similarly, a higher temperature can increase the electrolytic velocity, thus causing an increase in the hydrogen production rate. However, a higher CB concentration does not mean a greater rate of hydrogen production. Compared with Figs. 10 (a) and 11 (a) also shows oscillations for rate curves with the increasing of temperature but does not show any linear trend as expected. This proves these two side effects exist and connect with temperature and CB concentration. There is a possible reason that can explain this phenomenon. Firstly, even though nanoparticles can increase the conductivity of the electrolyte, there are inhibitory effects that have negative impacts on electrolysis. For example, every single CB particle is charged due to the electrical double layer. With the increase of the temperature, mass flow and convection become stronger. Considering Brownian motion and electrophoresis, the movement of particles is highly random, which causes the uneven distribution and irregular movement of charges. On the other hand, the CB concentration increases as the reaction progresses. Thus, the electrical conductivity decreases when beyond the critical concentration. Moreover, in this study, SS functioned as a kind of salt that destabilized the nanofluid at higher temperature, which could also affect electrolysis. These negative effects together with positive effects (increasing electrical conductivity and reaction rate) caused the oscillations. Therefore, at the first stage, the electrolysis proceeded normally. When reaching the second stage, negative effect became prominent, so the rate increase paused. Nonetheless, at the third stage, since the temperature was high enough, the rate restarted and increased accordingly.

Fig. 11 (b) reveals how temperature affects the hydrogen production rate when using a screen. The whole curves can be divided into two parts as they have a similar trend as in Fig. 11 (a): a rapid rise stage and steady stage. At first, the rates increase faster and then decrease until 304 K. When the temperature is greater than 304 K, all the curves maintain dynamic stability. There are two differences compared with Fig. 11 (a): decreasing and no second increasing. The aforementioned statement could also be used to explain this. The temperature gradient strengthened the negative effects so that these two side effects could not maintain a balance at a relatively low temperature. Likewise, from Fig. 11 (b), the hydrogen production rates stayed within a certain range when the temperature reached 304 K and did not increase at a higher temperature. This phenomenon just proved that the temperature must reach a certain value to make positive effects stronger than negative effects. In these experiments, the critical temperature is 315 K. It should be emphasized that the larger heat loss and CB agglomeration could also affect the results.

That the temperature increases with an increasing of CB concentration, and then decreases, as shown in Fig. 11 (a), was

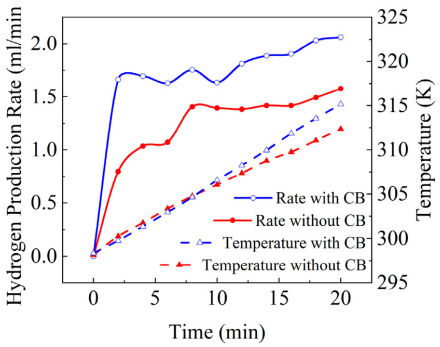

Fig. 12 – Comparison of production rate and temperature for electrolytes with and without CB.

also observed by other researchers. Ulset et al. [51] demonstrated that superheat of CB nanofluid steam was dependent on the CB concentration and reached a maximum value at 1 wt %. However, the maximum value occurred at 0.1 wt % and 0.001 wt % in our study. Because Ulset et al. heated the nanofluid until boiling, and the fluid did not reach the maximum temperature in their experiments, the temperature increasing rate may vary during the whole process that caused different results.

Comparison of CB effects

To have a more intuitive comparison of the effects of CB on a salt electrolyte, Fig. 12 shows the temperature and hydrogen production rate changes during the reaction for electrolytes with CB and without CB. The concentration of SS was 10 wt % for both electrolytes, and the concentration of CB was 0.1 wt %. During the first 8 min, there was no evident difference between the temperatures of the two electrolytes. When the reaction started, only CB on the surface of the electrolyte absorbed the heat, and CB in the inner part was unlikely to be radiated as the CB on the surface formed a "shield" to block the light. As a result, it was mainly thermal conduction in the electrolyte that induced the temperature to increase slowly. However, for electrolytes without CB, light could penetrate the solution due to its transparency, which means the temperature could increase fast. Therefore, the temperatures had the same increasing rate. However, during this period of time, the hydrogen production rates revealed high discrepancies. It is easier for a CB-based electrolyte to start the electrolysis at a higher reaction rate (1.66 ml/min) and maintain a slow growth rate due to the increased electrical conductivity of the electrolyte caused by the presence of CB. On the contrary, the hydrogen production rate for the SS solution starts at 0.79 ml/min, which is about half of the initial rate for a CB-based electrolyte, and then it increases fast. Compared with thermal properties, the electrical properties of CB have a greater impact on the process.

After 8 min, from Fig. 12, the impacts of thermal properties dominated the electrical properties. The temperature increases fast for CB-based electrolytes, and the hydrogen production rate also shows a visible rising trend. Similarly, the rate of hydrogen production and temperature for electrolytes without CB have an increasing trend, but they are significantly lower than electrolytes with CB. Heat conduction was strong during this time in the inner part of the electrolyte with CB, so the growth of temperature was faster. Afterwards, as mentioned before, the higher the temperature, the faster the tares. During the 20 min, the hydrogen production rates were 2.06 ml/min and 1.58 ml/min for electrolytes with CB and without CB, and the temperatures are 315.15 K and 312.35 K, respectively. Using CB makes the hydrogen production rate increase by 30.37%.

Electrolysis efficiency

In the previous sections, we found that CB does have positive effects on electrolysis. In this section, we evaluate the performance by estimating the efficiency of the process. For now, the objective of almost all the research for electrolysis is to increase electrolysis efficiency. Higher efficiency means less loss, and it can save energy.

There are numerous ways to evaluate the efficiency of an electrolyser. These include cell efficiency, energy efficiency, current efficiency, and thermal efficiency. Chakik et al. [52] summarized a model to calculate the electrolysis efficiency of water electrolysis:

$$\eta = \frac{V_{H_2}}{\frac{I \cdot V_m \cdot t}{2F}} \tag{10}$$

where η is the electrolysis efficiency, V_{H_2} is the volume of produced hydrogen, I is current, V_m is the molar volume (24.47 L/mol in 25 °C), t is reaction time and F is the Faraday constant (96 485 s A/mol).

In our study, the electrolysis efficiency can be calculated by:

$$\eta = \frac{E_{H_2}}{W_E} \tag{11}$$

$$E_{H_2} = n \cdot HHV \tag{12}$$

$$W_E = U \cdot I \cdot t, \tag{13}$$

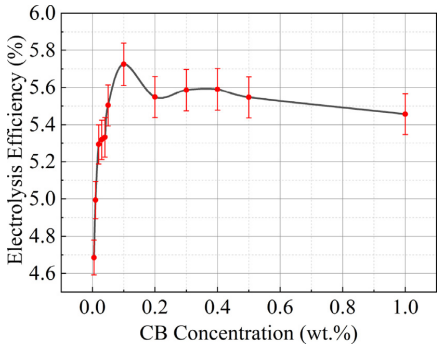

Fig. 13 – Electrolysis efficiency vs. CB concentration.

where E_{H_2} is the energy produced by electrolysis, i.e., energy stored in hydrogen, W_E is the energy consumed by electrolysis, i.e., electrical energy, n is the amount of substance, HHV is the higher heating value (=286 kJ/mol for hydrogen) and U is the voltage.

Fig. 13 shows the electrolysis efficiency for different CB concentrations. Similar to Fig. 9, one can clearly observe a rapid increase of efficiency with respect to concentration in cases when the concentration was low. For higher values of concentration, the efficiency decreases but with a lower rate. The maximum efficiency is 5.72% for the concentration 0.1 wt %, whereas the minimum efficiency is 4.69% for 0.005 wt%. This indicates that the efficiency increased by about 21.96%. These efficiencies are much lower than the industrial electrolysers as only simple electrodes and electrolytes were used, but the results are still meaningful. The reason is that the higher temperature induced a higher current and increased the consumption of electrical power. At first, temperature raises the ionic conductivity and enhances the current flow into the system. Therefore, the overall efficiency of the system in this work tends to increase with temperature. When increasing the concentration of CB, the temperature and the current density increase fast. As expressed by Ohm's law, the resistance in the system becomes more prominent when the current density increases. The efficiency of an electrolyser diminishes with increased temperature because at elevated temperatures the current density intensifies, resulting in higher activation and ohmic overpotentials. Another potential reason for the decrease is the coverage of the electrode surface by the NPs. The electrical double layer could catch the electrons that have a negative influence on the water electrolysis efficiency.

Concluding remarks

This study focused on the results of electrolyzing a carbon balance nanofluid-based electrolyte and analysed the effect of CB NF on the electrolysis. The results of the first part reveal that CB and light can increase the hydrogen production rate. The former increased the electrical conductivity of the electrolyte, and the latter increased the temperature of the electrolyte. The results of the second parts show that different CB concentrations have a different effect on the hydrogen production rate. The maximum hydrogen production rate occurred at the concentration of 0.1 wt %. When a screen was used to block the light, the maximum rate occurred at a concentration of 0.05 wt %. However, increasing the CB concentration leads to an increase in the hydrogen production rate up to the maximum value and then decreases for both situations. The results of the third part indicate that there may be a positive effect and negative effect of nanoparticles on the electrolysis as the average hydrogen production rates for every 2 min did not always increase or decrease. Thus, the whole electrolysis process can be treated as a “dynamic balance”.

For a future work, other types of fluids can be tested. An example is the use of different nanofluids, not necessarily CB. Also, biodegradable fluids that have recently gained popularity [36] should also be considered.

Declaration of competing interest

The authors declare that they have no known competing financial interests or personal relationships that could have appeared to influence the work reported in this paper.

Acknowledgments

Shihao Wei gratefully acknowledges financial support from China Scholarship Council. Boris Balakin thanks Russian Foundation for Basic Research (Project 20–58-53022).

REFERENCES

[1] Guido Collodi, Wheeler Foster. Hydrogen production via steam reforming with CO2 capture. Chem Eng Trans 2010;19:37–42.
[2] Lewis Larry N. Chemical catalysis by colloids and clusters. Chem Rev 1993;93(8):2693–730.
[3] Godula-Jopek Agata. “Hydrogen Production: by electrolysis”. en. 2015. p. 425. ZSCC: 0000074.
[4] Gandia Luis M, Arzamedi Gurutze, Diéguez Pedro M. Renewable hydrogen technologies: production, purification, storage, applications and safety. Newnes; 2013.
[5] Xu S, Zhao H, Li T, Liang J, Lu S, Chen G, Gao S, Asiri AM, Wu Q, Sun X. Iron-based phosphides as electrocatalysts for the hydrogen evolution reaction: recent advances and future prospects. J Mater Chem 2020;8(38):19729–45.
[6] Liu T, Liu D, Qu F, Wang D, Zhang L, Ge R, Hao S, Ma Y, Du G, Asiri AM, Chen L. Enhanced electrocatalysis for energy-efficient hydrogen production over CoP catalyst with nonelectroactive Zn as a promoter. Adv Energy Mater 2017;7(15):1700020.
[7] Zhang Y, Liu Y, Ma M, Ren X, Liu Z, Du G, Asiri AM, Sun X. A Mn-doped Ni_2 P nanosheet array: an efficient and durable hydrogen evolution reaction electrocatalyst in alkaline media. Chem Commun 2017;53(80):11048–51.
[8] Li X, Zhang R, Luo Y, Liu Q, Lu S, Chen G, Gao S, Chen S, Sun X. A cobalt–phosphorus nanoparticle decorated N-doped carbon nanosheet array for efficient and durable hydrogen evolution at alkaline pH. Sustain Energy Fuels 2020;4(8):3884–7.
[9] Gholamrezaei S, Ghiyasiyan-Arani M, Salavati-Niasari M, Moayedi H. Multidisciplinary methods (co-precipitation, ultrasonic, microwave, reflux and hydrothermal) for synthesis and characterization of $CaMn_3O_6$ nanostructures and its photocatalytic water splitting performance. Int J Hydrogen Energy 2019;44(48):26373–86.
[10] Ghanbari D, Salavati-Niasari M, Sabet M. Preparation of flower-like magnesium hydroxide nanostructure and its influence on the thermal stability of poly vinyl acetate and poly vinyl alcohol. Compos B Eng 2013;45(1):550–5.
[11] Salavati-Niasari M, Sobhani A, Davar F. Synthesis of star-shaped PbS nanocrystals using single-source precursor. J Alloys Compd 2010;507(1):77–83.
[12] Salavati-Niasari M, Davar F, Loghman-Estarki MR. Controllable synthesis of thioglycolic acid capped ZnS (Pn) 0.5 nanotubes via simple aqueous solution route at low temperatures and conversion to wurtzite ZnS nanorods via thermal decompose of precursor. J Alloys Compd 2010;494(1–2):199–204.

[13] Zinatloo-Ajabshir S, Morassaei MS, Salavati-Niasari M. Eco-friendly synthesis of $Nd_2Sn_2O_7$–based nanostructure materials using grape juice as green fuel as photocatalyst for the degradation of erythrosine. Compos B Eng 2019;167:643–53.
[14] Salavati-Niasari M. Zeolite-encapsulation copper (II) complexes with 14-membered hexaaza macrocycles: synthesis, characterization and catalytic activity. J Mol Catal Chem 2004;217(1–2):87–92.
[15] Salavati-Niasari M. Nanoscale microreactor-encapsulation 14-membered nickel (II) hexamethyl tetraaza: synthesis, characterization and catalytic activity. J Mol Catal Chem 2005;229(1–2):159–64.
[16] Razavi FS, Sobhani A, Amiri O, Ghiyasiyan-Arani M, Salavati-Niasari M. Green sol-gel auto-combustion synthesis, characterization and investigation of the electrochemical hydrogen storage properties of barium cobalt oxide nanocomposites with maltose. Int J Hydrogen Energy 2020 Jul 10;45(35):17662–70.
[17] Li Yanjiao, Zhou Jing'en, Tung Simon, Schneider Eric, Xi Shengqi. "A Review on Development of Nanofluid Preparation and Characterization". en. In: Powder Technology 196.2; Dec 2009. p. 89–101. ZSCC: NoCitationData [s1].
[18] Goudarzi K, Nejati F, Shojaeizadeh E, Asadi Yousef-abad SK. Experimental study on the effect of pH variation of nanofluids on the thermal efficiency of a solar collector with helical tube. Exp Therm Fluid Sci 2015;vol. 60:20–7.
[19] Maxwell JC. A treatise on electricity and magnetism, vol. 1. Clarendon Press; 1881.
[20] Choi Stephen US, Eastman Jeffrey A. Enhancing thermal conductivity of fluids with nanoparticles. Tech. rep. Argonne National Lab; 1995. IL (United States).
[21] Fendler Janos H. Colloid chemical approach to nanotechnology. Kor J Chem Eng 2001;18(1):1–13.
[22] Otanicar Todd P, Phelan Patrick E, Golden Jay S. Optical properties of liquids for direct absorption solar thermal energy systems. Sol Energy 2009;83(7):969–77.
[23] Otanicar Todd P, Phelan Patrick E, Ravi S Prasher, Gary Rosengarten, Taylor Robert A. Nanofluid-based direct absorption solar collector. J Renew Sustain Energy 2010;2(3). 033102.
[24] Prastiwi Yohanna. Unit operations of chemical engineering. 5th ed. Mc Cabe And Smith; 2008. English.
[25] Sani E, Mercatelli L, Barison S, Pagura C, Agresti F, Colla L, Sansoni P. Potential of carbon nanohorn-based suspensions for solar thermal collectors. Sol Energy Mater Sol Cell 2011;95(11):2994–3000.
[26] Han Dongxiao, Meng Zhaoguo, Wu Daxiong, Zhang Canying, Zhu Haitao. "Thermal Properties of Carbon Black Aqueous Nanofluids for Solar Absorption". en. Nanoscale Res Lett 2011;6(1):457. https://doi.org/10.1186/1556-276X-6-457. 1556-276X.
[27] Ganley Jason C. High temperature and pressure alkaline electrolysis. Int J Hydrogen Energy 2009;34(9):3604–11.
[28] Christopher MA. Brett and Ana Maria Oliveira Brett. Electrochemistry: principles, Methods, and Applications. en. Oxford Science Publications. Oxford; New York: Oxford University Press; 1993.
[29] Lobato J, Oviedo J, Cañizares P, Rodrigo MA, Millán M. Impact of carbonaceous particles concentration in a nanofluidic electrolyte for vanadium redox flow batteries. Carbon 2020;156:287–98.
[30] Bose P, Deb D, Bhattacharya S. Ionic liquid based nanofluid electrolytes with higher lithium salt concentration for high-efficiency, safer, lithium metal batteries. J Power Sources 2018;406:176–84.
[31] Yen PH, Wang JC. Power generation and electric charge density with temperature effect of alumina nanofluids using dimensional analysis. Energy Convers Manag 2019;186:546–55.
[32] Amin Asadi, Pourfattah Farzad, Miklós Szilágyi Imre, Afrand Masoud, Żyła Gaweł, Ahn Ho Seon, Wongwises Somchai, Nguyen Hoang Minh, Ahmad Arabkoohsar, Mahian Omid. "Effect of Sonication Characteristics on Stability, Thermophysical Properties, and Heat Transfer of Nanofluids: a Comprehensive Review". en. In: Ultrasonics sonochemistry 58; Nov 2019. p. 104701. ZSCC: NoCitationData[s1].
[33] Zhang C, Weldetsadik NT, Hayat Z, Fu T, Zhu C, Jiang S, Ma Y. The effect of liquid viscosity on bubble formation dynamics in a flow-focusing device. Int J Multiphas Flow 2019;117:206–11.
[34] Hwang Y, Lee JK, Lee JK, Jeong YM, Cheong SI, Ahn YC, Kim SH. Production and dispersion stability of nanoparticles in nanofluids. Powder Technol 2008;186(2):145–53.
[35] Ulset ET, Kosinski P, Balakin BV. Solar steam in an aqueous carbon black nanofluid. Appl Therm Eng 2018;137:62–5.
[36] Kosinska A, Balakin BV, Kosinski P. Use of biodegradable colloids and carbon black nanofluids for solar energy applications. AIP Adv 2021;11:055214.
[37] Romanelli MF, Moraes MCF, Villavicencio ALCH, Borrely SI. Evaluation of toxicity reduction of sodium dodecyl sulfate submitted to electron beam radiation. Radiat Phys Chem 2004;71(1–2):411–3.
[38] Lechuga M, Fernandez-Serrano M, Ríos F, Fernández-Arteaga A, Jiménez-Robles R. Environmental impact assessment of nanofluids containing mixtures of surfactants and silica nanoparticles. 2021.
[39] Godula-Jopek A. Hydrogen production: by electrolysis. John Wiley & Sons; 2015.
[40] Khani M, Habibzadeh S, Moraveji MK, Ebrahim HA, Alizadeh J. Novel α-alumina@ CuO-Fe_2O_3nanofluid for potential application in PEM fuel cell cooling systems: towards neutralizing the increase of electrical conductivity. Thermochim Acta 2021;695:178818.
[41] Shoghl SN, Jamali J, Moraveji MK. Electrical conductivity, viscosity, and density of different nanofluids: an experimental study. Exp Therm Fluid Sci 2016;74:339–46.
[42] Mashali F, Languri E, Mirshekari G, Davidson J, Kerns D. Nanodiamond nanofluid microstructural and thermo-electrical characterization. Int Commun Heat Mass Tran 2019;101:82–8.
[43] Ijam A, Saidur R, Ganesan P, Golsheikh AM. Stability, thermo-physical properties, and electrical conductivity of graphene oxide-deionized water/ethylene glycol based nanofluid. Int J Heat Mass Tran 2015;87:92–103.
[44] Maxwell JC. A treatise on electricity and magnetism, vol. 1. Oxford: Clarendon Press; 1873.
[45] Shen LP, Wang H, Dong M, Ma ZC, Wang HB. Solvothermal synthesis and electrical conductivity model for the zinc oxide-insulated oil nanofluid. Phys Lett 2012;376(10–11):1053–7.
[46] Lavasani AM, Vakili M. Experimental study of photothermal specifications and stability of graphene oxide nanoplatelets nanofluid as working fluid for low-temperature Direct Absorption Solar Collectors (DASCs). Sol Energy Mater Sol Cell 2017;164:32–9.
[47] Heyhat MM, Irannezhad A. Experimental investigation on the competition between enhancement of electrical and thermal conductivities in water-based nanofluids. J Mol Liq 2018;268:169–75.
[48] Mashali F, Languri E, Mirshekari G, Davidson J, Kerns D. Nanodiamond nanofluid microstructural and thermo-electrical characterization. Int Commun Heat Mass Tran 2019;101:82–8.

[49] Zawrah MF, Khattab RM, Girgis LG, El Daidamony H, Aziz REA. Stability and electrical conductivity of water-base Al2O3 nanofluids for different applications. HBRC journal 2016;12(3):227–34.
[50] Choi D, Lee KY. Experimental study on water electrolysis using cellulose nanofluid. Fluid 2020;5(4):166.
[51] Ulset ET, Kosinski P, Zabednova Y, Zhdaneev OV, Struchalin PG, Balakin BV. Photothermal boiling in aqueous nanofluids. Nano Energy 2018;50:339–46.
[52] Chakik FE, Kaddami M, Mikou M. Effect of operating parameters on hydrogen production by electrolysis of water. Int J Hydrogen Energy 2017;42(40):25550–7.

This paper was accepted for publication in the Experimental Heat Transfer

Experimental and Numerical Investigation of Direct Absorption Solar Collectors (DASCs) Based on Carbon Black Nanofluids

Shihao Wei[a], Lisbeth Espedal[a], Boris V. Balakin[b], Pawel Kosinski[a]*

[a]*Department of Physics and Technology, University of Bergen, Bergen, Norway;* [b]*Department of Mechanical and Marine Engineering, Western Norway University of Applied Sciences, Bergen, Norway*

*Corresponding author: Pawel Kosinski

Email: pawel.kosinski@uib.no

Direct Absorption Solar Collectors (DASCs) typically achieve high efficiency due to the volumetric heat absorption process facilitated by the working fluids. In this study, carbon black (CB) nanofluids were utilized as the working fluid to experimentally and numerically investigate the thermal performance of a rectangular DASC. The findings suggest that the nanoparticles have the potential to enhance the efficiency of the DASC.

Department of Physics and Technology, University of Bergen, Bergen, Norway

This paper was accepted for publication in the Experimental Heat Transfer

Experimental and Numerical Investigation of Direct Absorption Solar Collectors (DASCs) Based on Carbon Black Nanofluids

Direct absorption solar collectors (DASCs) are known for their high efficiency, which is achieved through the volumetric heat absorption process provided by the working fluids In this study, carbon black (CB) nanofluids were used as these working fluids to study the thermal performance of a rectangular DASC. The experiments were conducted using water and nanofluids with 0.05 wt.% nanoparticle concentration, at different flow rates and tilt angles, under a concentrated simulated solar power source. Our results show that the efficiency of the DASC increased as the flow rate increased. The DASC was more efficient when the receiving surface was facing downwards (tilt angle of 0°), and the efficiency was 35% higher than when the receiving surface was facing upwards (tilt angle of 180°). A computational fluid dynamics (CFD) model, which was validated against our experimental results, analyzed the DASC performance under different CB concentrations. According to the simulations, the highest efficiency occurred at a concentration of 0.05 wt.%. The study also highlighted the distribution of temperature and velocity of the nanofluids, as well as the volume fraction of carbon black during the flow process.

Keywords: direct absorption solar collector; carbon black; nanofluids; CFD; extinction coefficient

1 Introduction

With the rapid increase in energy consumption, the need for renewable and clean energy has become urgent [1]. Solar energy can be considered the best target. Furthermore, equipment that can efficiently capture and utilize solar energy is also in substantial demand [2]. Nowadays, solar energy utilization focuses mainly on converting solar energy into other energy types that can be used directly, such as electricity, heat and fuel [3]. Solar collectors are a type of equipment that can absorb incident solar radiation and convert solar energy into thermal energy [4].

The efficiency of solar collectors relies mainly on the thermal properties of the working fluids inside them. Recently, attempts have been made to exploit nanofluids as working fluids in solar collectors and heat exchange devices [5-7]. Nanofluids are colloidal suspensions of nanometer-sized particles [8] with enhanced thermal properties (relative to the base fluid). Fekadu et al. [9] reported a heat transfer coefficient enhancement of 4.712% and 5.94% for carbon soot nanofluids at a concentration of 0.5% and 0.75%, respectively. They are therefore considered to be promising working fluids

[10]. When used in direct absorption solar collectors (DASCs), nanofluids offer improved optical absorption of solar heat.

Many researchers have investigated the performance of nanofluids in different solar collectors. Bioucas [11] conducted an experimental study of thermal performance in a flat plate solar collector (FPSC) with different concentrations of nanographene. The maximum efficiency of FPSC was 60.6% when the nanofluid concentration was 0.1 wt.%, compared to 54.7% for the base fluid. This corresponded to a 5.9% enhancement. Sarsam et al. [12] numerically evaluated the properties of multi-wall carbon nanotubes (MWCNT) in an FPSC by the performance index and reported a positive impact on pressure drop. Mwesigye et al. [13] numerically investigated the thermal properties of a parabolic trough solar collector (PTSC) exploiting SWCNT (single-wall carbon nanotubes)-Therminol VP-1-based nanofluids. The results showed a two-fold enhancement of heat transfer performance when using the nanofluid, and the thermal efficiency increased by about 4.4% as the nanoparticle volume fraction rose from 0 to 2.5%. Natividade et al. [14] evaluated the thermal efficiency of an evacuated tube solar collector (ETSC) at low volume fractions of multi-layer graphene (MLG) nanofluids. The thermal efficiency increased by 31% and 76%, corresponding to the concentrations of 0.00045 vol. % and 0.00068 vol. %, compared to the base fluid. Xu et al. [15] explored the performance of a direct absorption solar collector at low temperatures with reduced graphene oxide (RGO)/water-ethylene glycol (EG) nanofluids as working fluids. The nanofluid showed better anti-freeze properties that allowed the DASC to be used in low temperatures, and the efficiency increased by around 70% compared to the base fluid.

Compared to other solar collectors, DASC utilizes fluid as the absorbing medium for incident sunlight, instead of a solid absorber. It can provide greater efficiency than the collectors with surface absorption [16]. Furthermore, various parameters can affect the efficiency of DASC. Bhalla et al. [17] numerically studied the effect of geometrical parameters on the performance of DASC. With an increase in collector length, an apparent efficiency reduction was seen, due to greater heat loss. Sharaf et al. [18] used a suspension of graphite nanoparticles in two different base fluids, including water and Therminol VP-1, to investigate the effect of nanofluid film thickness. Greater efficiency was observed when the depth of the collector was 10 mm, compared to a depth of 0.5 mm. It was also found that the base fluid had an impact on the performance of the collector. When the volume fraction of nanofluids was lower than 0.005%, the water-based nanofluids offered stronger radiation absorption. The base fluid is therefore still an essential factor that affects the thermal efficiency of DASC.

According to the experimental study conducted by Otanicar et al. [19], the solar-weighted absorption efficiencies for water, ethylene glycol (EG), propylene glycol (PG), and Therminol VP-1 were 13.6%, 9.30%, 9.1%, and 2.1%, respectively, measured by a standard scanning wavelength spectrophotometer. Struchalin et al. [20] investigated the thermal performance of carbon-based nanofluids in a tubular DASC experimentally and numerically. The results showed that the efficiency of DASC was at most 37.9% greater than the surface absorption collector. They also discovered that when the flow rate was above 6.0 l/min, the particle deposition was less than 5.0%, from simulation results. The above review indicates that nanofluids can enhance the thermal performance of solar collectors, and most of the research mainly evaluated the impact of the nanofluids' concentration. However, not all the researchers reported positive results for DASCs. Li et al. [21] investigated the thermal performance of a vacuum-packaged volumetric receiver and of a vacuum-packaged black chrome-coated receiver using MWCNT nanofluids at 80°C and 200°C, respectively. The results showed efficiencies of 54% and 26% for the volumetric receiver, which is lower than the surface receiver, with

efficiencies of 68% and 47%, respectively. They explained this as optical reflective losses from the outer glass surface. After mathematical calculation, the authors found that only 90% of the effective radiation was transmitted to the glass and absorbed by the nanofluids. Therefore, the anti-reflective coating might be a good option to improve the optical efficiency of the volumetric receiver.

This important discovery was adopted by Struchalin et al. [20] to improve their simulation model that can effectively prevent overpredicting. Nonetheless, it should be noted that the thermal efficiency of solar collectors depends on many factors, such as geometry, base fluid and exposure time. It can even be affected by the surfactant used to stabilize the nanofluids [22]. Furthermore, nanoparticle material plays a vital role because various nanoparticles have different optical properties. Carbon-based nanomaterials like graphene and nanotubes in particular are excellent anti-corrosion additives for spectrally selective solar absorbers that are an ideal material for the utilization of heat transfer applications [2]. Carbon black (CB) is also a carbon-based nanomaterial with good photothermal properties. In our previous research, we investigated the photothermal properties of CB, such as photothermal conversion [23] and photothermal boiling [24]. Likewise, we experimentally and numerically studied the thermal efficiency of a DASC with Fe_2O_3-based nanofluids [25]. However, to use CB-based nanofluids in a DASC, more knowledge about their optical properties and characteristics needs to be acquired, since little information can be obtained from the literature. Moreover, none of the aforementioned studies were focused on concentrated solar light, so this field needs to be investigated. The light intensity is typically around 1000 W/m^2 on a sunny day, but concentrated solar light intensity can exceed 2000 W/m^2. Therefore, making proper use of concentrated solar light can improve the efficiency of solar energy utilization.

In this work, a series of indoor experiments were conducted to investigate the performance of the DASC based on carbon black (CB) nanofluids under a simulated light source corresponding to concentrated solar light in terms of power. A rectangular DASC with baffles inside the receiver was designed. A halogen lamp was used to simulate the sun and concentrated solar radiation. The temperature histories for different flow rates and tilt angles using both nanofluids and water as base fluids were obtained.

In this study, we developed a volumetric heat transfer model based on Beer-Lambert's law to analyze the flow pattern and distribution of CB nanoparticles in DASCs. The key parameter of our model was the extinction coefficient of CB nanofluids, which we determined by measuring the reduction in heat flux when light passed through the nanofluids. The simulation results showed the behavior and deposition of the nanofluids, and we compared the efficiency of our system with experimental results and some typical commercial models.

Although traditional DASCs used circular cross-section pipes, rectangular channels were commonly used in engineering despite their tendency for uneven heat distribution and nanoparticle deposition. Our study focused on these two issues to improve thermal efficiency, and we combined experimental and simulation methods to investigate the performance of rectangular DASCs. To the best of our knowledge, this aspect has not been adequately addressed in recent research.

Our findings have important implications for the design and use of commercial DASCs, providing valuable insights into how to optimize their performance."

2. Experiments

2.1 Preparation of nanofluids and stability analysis

A typical two-step method was used to prepare stable CB-based nanofluids. We chose carbon black because its nanofluids are easier to stabilize and have photothermal properties that are less susceptible to environmental factors like temperature, pressure, humidity, and so on. First, CB nanoparticles and SDS were added to distilled water in a beaker. 1.0 wt.% SDS constituted the surfactant that was necessary to stabilize the nanofluids [23]. Secondly, a ceramic magnetic stirrer plate with a maximum stirrer speed of 2000 rpm and a magnetic stirrer bar was used to stir the mixed sample for at least 15 minutes, to acquire a more uniform mixture. Finally, the beaker was put into the tank of an ultrasonic cleaner, so that the liquid in the tank covered the nanofluid. The sample was sonicated for 60 minutes. The cleaner had a frequency of 40 kHz and a maximum power of 335 W, with a maximum capacity equivalent to 6 L. The objective of the process was to break the agglomerates into primary particles. This method has been shown to be effective in numerous scientific papers [21,23,24].

The stability of the prepared nanofluids was evaluated by examining the particle size distribution. To investigate the particle size distribution, we employed the static light scattering (SLS) method, which measures the time-averaged intensity of incident light and determines the particle size distribution over a short period of time. Fig. 1 (a) shows the particle size distribution for the nanofluid after sonication and after 24 hours, as recorded by Malvern Mastersizer 2000. After the sonication, the particle size distribution was between 480 nm and 10000 nm, and the average size was around 750 nm. After 24 hours, the particle size range shifted to smaller sizes, apparently due to the deposition of the particles. The particle size range was between 35 nm and 400 nm, and the average size was around 52.4 nm. The maximum particle size number frequency occurred between 50 nm and 60 nm, which corresponds to the CB primary particle size of 51.1±17.0 nm. We also performed a similar measurement of the sample after seven days, but we did not observe any further change in the particle size distribution.

Fig. 1 shows sedimentation at the bottom of the container, with (b) depicting sedimentation from a sample after preparation and (c) showing another sample from the reservoir tank after the DASC experimental test. Comparing the two figures, the second sample exhibited a higher level of sedimentation due to damage to the bonding between the surfactant and nanoparticles from repeated heating and circulation during testing, leading to agglomeration and sedimentation. However, the small amount of sediment after seven days indicates the partial long-term stability of the nanofluids. This indicated satisfactory dispersion stability of the CB nanofluids.

2.2 Experimental setup

The DASC used in this study comprised three main elements: a glass surface, an inner plate structure with three baffles, and an external aluminum box with hose connectors, as shown in Fig. 2. An Osram 400 W/230 V R7S halogen lamp was used to simulate the solar light. The simulated light has non-uniform intensity distribution at the DASC surface. We therefore used the infrared radiometer from Linshang Technology, with an accuracy of ±0.10%, to measure the irradiance intensity. Fig. 3 shows the intensity distribution on the DASC at a distance of 21 cm from the halogen lamp frame. Using the intensity distribution, we calculated the average intensity to be 1,103 W/m^2, which was

slightly higher than the standard solar intensity.

The entire experimental system is depicted in Fig. 4. Four Pt100 sensors monitored the inlet and outlet temperatures of the DASC, the ambient temperature and the bulk fluid temperature in the reservoir tank, respectively. The data logger provided a given resolution of 0.001°C and accuracy of 0.015°C. The working fluid was circulated from a 12-l reservoir tank made of thermoplastic material (PMMA) through a 20-m plastic tube. The 12/10-mm tube was made of polytetrafluoroethylene (PTFE), a synthetic fluoropolymer that is a hydrophobic material with a very low friction coefficient. The turbine flow meter was used to control the volumetric flow rate through the system. The flow rate could be adjusted by a flow-control valve placed after the pump. The turbine flow meter used in this work had a given accuracy of 10%. The entire system was insulated thermally to reduce heat loss. The commercial insulation Armaex class 0 SK, with thermal conductivity of K_i = 0.003 W/(m·K), was used in the DASC. The tubes were thermally insulated with 13 mm of polyethylene foam.

2.3 Experimental procedure

As previously discussed, the fluid (water or nanofluid) was circulated continuously through the system prior to the experiments for two main reasons. This took place primarily to heat the system to a point near thermal equilibrium with its surroundings, and secondarily to avoid the presence of air bubbles in the system. The lamp was turned on immediately after the temperature logging started. During the experiments, all temperatures were sampled every 60 seconds until the DASC inlet and outlet temperatures achieved a steady-state condition. After stabilization, the recording was continued for roughly 100 samples, as this resulted in adequate statistics for each experiment. The four working fluid flow rates chosen for this experimental study were 1 l/min, 2 l/min, 3 l/min and 4 l/min, respectively. For nanofluids, the concentration was 0.05 wt.%. This concentration of CB nanoparticles has been demonstrated to be optimal in many other scientific papers [21, 24, 26-28]. In addition, a surface absorption experiment was conducted at the flow rates of 0.48 l/min, 1.15 l/min, 1.66 l/min and 2.33 l/min, with water as the working fluid. For this, the glass surface of the collector was covered by black tape. Furthermore, we adjusted the inclination of the DASC by 0°, 15°, 45° and 180°. The inclination angle of 0° referred to the case where the glass surface was oriented along gravity.

The main source of experimental error in this study was the agglomeration of CB nanoparticles. Agglomerates can affect the penetration of light and heat transfer, and even a stable nanofluid cannot completely avoid their formation. During the experiments, the nanofluids were exposed to multiple cycles of heating and circulation, which increased the chance of nanoparticle collision and resulted in agglomeration."

3 CFD model

3.1 Geometry and mesh

For CFD simulations, the computational domain had a rectangular shape with three baffles. The length of the domain was 0.39 m, the width was 0.23 m, and the depth was 0.02 m. The length of the baffles was 0.15 m, and their width was 0.02 m. All the dimensions corresponded to the experimental setup, as shown in Figs. 5-6. The fluid entered the domain via a small pipe located in the lower left-hand corner in Fig. 5, and the inlet boundary condition was set there. The pressure outlet boundary was located symmetrically on the right-hand side. Both inlet and outlet were connected to the DASC.

The surface on the opposite side was the receiving surface (glass surface). This surface was irradiated by light and was also subject to heat loss. A trimmed mesh was used when generating the computational cells in the CFD software. The basic size was 0.001 m and the minimum surface size was 0.0001 m, the number of prism layers was 5, and the prism layer total thickness was set as 1/3 with respect to the base size.

3.2 Governing equations

We consider an unsteady incompressible flow, described by the Navier-Stokes equations. The continuity equation reads [27]:

$$\frac{D(\alpha_i \rho_i)}{Dt} = 0, \tag{1}$$

where $\frac{D}{Dt}$ is the substantial derivative, α_i is the volume fraction, and ρ_i is density. The subscript i denotes the phases where $i = p$ for the nanoparticle and $i = f$ for the base fluid, $\alpha_f + \alpha_p = 1$.

The momentum equation is given by [28]:

$$\frac{D(\alpha_i \rho_i \boldsymbol{v}_i)}{Dt} = \alpha_i \nabla p + \alpha_i \boldsymbol{\tau_i} + \alpha_i \rho_i \boldsymbol{g} + \boldsymbol{F}_{D,ij}, \tag{2}$$

where $\boldsymbol{v}_i$ is the velocity vector, p is the pressure and $\boldsymbol{\tau_i}$ is the viscous stress tensor, respectively, $\boldsymbol{g}$ is the acceleration due to gravity and $\boldsymbol{F}_{D,ij}$ is the drag force. Strictly, the motion of nanoparticles should also be affected by Brownian force and thermophoretic force. The Brownian force and thermophoretic force were around at least seven orders and two orders smaller than the drag force, respectively. According to Lutro [29], thermophoretic force has less impact on the nanoparticle motion. Therefore, we assume the Brownian force and thermophoretic force to be negligible. The viscous stress tensor for the particulate phase is computed by the viscosity of the base fluid. This is a viable assumption for low concentrations of carbon-based nanofluids, as confirmed by Struchalin et al. [20].

The drag force was computed as follows [30]:

$$\boldsymbol{F}_{D,ij} = \frac{\pi d^2}{8} N_p \rho_f C_D \left|\boldsymbol{v}_i - \boldsymbol{v}_j\right| (\boldsymbol{v}_i - \boldsymbol{v}_j), \tag{3}$$

where N_p is the number density for the nanoparticles, d is the diameter of the carbon black nanoparticles and C_D is the drag coefficient computed using the standard expression by Schiller- Naumann [28].

The energy equation is given by [31]:

$$\begin{aligned} \frac{D(\alpha_i \rho_i (e_i + 0.5|\boldsymbol{v_i}|^2))}{Dt} \mathrm{s} \\ = -\alpha_i \nabla \cdot (P \cdot \boldsymbol{v_i}) + \alpha_i \nabla \cdot \nabla (K_i T_i) + q_{ij} + \alpha_i q_{v,i} + \alpha_i \rho_i \boldsymbol{v_i} \cdot \boldsymbol{g} \\ + \alpha_i \nabla \cdot (\boldsymbol{\tau_i} \cdot \boldsymbol{v_i}), \end{aligned} \tag{4}$$

where $\boldsymbol{e}_i = C_{p,i} T_i$ is the phase-specific enthalpy, K_i is the thermal conductivity and q_{ij} is the inter-phase heat transfer term. Assuming that the convective heat transfer is established between the phases, the inter-phase heat transfer term is computed according to the Ranz-Marshall expression [28]. Furthermore, q_v is the volumetric heat generation due to the absorption of light. We simplified the thermal re-radiation behavior by assuming that it only occurred at the glass surface of the collector. Likewise, the heat loss only occurred at the glass surface by convection and radiation. Also, we neglected emission and scattering terms for the light in the fluid. The incident heat flux was dissipated as a local heat release. Thus, the volumetric heat generation can be treated as the energy change in the z direction:

$$q_v = -\frac{dI(z)}{dz}, \tag{5}$$

where z is the length of the light path in the z direction, $I(z)$ is the radiative intensity from the glass surface of the incident light, and when z = 0, $I(0)$ represents the intensity of the incident radiation at the glass surface. $I(z)$ can be determined by Beer-Lambert's law [32]:

$$I(z) = I(0)e^{-k_{nf}z}, \tag{6}$$

where k is the extinction coefficient [33], and subscript *nf* represents the nanofluid. It is the most important parameter of nanofluids.

Following Struchalin et al. [20], the average extinction coefficient of nanofluid at different concentrations can be fit as:

$$k_{nf} = k_f + \alpha_p \mathcal{A}\left(1 + \frac{d^2}{\mathcal{B}}\right), \tag{7}$$

where $\mathcal{A}$ and $\mathcal{B}$ are the fitting constants. Integrating Eq. (6) and substituting them into Eq. (5), the volumetric heat generation term reads:

$$q_{v,i} = I(0)k_i e^{-k_{nf}z}, \tag{8}$$

3.3 Efficiency

The efficiency of a solar thermal collector is the ratio of collected thermal energy to the total incident energy:

$$\eta = \frac{C_{nf}\dot{m}(T_{out} - T_{in})}{I(0)S}, \tag{9}$$

where η is the efficiency, C_{nf} is the specific heat of nanofluids, $\dot{m}$ is the mass flow rate of the fluid in the collector, T_{out} and T_{in} are the temperatures of the nanofluid at the outlet and inlet, respectively, $I(0)$ is the solar irradiance and S is the solar collector surface area. The specific heat capacity of nanofluids should consider the concentration of the nanoparticles, and it can be calculated by [34]:

$$C_{nf} = \frac{C_p\alpha_p\rho_p + C_f\alpha_f\rho_f}{\alpha_p\rho_p + \alpha_f\rho_f}. \tag{10}$$

3.4 Boundary conditions and numerical scheme

The working fluid was a combination of distilled water and CB nanoparticles. Table 1 shows the physical properties of the CB used in this study. These properties, together with the other properties that corresponded to the graphene in the database of the commercial CFD software STAR-CCM, were used to define the nanoparticle in the simulation. IAPWS-IF97 formulation [35] was used to define the thermal properties of the distilled water.

All the surfaces were set as adiabatic, apart from the inlet, the outlet and the glass surface. The environmental temperature and the inlet temperature were set as 300 K and 310.5 K, which correspond to the experimental record. Therefore, the convective heat loss and radiant heat loss at the glass surface can be calculated as in [36]:

$$q_{loss} = h\left(T_{suf} - T_{amb}\right) - \varepsilon\sigma\left({T_{suf}}^4 - {T_{amb}}^4\right), \tag{11}$$

where q_{loss} is the thermal loss, T is the temperature, subscript *suf* and *amb* represent the glass surface and ambient conditions, ε is the emissivity of the receiver (for glass ε = 0.85), σ is the Stefan–Boltzmann constant, and h is the natural convective heat loss coefficient determined by Raleigh number [37]:

$$h = \begin{cases} \left(\frac{K_{nf}}{L}\right) 0.54\, Ra^{\frac{1}{4}}, & Ra \le 10^7 \\ \left(\frac{K_{nf}}{L}\right) 0.15\, Ra^{\frac{1}{3}}, & Ra > 10^7 \end{cases} \quad (12)$$

In the above, K_{nf} is the thermal conductivity of the nanofluid, L is the length of the DASC, and Ra is the Raleigh number that can be calculated by [38]:

$$Ra = \frac{C_a \left|\frac{\partial \rho_a}{\partial T}\right| \rho_a g \left|T_{suf} - T_{amb}\right| L^3}{K_a \mu_a}, \quad (13)$$

where C_a is the specific heat of air, ρ_a is the density of air, K_a is the thermal conductivity of air, and μ_a is the dynamic viscosity of air.

All the walls were non-slip walls. The ambient temperature was set as 27 °C according to the lab environment. The different flow rates of 1 l/min, 2 l/min, 3 l/min and 4 l/min, and the different CB concentrations of 0.01 wt.%, 0.05 wt.%, 0.1 wt.%, 0.5 wt.% and 1 wt.%, were chosen for the numerical study.

Equations (1) - (5) were solved using STAR-CCM+ 15.02.007. The numerical solution was obtained using an implicit SIMPLE method. The following relaxation coefficients were applied: 0.3 for pressure, 0.7 for velocity, 0.5 for phase volume fraction, 0.9 for the enthalpy and 0.8 for the turbulence model. The governing equations were discretized temporally with the second-order Euler technique marching at 1.0 ms. The upwind scheme was applied for spatial discretization [28].

4 Results and discussion

4.1 Extinction coefficient

The radiation spectrum of the halogen lamp used in the experiments was measured by Ulset [39]. The maximum intensity of the light from the halogen lamp occurred between the wavelengths of 750-950 nm. In our research, the intensity at different optical path lengths was tested for the CB concentrations of 0.005 wt. %, 0.01 wt. %, 0.05 wt. % and 0.1 wt. %, as shown in Fig. 7. The intensity at the optical length of 0 mm represented the intensity of incident light at the nanofluid surface. According to Eq. (6), the extinction coefficients for different concentrations were calculated, and the results are shown in Fig. 8. As follows from the figure, the relationship between the extinction coefficient and the concentration could be roughly approximated by a linear function. This corresponds to Eq. (7), where the second term in the brackets is in practice negligible, as the particle diameter is very low. A similar result was obtained by Choi et al. [40], who tested the extinction coefficient for different concentrations of carbon nanotube-based nanofluids under the radiation wavelength of 632.8 nm. The results show that when the volume fraction of the carbon nanotube is less than 0.05%, the extinction coefficient increases linearly with the volume fraction, as illustrated by the black line in Fig. 8. However, when the volume fraction is greater than 0.05%, the increase is less rapid.

Furthermore, if we compare the red and black curves, we see that the extinction coefficient for carbon nanotubes is less than for carbon black. It must be noted that this result is not only affected by the optical properties of nanoparticles, but also by the wavelengths of light sources. This is concluded by Ahmad et al. [41], who investigated the extinction coefficient change on carbon-based nanofluids by varying types of base fluid, and found that when the wavelength increased, the extinction coefficients of all the nanofluids increased. Therefore, the extinction coefficients of the base fluid and nanofluid obtained can be used to complete the volumetric heat transfer model shown in Eq. (8).

4.2 Experimental results

4.2.1 Effect of flow rate

The average temperature change of the working fluids after flowing through the DASC (T_{out} - T_{in}) against time is plotted in Fig. 9. When the working fluid is water, the DASC becomes a surface collector, due to the black tape. The solid lines represent the nanofluid, and the dash-dot lines indicate the water. It can be seen that the working fluid temperatures have a clear tendency to rise under the irradiance of concentrated light. With the flow rate increase, the temperature augmentation declines. However, it is easier for nanofluids to reach a stable temperature state. When the system entered into the thermally stable state, we kept recording the temperature for 280 minutes and calculated the average temperature as the final temperature, to evaluate the efficiency. The results are shown in Fig. 10. Comparing the average temperature increase, the red line and the green line, the nanofluids show a higher temperature increase at the same flow rate. Hence, the thermal efficiency of the DASC also exceeds the surface collector, and is around 10% at 2 l/min. Following the increase in the flow rate, the total thermal efficiency of nanofluids has an increasing tendency, while for water the opposite applies. In the case of the surface collector, the heat is absorbed by the surface, and transferred by conduction within the water. For the DASC on the other hand, nanoparticles can absorb the irradiance directly, so the heat is transferred by radiation and convection. Therefore, the temperature rises faster and higher for nanofluids. On increasing the flow rate, the residence time for the working fluid inside the collector decreases, and this causes less heat to be absorbed by the working fluid. As a result, the higher the flow rate, the lower the temperature rise. Nevertheless, less residence time also means less heat loss, which leads to higher thermal efficiency for a DASC. However, for the surface collector, the heat is mainly lost from the surface, which has less impact on the residence time of the working fluid. The efficiency of the surface collector therefore decreases with the increase in flow rate. This corresponds to the behavior observed by both Eggers et al. [42] and Gupta et al. [43], who also tested the influence of the flow rate on a DASC. Increasing the flow rate in a DASC system generally leads to greater efficiency, since it reduces the heat loss from the system to the surroundings. However, the dependency is somewhat mitigated, due to the volumetric absorption. For a volumetric absorber, the heat is released within the fluid volume. Eggers et al. [42] explained that most of the incident radiation absorbed by the fluid volume results in a temperature increase close to the walls, where the average flow rate is lower than at the center of the collector. This results in a temperature rise close to the walls. Our results show agreement with other research that was summarized in the introduction [15, 18, 19].

4.2.2 Effect of tilt angle

In this section, we examine how the inclination of the DASC affects efficiency, and the results are presented in Fig.11. When we incline the DASC, the efficiency change with flow rate tendency shows agreement with the results of the 0° tilt angle. The maximum efficiency occurs at the tilt angle of 0°, while the efficiency does not decline with the increase in the tilt angle at all ranges. Therefore, the lowest efficiency might exist at a tilt angle. To verify the hypothesis, we predict the change tendency between efficiency and tilt angle in the range of 0°~180°. The black dashed line in Fig. 12 is the fitting line, according to our experimental results. With the increase of tilt angle, the efficiency tends to decrease first and then increase, and the minimum efficiency shows between 90° ~ 105°, while the efficiency of the 0° tilt angle is around 35% higher than the 180° tilt angle.

This result corresponds to previous research by Balakin et al. [44], as shown in the red line of Fig. 12. They numerically investigated the thermal efficiency of a cylindrical column collector with graphene nanofluids (the height is 1.0 cm, and the intensity is 2.3 sun). According to their study, increasing the tilt angle will reduce the convective pattern, until a minimum is reached at 90°, while the collector efficiency increases to a point where the 180° tilt angle is preferred compared to 45°. The comparison between the 0° and 180° tilt angles at different flow rates is also shown in Fig. 10.

When the tilt angle is 0°, the DASC is illuminated from the bottom. The outer layer absorbs the heat first, and then a temperature gradient inside the nanofluid is formed. With the increase in temperature, the density of the nanofluid decreases. The buoyant force drives the outer layer nanofluid to move upwards, which leads to macroscopic convection. Wang et al. [45] pointed out that heat transfer is dominated by convection, rather than conduction, in this situation, and this phenomenon is called Rayleigh-Benard convection. Since the direction of the buoyant force is opposite to gravity, the Rayleigh-Benard convection will be affected by inclining the DASC. With the increase in the tilt angle, the angle between buoyance and radiation increases, and the Rayleigh-Benard convection is weakened. Moreover, the working flow can hinder the Rayleigh-Benard convection at the 90° tilt angle. Therefore, the minimum efficiency shows when the tilt angle is 90°. When the tilt angle reaches 180°, the irradiation light comes from the top surface. The heat is absorbed by the top layer and transferred inside the nanofluid by conduction, leading to a higher temperature gradient compared to the 0° tilt angle. Even though the nanoparticles can absorb the heat directly, the Rayleigh-Benard convection is still the predominant factor in reducing the temperature gradient. In this situation, there are numerous heat losses to the environment. Furthermore, Wang et al. [45] also realized that nanoparticles did not easily form sedimentation when the tilt angle was 0°, because the macroscopic convection made the nanoparticles move continuously. Therefore, the DASC 0° tilt angle has a stronger thermal absorption and conversion ability than the DASC 180° tilt angle.

4.3 Model validation

In this research, we also performed CFD simulations using STAR-CCM+, as indicated previously. The efficiencies of the DASC were calculated for all iterations, but the simulation only simulated one iteration. Therefore, we validated the CFD model by comparing the overall temperature increase at the outlet with the experimental results for different flow rates at 0° tilt angle.

We consider laminar flow in the simulations. As shown in Fig. 10 for the flow rates of 1 l/min and 2 l/min, the average overall temperature increase is 1.36 ℃ and 0.66℃, respectively.

Table 2 shows the comparison of experimental results and simulation results with flow rates of 1.0 l/min and 2.0 l/min. There is a clear agreement between the simulation results and the experimental results when using CB-based nanofluid as the working fluid. The maximum error was 0.344% when the flow rate was 2.0 l/min. This indicates that the proposed model can be used to analyze the photothermal performance of the DASC for CB-based nanofluids.

4.4 Mesh independence study

To ensure mesh independence, we tested five different mesh sizes for our simulation model, following the same strategy as in previous works, including [17, 22, 23]. The mesh sizes studied and grid cell numbers are shown in Table 3. As a critical factor, heat transfer

is the most typical parameter we focus on in the simulation. Therefore, we examined the efficiency of the DASC at the glass surface for different mesh sizes [46].

The results are shown in Fig. 13. There is a clear tendency for efficiency to decrease due to the increase in cell mesh size. The results showed less precision for larger computational cells, in particular close to the system boundaries, where steep concentration gradients occur. As a result, the interfacial area between nanofluid layers of two different concentrations increased, and more mesh numbers were required to achieve the mesh-independent solutions. Similar results were obtained by Hadjigeorgiou et al. [47], who found that a high concentration gradient existed within each unit cell, except for the last two-unit cells, where the solutions are almost thoroughly mixed. Following the increase in the mesh size, the average Nusselt number rose slightly. The reason was the different boundary conditions for different mesh sizes. The temperature in the cells at the boundary is too high compared to the next cell. This resulted in greater heat loss and also lower thermal efficiency. These results correspond to the paper by Abbassi et al. [48], in which a more refined mesh was needed to achieve mesh-independent results at higher Rayleigh numbers. The average mesh size of 10 mm was therefore chosen to complete the simulation, to ensure mesh independence and reduce the computational cost.

4.5 Simulation results

4.5.1 Effect of CB concentration

Fig. 14 shows the thermal efficiency and outlet temperature for different CB concentrations at the flow rate of 1.0 l/min. According to the figure, the efficiency and outlet temperature increase with the CB concentration and reach the maximum of 0.88 and 314.67 K, respectively. This maximum occurs at a CB concentration of 0.05 wt.%. The nanoparticles enhance the absorption of solar radiation in the base flow. However, as the CB concentration increases further, the efficiency and temperature decrease. When the number of nanoparticles in the base flow is low, the solar light can penetrate the nanofluid and easily reach the upper surface of the DASC. Hence, the fluid layer near the internal surface of the DASC extracts heat from this surface. This results in a more uniform temperature distribution and a lower temperature gradient between the fluid layers. When the concentration is too high, however, there is a large number of nanoparticles that can form a "shield" on the glass surface that blocks the solar light. As a result, only a thin layer of the nanoparticles can absorb the solar radiation directly, and the heat transfer is lower at these concentrations compared to low concentrations within the nanofluid. Accordingly, there will be a larger temperature gradient in these concentrations, causing more heat loss to the surroundings. In our simulation model, all the surfaces were set as adiabatic, except the glass surface, so the heat loss only occurs at the outer layer of this surface. This results in a decrease in the outlet temperature and efficiency. It should be noted that there will have been an optical loss, due to light reflection and glass absorption. Therefore, the actual efficiency and temperature are lower than the simulation results.

Similar results were obtained by some researchers. Otanicar et al. [49] studied the performance of a micro-DASC using an experimental setup and the aqueous suspensions containing silver and graphite nanoparticles and carbon nanotubes as the working fluids. The results show that the collector efficiency is enhanced by the increase in the nanofluid volume fraction because the solar absorption of nanofluid increases. However, this

increase continues for a certain amount of volume fraction, and then the reflection of solar radiation from the nanofluid increases, which results in a reduction of efficiency.

4.5.2 Flow patterns

Figs. 15-16 (a) show distributions of nanofluid temperature on the middle surface and velocity on the glass surface with a CB concentration of 0.05 wt.% and a flow rate of 2.0 l/min. Due to the viscosity, the velocity on the glass surface and internal surface were almost 0. Therefore, we only show the velocity distribution on the middle surface. The middle surface is located in the middle of the DASC, where the height was 1 mm. At the inlet, the temperature was low and a number of vortices occurred due to the sudden change in the cross-section radius and flow direction. When the fluid passed the first baffle, the temperature increased, and the velocity direction became clearly defined. The maximum temperature occurred after the third baffle, and the flow showed a clear path to the outlet. By comparing Fig. 15 and Fig. 16, we see that the area with the higher velocity tended to have a lower temperature. This is due to a shorter thermal exposure time for nanoparticles in these regions.

The presence of the baffles increased the residence time of the nanofluid inside the DASC and thus made it possible to extend the duration of absorption. As can be noted, due to the flow inertia the maximum velocity did not occur in the center of the pipeline. Instead, the maximum velocity was shifted to the right. Therefore, the areas on the opposite side of the baffles had a higher temperature. It is worth emphasizing that in these high-temperature areas, there was a displacement of the fluid towards the internal surface [50]. This phenomenon can be confirmed in Fig. 17 (a) and Fig. 17 (b), which show the volume fraction distribution at the glass and internal surfaces. At the glass surface, the volume fraction distribution resembles the velocity field. However, no compaction of particles occurred in the low-velocity regions (compare Fig. 15 with Fig. 17). As the flow proceeded, it was inevitable that the deposition was formed. In a stable nanofluid, the existence of an electrical double layer (EDL) ensured the repulsion between nanoparticles. When the stable state was affected by other factors, such as temperature gradient, Brownian motion, buoyancy, etc., that could accelerate the movement of nanoparticles, agglomeration was formed, due to the high chance of collision between nanoparticles. With the growth of the agglomeration, the flow pushed them to deposit near edges and corners. A higher particle volume fraction was thus observed close to the baffles. However, the deposition should occur abundantly on the glass surface due to gravity. In this case, the volume fraction on the internal surface was evidently higher than on the glass surface. Therefore, there must be a heat flow towards the interior of the fluid volume that drives the deposition to move, namely, Rayleigh-Benard convection.

Knowing the distribution of flow patterns could potentially help to increase the efficiency of the DASC for commercial use. The higher temperature makes the DASC more effective, but this is also accompanied by higher heat losses. Therefore, this should be considered when designing DASCs, for example by considering thermal insulation if possible.

5 Conclusions and future work

In this study, a series of experiments were conducted in a rectangular DASC, to test its thermal performance when using CB-based nanofluids as working fluids at different flow rates and tilt angles. For comparison, a surface collector with water as a working fluid was also used. The thermal efficiency of the DASC showed a rising trend with the flow rate increase and reached 0.57 when the flow rate was 4 l/min. The thermal efficiency of

the DASC is higher than the surface collector, and it was 10% higher at 2.0 l/min. Furthermore, the thermal efficiency depends on the DASC orientation in the gravity field with respect to the light source. With the increase of the incline angle of the DASC, the total thermal efficiency decreases, until the tilt angle reaches 90°, and then increases. The results prove that the 0° (down-faced) tilt angle outperforms 180°, and the efficiency is around 35% higher, due to the reduced heat loss and stronger macroscopic convection.

A CFD model of a rectangular DASC was used to analyze the optical properties of CB nanoparticles and the parameters of the DASC. According to the results, CB nanoparticles can increase the absorption of solar radiation in the base flow, and the efficiency of the DASC. As the CB concentration increases, the outlet temperature and efficiency tend to increase first and then decrease. Both the outlet temperature and the efficiency become optimal for the CB concentration of 0.05 wt. %. According to the temperature and velocity distributions, there will be a low flow velocity, but a high-temperature zone, in the rectangular DASC, which can lead to heat loss. Besides, CB nanoparticles will deposit in some places near the internal surface edges, due to the inward heat flow. These reveal the potential improvement for the DASC, to avoid thermal loss.

Optimizing the numerical model is the first objective of our future work. In the future, the efficiencies for different nanofluids and different geometries of DASCs should be considered.

Acknowledgments

Shihao Wei gratefully acknowledges financial support from the China Scholarship Council.
The computations were performed on resources provided by UNINETT Sigma2 - the National Infrastructure for High Performance Computing and Data Storage in Norway.
Boris Balakin thanks the Norwegian Research Council for funding (project 300286).

The authors report there are no competing interests to declare.

References

[1] T. B. Johansson, A. P. Patwardhan, N. Nakićenović, and L. Gomez-Echeverri, *Global energy assessment: toward a sustainable future*. Cambridge University Press, 2012.

[2] M. Karami, M. Bozorgi, and S. Delfani, “Effect of design and operating parameters on thermal performance of low-temperature direct absorption solar collectors: a review,” *Journal of Thermal Analysis and Calorimetry*, vol. 146, no. 3, pp. 993–1013, 2021.

[3] Y. Tripanagnostopoulos, “Photovoltaic/thermal solar collectors,” *Comprehensive renewable energy*, vol. 3, pp. 255–300, 2012.

[4] Z. Haddad, C. Abid, H. F. Oztop, and A. Mataoui, “A review on how the researchers prepare their nanofluids,” *International Journal of Thermal Sciences*, vol. 76, pp. 168–189, 2014.

[5] G. Peker, C. Yıldız, G. Çakmak, Y. Bilgiç, and A. Yıldız, “Thermal performance of new type plate heat exchanger with spring turbulence generator using nanofluid flow,” *Experimental Heat Transfer*, pp. 1–15, May 2022, doi: 10.1080/08916152.2022.2081886.

[6] Abd. R. Abu Talib and S. Salman, "Heat transfer and fluid flow analysis over the microscale backward-facing step using β Ga 2 O 3 nanoparticles," Experimental Heat Transfer, pp. 1–18, Feb. 2022, doi: 10.1080/08916152.2022.2039328.

[7] S. M. H.M and R. N. Hegde, "Investigations on the effect of disturbed flow using differently configured turbulators and Alumina nanofluid as a coolant in a double tube heat exchanger," *Experimental Heat Transfer*, vol. 35, no. 3, pp. 282–307, Apr. 2022, doi: 10.1080/08916152.2020.1860159.

[8] R. Saidur, K. Leong, and H. A. Mohammed, "A review on applications and challenges of nanofluids," *Renewable and sustainable energy reviews*, vol. 15, no. 3, pp. 1646–1668, 2011.

[9] B. Fekadu, R. Kathiravan, and P. Saravanan, "Augmentation of pool boiling heat transfer characteristics using naphtha carbon soot nanoparticles–water based nanofluids," *Experimental Heat Transfer*, pp. 1–16, 2021.

[10] R. Maithani, R. Agarwal, A. Kumar, and S. Sharma, "Parametric optimization of impinging air jet on hemispherical protrusion of a solar thermal collector," *Experimental Heat Transfer*, pp. 1–22, May 2022, doi: 10.1080/08916152.2022.2075989.

[11] F. Bioucas, S. Vieira, M. Lourenço, F. Santos, and C. N. de Castro, "Performance of heat transfer fluids with nanographene in a pilot solar collector," *Solar Energy*, vol. 172, pp. 171–176, 2018.

[12] W. S. Sarsam, S. Kazi, and A. Badarudin, "Thermal performance of a flat-plate solar collector using aqueous colloidal dispersions of multi-walled carbon nanotubes with different outside diameters," *Experimental Heat Transfer*, vol. 35, no. 3, pp. 258–281, 2022.

[13] A. Mwesigye, İ. H. Yılmaz, and J. P. Meyer, "Numerical analysis of the thermal and thermodynamic performance of a parabolic trough solar collector using SWCNTs-Therminol® VP-1 nanofluid," *Renewable Energy*, vol. 119, pp. 844–862, 2018.

[14] P. S. G. Natividade, G. de Moraes Moura, E. Avallone, E. P. Bandarra Filho, R. V. Gelamo, and J. C. de S. I. Gonçalves, "Experimental analysis applied to an evacuated tube solar collector equipped with parabolic concentrator using multilayer graphene-based nanofluids," *Renewable Energy*, vol. 138, pp. 152–160, 2019.

[15] X. Xu, C. Xu, J. Liu, X. Fang, and Z. Zhang, "A direct absorption solar collector based on a water-ethylene glycol based nanofluid with anti-freeze property and excellent dispersion stability," *Renewable Energy*, vol. 133, pp. 760–769, 2019.

[16] C. H. Li and G. Peterson, "Experimental investigation of temperature and volume fraction variations on the effective thermal conductivity of nanoparticle suspensions (nanofluids)," *journal of applied physics*, vol. 99, no. 8, p. 084314, 2006.

[17] V. Bhalla, V. Khullar, and H. Tyagi, "Investigation of factors influencing the performance of nanofluid-based direct absorption solar collector using Taguchi method," *Journal of Thermal Analysis and Calorimetry*, vol. 135, no. 2, pp. 1493–1505, 2019.

[18] O. Z. Sharaf, D. C. Kyritsis, A. N. Al-Khateeb, and E. Abu-Nada, "Effect of bottom surface optical boundary conditions on nanofluid-based DASC: Parametric study and optimization," *Solar Energy*, vol. 164, pp. 210–223, 2018.

[19] T. P. Otanicar, P. E. Phelan, and J. S. Golden, "Optical properties of liquids for direct absorption solar thermal energy systems," *Solar Energy*, vol. 83, no. 7, pp. 969–977, 2009.

[20] X. Li *et al.*, "Numerical analysis of photothermal conversion performance of MXene nanofluid in direct absorption solar collectors," *Energy Conversion and Management*, vol. 226, p. 113515, 2020.

[21] P. Struchalin *et al.*, "Performance of a tubular direct absorption solar collector with a carbon-based nanofluid," *International Journal of Heat and Mass Transfer*, vol. 179, p. 121717, 2021.
[22] T. J. Choi, S. P. Jang, and M. Kedzierski, "Effect of surfactants on the stability and solar thermal absorption characteristics of water-based nanofluids with multi-walled carbon nanotubes," *International Journal of Heat and Mass Transfer*, vol. 122, pp. 483–490, 2018.
[23] A. Kosinska, B. V. Balakin, and P. Kosinski, "Photothermal conversion of biodegradable fluids and carbon black nanofluids," *Scientific Reports*, vol. 12, no. 1, pp. 1–13, 2022.
[24] E. T. Ulset, P. Kosinski, Y. Zabednova, O. V. Zhdaneev, P. G. Struchalin, and B. V. Balakin, "Photothermal boiling in aqueous nanofluids," *Nano Energy*, vol. 50, pp. 339–346, 2018.
[25] A. Sözen, M. Gürü, T. Menlik, U. Karakaya, and E. Çiftçi, "Experimental comparison of Triton X-100 and sodium dodecyl benzene sulfonate surfactants on thermal performance of TiO2–deionized water nanofluid in a thermosiphon," *Experimental Heat Transfer*, vol. 31, no. 5, pp. 450–469, 2018.
[26] B. V. Balakin, M. Stava, and A. Kosinska, "Photothermal convection of a magnetic nanofluid in a direct absorption solar collector," *Solar Energy*, vol. 239, pp. 33–39, 2022.
[27] B. V. Balakin, O. V. Zhdaneev, A. Kosinska, and K. V. Kutsenko, "Direct absorption solar collector with magnetic nanofluid: CFD model and parametric analysis," *Renewable Energy*, vol. 136, pp. 23–32, 2019.
[28] R. Bårdsgård, D. M. Kuzmenkov, P. Kosinski, and B. Balakin, "Eulerian CFD model of direct absorption solar collector with nanofluid," *Journal of renewable and sustainable energy*, vol. 12, no. 3, p. 033701, 2020.
[29] H. F. Lutro, "The effect of thermophoresis on the particle deposition on a cylinder," 2012.
[30] T. Cosgrove, *Colloid science: principles, methods and applications*. John Wiley & Sons, 2010.
[31] H. M. Al-Ali and N. H. Hamza, "Numerical and experimental study of the influence of extended surfaces in rectangular channel subjected to constant heat flux," *Experimental Heat Transfer*, pp. 1–19, Feb. 2023, doi: 10.1080/08916152.2023.2176567.
[32] M. Kalteh, A. Abbassi, M. Saffar-Avval, and J. Harting, "Eulerian–Eulerian two-phase numerical simulation of nanofluid laminar forced convection in a microchannel," *International journal of heat and fluid flow*, vol. 32, no. 1, pp. 107–116, 2011.
[33] C. F. Bohren and D. R. Huffman, *Absorption and scattering of light by small particles*. John Wiley & Sons, 2008.
[34] R. A. Taylor, P. E. Phelan, T. P. Otanicar, R. Adrian, and R. Prasher, "Nanofluid optical property characterization: towards efficient direct absorption solar collectors," *Nanoscale research letters*, vol. 6, no. 1, pp. 1–11, 2011.
[35] IAPWS, TGD8-16(2019), "Application of Film Forming Substances in Fossil, Combined Cycle, and Biomass Power Plants."
[36] A. Lenert and E. N. Wang, "Optimization of nanofluid volumetric receivers for solar thermal energy conversion," *Solar Energy*, vol. 86, no. 1, pp. 253–265, 2012.
[37] T. L. Bergman, T. L. Bergman, F. P. Incropera, D. P. Dewitt, and A. S. Lavine, *Fundamentals of heat and mass transfer*. John Wiley & Sons, 2011.
[38] J. Liu, Z. Ye, L. Zhang, X. Fang, and Z. Zhang, "A combined numerical and

experimental study on graphene/ionic liquid nanofluid based direct absorption solar collector," *Solar Energy Materials and Solar Cells*, vol. 136, pp. 177–186, 2015.

[39] E. T. Ulset, "Utilizing solar vapour energy by use of nanofluids in a direct absorption solar collector," 2018.

[40] T. J. Choi, S. H. Kim, S. P. Jang, L. Lin, and M. A. Kedzierski, "Aqueous nanofluids containing paraffin-filled MWCNTs for improving effective specific heat and extinction coefficient," *Energy*, vol. 210, p. 118523, 2020.

[41] S. Ahmad, R. Saidur, I. Mahbubul, and F. Al-Sulaiman, "Optical properties of various nanofluids used in solar collector: a review," *Renewable and Sustainable Energy Reviews*, vol. 73, pp. 1014–1030, 2017.

[42] J. R. Eggers, E. M. Lange, and S. Kabelac, "Radiation and energetic analysis of nanofluid based volumetric absorbers for concentrated solar power," *Nanomaterials*, vol. 8, no. 10, p. 838, 2018.

[43] H. K. Gupta, G. D. Agrawal, and J. Mathur, "An experimental investigation of a low temperature Al2O3-H2O nanofluid based direct absorption solar collector," *Solar Energy*, vol. 118, pp. 390–396, 2015.

[44] B. V. Balakin, O. V. Zhdaneev, A. Kosinska, and K. V. Kutsenko, "Direct absorption solar collector with magnetic nanofluid: CFD model and parametric analysis," *Renewable Energy*, vol. 136, pp. 23–32, 2019.

[45] K. Wang *et al.*, "Significant photothermal conversion enhancement of nanofluids induced by Rayleigh-Bénard convection for direct absorption solar collectors," *Applied Energy*, vol. 254, p. 113706, 2019.

[46] M. Hatami and D. Jing, "Evaluation of wavy direct absorption solar collector (DASC) performance using different nanofluids," *Journal of Molecular Liquids*, vol. 229, pp. 203–211, 2017.

[47] A. G. Hadjigeorgiou, A. G. Boudouvis, and G. Kokkoris, "Thorough computational analysis of the staggered herringbone micromixer reveals transport mechanisms and enables mixing efficiency-based improved design," *Chemical Engineering Journal*, vol. 414, p. 128775, 2021.

[48] M. A. Abbassi, M. R. Safaei, R. Djebali, K. Guedri, B. Zeghmati, and A. A. Alrashed, "LBM simulation of free convection in a nanofluid filled incinerator containing a hot block," *International Journal of Mechanical Sciences*, vol. 144, pp. 172–185, 2018.

[49] T. P. Otanicar, P. E. Phelan, R. S. Prasher, G. Rosengarten, and R. A. Taylor, "Nanofluid-based direct absorption solar collector," *Journal of renewable and sustainable energy*, vol. 2, no. 3, p. 033102, 2010.

[50] M. Simonetti, F. Restagno, E. Sani, and M. Noussan, "Numerical investigation of direct absorption solar collectors (DASC), based on carbon-nanohorn nanofluids, for low temperature applications," *Solar Energy*, vol. 195, pp. 166–175, 2020.

Table 1 Properties of carbon black

Manufacturer	Bulk density	Specific heat	Average particle size	Thermal conductivity
TIMCAL ENSACO™	2250 kg/m^3	710 J/(kg·K)	60 nm	24 W/(m·K)

Table 2 Model validation

Results	1.0 l/min	2.0 l/min
Experiment	1.36 ℃	0.66 ℃.
Simulation	1.32 ℃	0.67 ℃.
Error	3.03%	-1.49%

Table 3 Mesh numbers for different mesh sizes

Mesh size (mm)	5	10	15	20	25
Grid cell number	13177488	2690156	944391	463989	285894

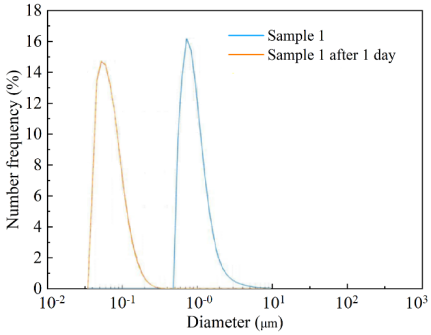

(a) Particle size distribution of the CB nanofluid measured on two consecutive days.

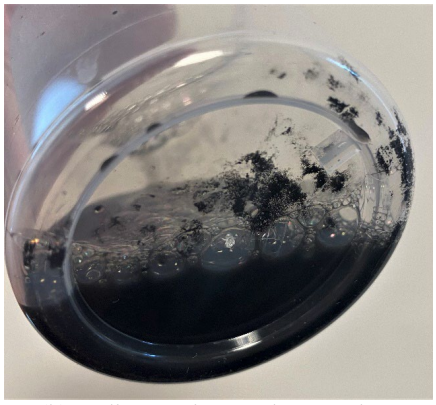

(b) Sedimentation on the container bottom after seven days (a sample was collected after preparation)

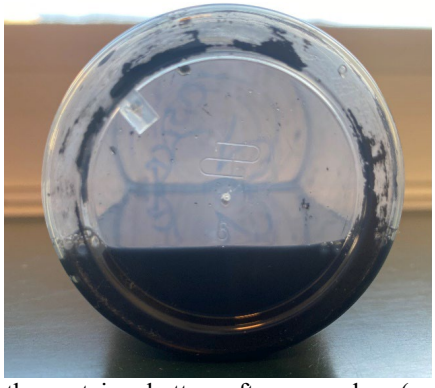

(c)Sedimentation on the container bottom after seven days (a sample was collected after the experiments)

Fig. 1 Stability analysis of the nanofluids

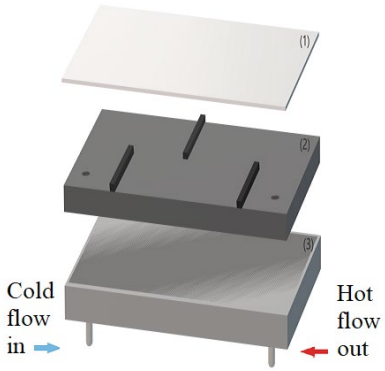

Fig. 2 Schematic of the DASC: (1) glass surface, (2) inner plate with three baffles, (3) external aluminium box.

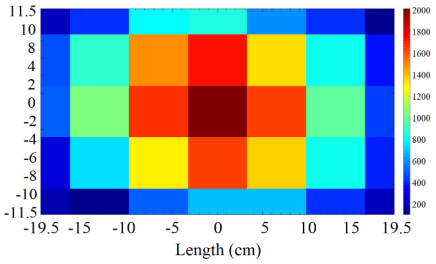

Fig. 3 Intensity distribution [W/m^2] on the DASC.

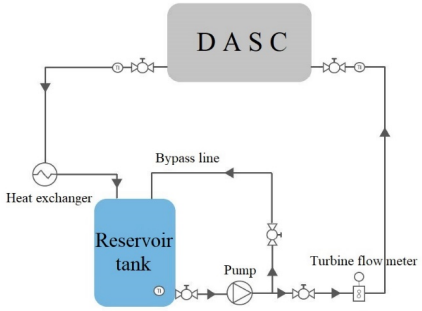

Fig. 4 Schematic of the experimental setup.

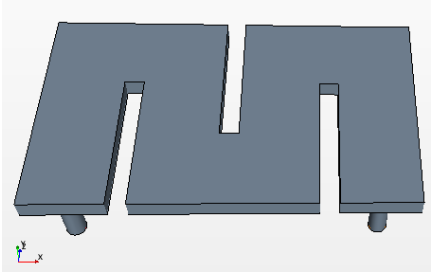

Fig. 5 Simulation model of the DASC.

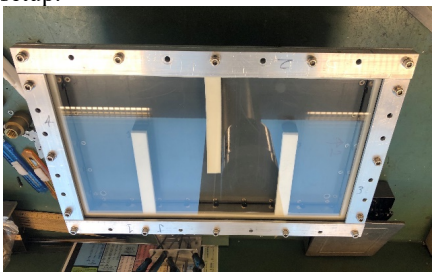

Fig. 6 Image of the DASC.

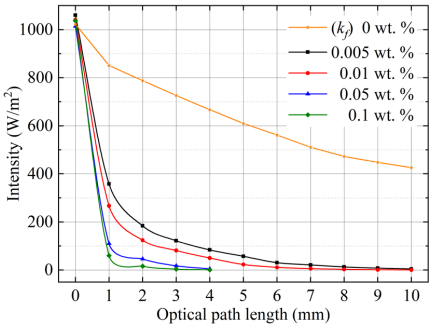

Fig. 7 Transmittance of CB nanofluids.

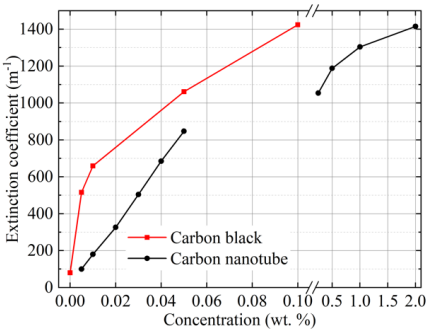

Fig. 8 Extinction coefficient of CB nanofluids (red line). The results are compared to the literature results [40] that focused on carbon nanotubes.

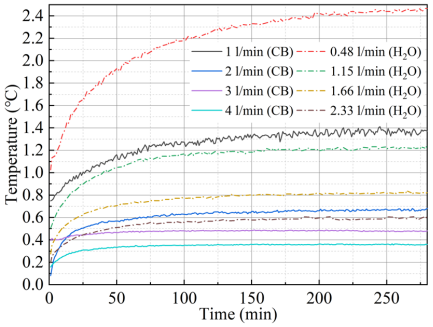

Fig. 9 Temperature difference histories in nanofluid and water (C_{CB}=0.05 wt.%).

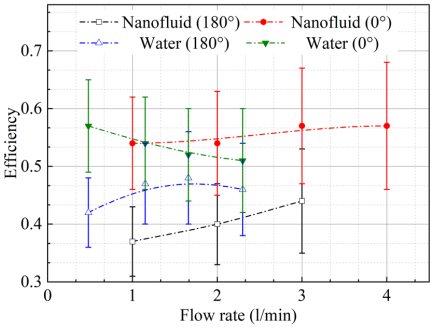

Fig. 10 Thermal efficiency at different flow rates and tilt angle for nanofluids and water (C_{CB}=0.05 wt.%).

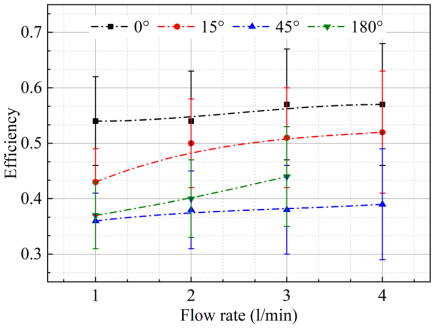

Fig. 11 Efficiency of nanofluid at different tilt angles and flow rates (C_{CB}=0.05 wt.%).

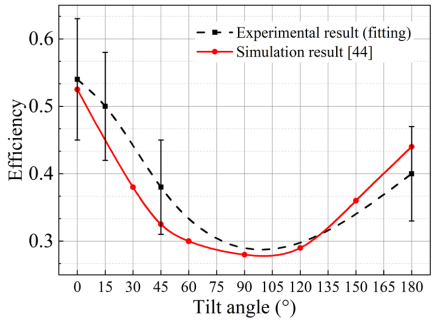

Fig. 12 Prediction of the change tendency between efficiency of nanofluid and tilt angles (C_{CB}=0.05 wt.%, Q=2 l/min). Compared with Balakin et al. [44].

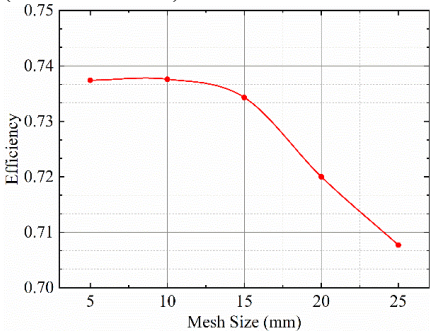

Fig. 13 Efficiency vs. mesh size (C_{CB}=0.05 wt.%, Q=1 l/min).

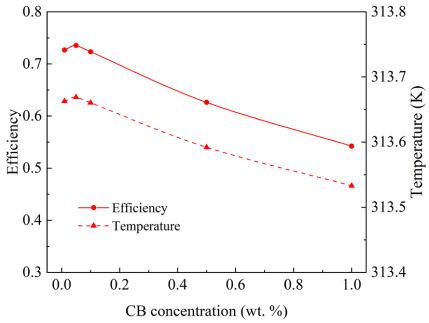

Fig. 14 Efficiency for different CB concentrations (Q=1.0 l/min).

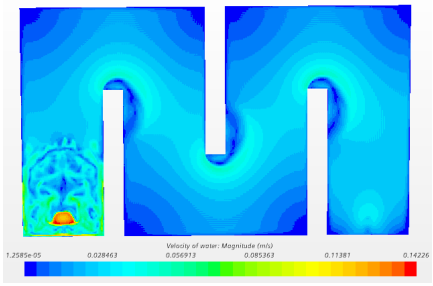

Fig. 15 Velocity distribution on the middle surface (height is 1 mm) (C_{CB}=0.05 wt.%, Q=2.0 l/min).

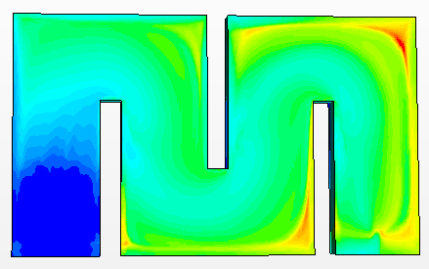

(a) glass surface

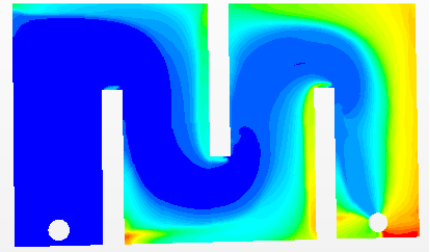

(b) internal surface

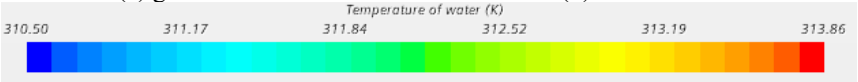

Fig. 16 Temperature distribution (C_{CB}=0.05 wt.%, Q=2 l/min).

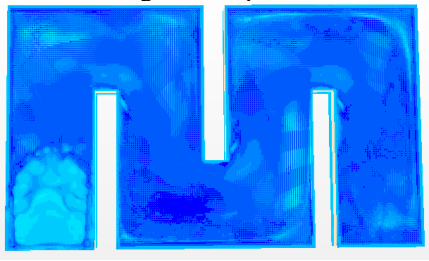

(a) glass surface

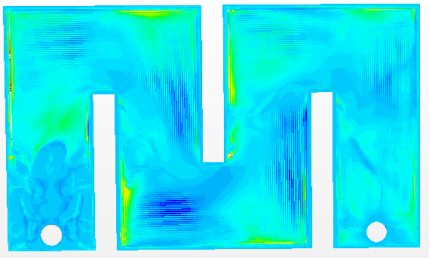

(b) internal surface

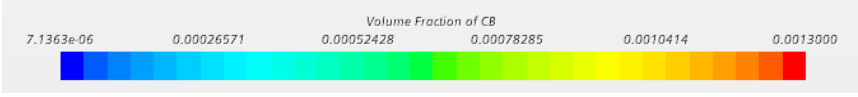

Fig. 17 CB volume fraction distribution (C_{CB}=0.05 wt.%, Q=2 l/min).

This paper was submitted for publication in the Journal of Cleaner Production

Investigation of nanofluids in alkaline electrolytes: stability, electrical properties, and hydrogen production

Shihao Wei[1], Boris V. Balakin[2], Pawel Kosinski[1,*]

[1]University of Bergen, Department of Physics and Technology, Bergen, Norway
[2]Western Norway University of Applied Sciences, Department of Mechanical and Marine Engineering, Bergen, Norway
* Corresponding author: pawel.kosinski@uib.no

Abstract: Utilizing solar energy efficiently and manufacturing hydrogen economically are the primary goals in the energy industry. In this paper, we present a novel method to solve both issues by exploiting the electrolysis of electrolyte-based nanofluids under the illumination of solar light. The carbon black nanoparticles/ sodium hydroxide solution mixture of electrolyte nanofluids were prepared, which were then electrolyzed in a Hoffman voltameter to produce hydrogen. The results showed the hydrogen production rate improved by 23.62% when carbon black was used in the electrolyte. The optimal carbon black concentration was 0.04% or 0.2% depending on the experimental set-up used. Finally, a theoretical model was built to evaluate the total hydrogen production, which showed a good agreement with the experimental results when the carbon black concentration was lower than 0.1 wt.%.

Keywords: Electrolysis, Carbon black, Nanofluids, Hydrogen production, Electrical properties

1. Introduction

In 2021, the European Commission released the 2030 climate target plan (European Commission, 2020). The commission proposed cutting greenhouse gas emissions by at least 55% by 2030 to achieve climate neutrality by 2050. Similarly, China set a 2060 carbon neutrality target in 2020 and hit a carbon emissions peak before 2030 (The state council of the people's republic of China, 2021). In order to achieve these targets, clean energy with zero greenhouse gas emissions that can replace fossil fuels is the critical factor. At present, good alternatives for fossil energy are hydrogen and solar energy.

Hydrogen is a renewable energy resource; its burnt product is only water. Although hydrogen is a principal element in nature, most of it that can be used in power engineering should be manufactured by water electrolysis (Léon, 2008.), which requires significant energy. However, when the electrolysis efficiency is insufficient, the energy cost to harness hydrogen is higher than the total energy that is converted into hydrogen formation. Nowadays, the widely used technologies in water splitting reactions that can increase efficiency and reduce consumption include operating at high pressure and temperature, photovoltaic technique, PEM membrane, etc. (Godula-Jopek, 2015).

Alternatively, solar energy has a huge potential in the energy resource field. A common way to use solar energy is by transferring it into thermal energy through solar collectors. Solar collectors are thermal systems that harvest solar irradiation through various working fluids, such as water, thermal oil, ethylene-glycol, etc. (Bellos et al., 2017). However, low energy efficiency is still the primary severe issue that engineers face in using solar energy.

To solve this problem, some researchers proposed to use nanofluids as working fluids due to their enhanced thermal conductivity (Kumar et al., 2015).

Nanofluids are colloids with dispersed nanosized particles in base fluids. Because of the high thermal conductivity of nanoparticles, the heat transfer coefficient of nanofluids is higher than that of traditional working fluids. Therefore, the utilization of nanofluids in solar collectors (Struchalin et al., 2021; Kosinska et al., 2022) and the thermophysical properties of nanofluids (Balakin et al., 2019; Balakin et al., 2022) has been widely investigated through simulations and experiments.

Moreover, another essential property of nanofluids that has not been given enough attention is electrical or thermoelectrical properties (Sheikholeslami et al., 2017). One important thermoelectrical property is that heat transfer performance can be enhanced in a nanofluid with a supplied electrical field or magnetic field (Wang et al., 2020). This critical discovery appealed to researchers who shifted study priority from thermo-convection to thermomagnetic convection (Khan et al., 2016; Khan et al., 2016). Another paramount electrical property is electrical conductivity. It was experimentally studied by researchers on different nanoparticle-based nanofluids (Zawrah et al., 2016; Bagheli et al., 2015), and an improved Maxwell model was derived to estimate the electrical conductivity of water-based nanofluids (Minea, 2019).

Therefore, an energy system that can make good use of the nanofluids' thermophysical and thermoelectrical properties has a promising prospect. Liu et al. (2016) used aluminum nanoparticles and ferro/ferricyanide solution to make electrolyte nanofluids (ENF). They demonstrated a possible thermogalvanic application as reported the enhanced mass transfer, electrical conductivity, and thermal conductivity. Another proposed application is using ENF inside batteries. Wang et al. (2016) investigated the performance of aluminum oxide-based nanofluids as an electrolyte of a battery. The results showed that aluminum oxide ENF could effectively improve the output and heat transfer of the battery due to electrochemical reactions within the ENF. Both proposed applications of ENF highly relied on the stability of the nanofluids, which makes their effectivity loss with time. In addition, they were one-time uses decided by the aluminum ions concentration, making them harmful to the environment.

Therefore, it is a sensible choice to combine solar energy, hydrogen, and nanofluids in energy conversion and storage. One specific device is the photovoltaic/thermal (PV/T) system, a combination of solar collectors and photovoltaic cells. Nanofluids have been proven to be excellent working fluids in the PV/T system (Sheikholeslami et al., 2021). However, the temperature rise in PV cells negatively affects electrical performance (Manikandan et al., 2022), which makes nanofluids primarily used in the cooling system due to their excellent heat transfer capabilities. Therefore, in our research, we considered the feasibility of using ENF and solar light for manufacturing hydrogen.

In (Hiraki et al., 2005), the authors dispersed waste aluminum dross with the size of 180 – 425 μm in a sodium hydroxide (SH) solution and tested the hydrogen production. The results showed that initial temperature significantly affected the reaction rate, and that using micro-sized aluminum-SH solution as an electrolyte only required 2% energy consumption and emitted 4% carbon dioxide compared to conventional methods to generate hydrogen. They owed this unexpected energy consumption to the aluminum dross. The micro-sized aluminum increased the total surface area in the solution, making the reaction faster. However, they pay more attention to the composition of aluminum hydroxide (another electrolysis product) in the study instead of how aluminum particles affected the electrolysis production. This study indicated that using ENF in producing hydrogen by water electrolysis and solar light irradiation can increase total hydrogen production.

First, the improved electrolysis efficiency requires a higher temperature, which can be achieved through the enhanced thermal properties of nanofluids when subjected to solar irradiation. Secondly, the nanoparticle motion in the electrolyte can promote electrolysis due to the electrical double layer (EDL). Thirdly, the applied electric field can enhance the convective heat transfer within nanofluids. To our knowledge, these factors were considered by only a few researchers, making it a completely new research field. As an example, we cite the work by Choi and Lee (2020), who reported a promotion in hydrogen production in water electrolysis using the cellulose nanofluids. However, as an organic nanofluid, the enhancement was caused by the nanostructure of cellulose instead of its thermoelectric properties. Hence, a deeper understanding of the properties of ENF and its performance in hydrogen production through water electrolysis is essential.

In this study, we focused on factors that can affect hydrogen production through water electrolysis. Based on our previous work (Wei et al., 2022), SH electrolyte-based carbon black (CB)-based sodium sulfate electrolyte nanofluids (SSENF) were synthesized. Their stability was compared with aqueous CB nanofluids and CB-based sodium hydroxide electrolyte nanofluids (SHENF). The alkaline ENF was then electrolyzed in a Hoffman apparatus at different nanofluids concentrations. The hydrogen production and current changes with CB concentrations were recorded. In the end, these results were used to build a simplified theoretical model to evaluate the total hydrogen production for alkaline electrolyte-based CB nanofluids. To our knowledge, this study is the first to investigate hydrogen production by electrolyzing alkaline ENF. The results are valuable in exploiting the use of nanofluids together with solar energy for hydrogen production.

2. Methodology

2.1 Preparation of nanofluids-based electrolyte

In the first stage of the work, we synthesized nanofluids that were later used for the production of electrolyte nanofluids. The process is shown in Figure 1. For this, the suitable volume fraction CB particles and 0.5 wt.% sodium dodecyl sulfate (SDS) were blended with distilled water and stirred in the mixture until no visible large particle cluster acquired a homogeneous suspension. Then, an ultrasonic bath (Branson 3510E-DTH, 355 W/ 220-230 V) was used to agitate nanoparticles to make a stable nanofluid.

The reason we choose CB nanoparticles as the main object in making nanofluids is that carbon is essentially inert under normal conditions, and it can maintain its properties in a chemical solution and during electrolysis.

SDS is an ionic surfactant that is able to stabilize nanofluids (Ulset et al., 2018). It makes nanoparticles possess surface charge, which overlaps with nanoparticles' EDL and makes them repel each other. This stabilization technique is known as electrostatic stabilization. However, SDS shows inadequate performance in breaking large agglomerates and needs sufficient time to respond (Taylor et al., 2013). Hence, we adopt ultrasonic agitation after adding SDS. This technique, known as mechanical stabilization, uses ultrasonic waves on the nanofluid to break down the clusters and agglomerations incidentally (Chung et al., 2009).

Finally, when the stable nanofluid was made, SH bulks were added to the nanofluid and kept stirring until the bulks were wholly dissolved. The magnetic stirring method (Timofeeva et al., 2011), which consists of a ceramic magnet stirrer plate (VWR VMS-C4 advanced, 270 W/ 230 V) and magnet stirrer bar, was applied for dissolution to maintain

the stability of the prepared nanofluid. This process was carried out at room temperature and the stirring speed was set as 1000 rpm.

We chose salt electrolyte in the past (Wei et al., 2022) because it is unable to oxidate nanoparticles. Nonetheless, as a mature technique, the alkaline electrolyzer is widely used in large-scale hydrogen production industries. The purity of produced hydrogen in an alkaline electrolyzer is expected to be more than 99.99%, and the rest of 0.01% is caused by the gas crossover (Ezzahra-Chakik et al., 2017). Schalenbach et al. (2016) experimentally investigated the performance of water electrolysis cells with acidic and alkaline electrolytes. The results showed that alkaline water electrolyzers were more efficient than acidic water electrolysis. The abovementioned advantages make the investigation of nanoparticles in alkaline electrolytes meaningful.

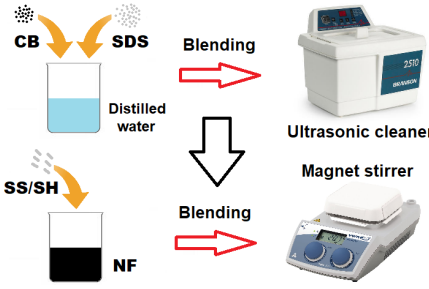

Figure 1 The process of electrolyte nanofluids' preparation.

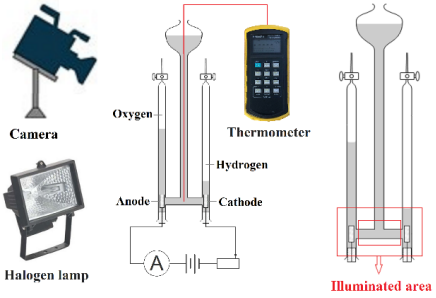

(a) (b)

Figure 2 Schematic representation of experimental apparatus

2.2 Experimental procedure

Figure 2 (a) shows the framework of the experimental setup for the hydrogen production study. A Hoffman voltameter was used to electrolyze the ENF. CB nanoparticles were unable to be oxidated under the condition of this experiment. Hence, the reactions for alkaline ENF in this work were as follows:

$$\text{Anode: } 2OH^- = H_2O + 1/2O_2 + 2e^- \quad (1)$$

$$\text{Cathode: } 2H_2O + 2e^- = H_2 + 2OH^- \quad (2)$$

$$\text{Overall Reaction: } H_2O = H_2 + 1/2O_2 \quad (3)$$

The produced hydrogen and oxygen were gathered at the top of the two vertical pipes of the Hoffman voltameter. The volume of the gases could be read directly from the scale on the pipes with each graduated 60 × 0.2 ml, and the distance between them were 0.1 m. A DC source from Peakteck supplied the power for electrolysis. The maximum output current and voltage were 2 A and 30 V, respectively, and the accuracy was ±1%+5 digits. A thermocouple was used to test the temperature of the horizontal pipe of the Hoffman voltameter, as shown by the red line in Figure 2 (a). The temperature could be read and recorded by a datalogger (Omega HH506RA), and its error range was ±0.05%. A halogen lamp (Osram R7S 400 W /230 V) was used to simulate the sun and produce solar radiation. The irradiance was measured by an irradiance meter (Linshang Technology) with an

accuracy of ±0.1%. The height of the halogen lamp was set to keep the light bulb and the horizontal pipe on the same level. We adjusted the distance between them to control the irradiance. The irradiance was selected as 1000 W/m^2.

After the ENF was prepared as described in Section 2.1, we filled the Hoffman voltameter until the liquid level reached the tick mark of 0 and closed the outlet of the pipe. The temperature of the prepared ENF was higher than room temperature due to sonification and stirring. Therefore, we let the system in a static condition until the thermal equilibrium was obtained. When the temperature of the sample reached the preset initial temperature (±1℃.), we turned on the camera, halogen lamp, and DC source simultaneously. In each case, the electrolysis was carried out for 16 minutes under 30 V voltage input, and the hydrogen production, temperature, and current were recorded every 2 minutes.

In this study, we focus on the three issues that can affect hydrogen production. The first one is the stability of ENF. Instability has adverse effects on nanofluids' thermophysical and thermoelectrical properties (Sharaf et al., 2020). Thus, the stability of nanofluid-based electrolytes becomes an essential factor affecting hydrogen production and deserves to be investigated. Three different nanofluids with three different concentrations were made in this work. The composition and concentration of each component are shown in Table 1. The nine suspensions were sealed in plastic beakers, as shown in Figure 3, and recorded their states with photographic equipment every 24 hours.

Table 1 Composition and concentration of samples

Samples	1	2	3	4	5	6	7	8	9
Composition and concentraion (wt.%)	CB/ 0.05	CB/ 0.1	CB/ 0.5	CB/ 0.05	CB/ 0.1	CB/ 0.5	CB/ 0.05	CB/ 0.1	CB/ 0.5
		-			SDS/ 0.5				
					SH/ 5			SS/ 10	
					Distilled water				

Secondly, the electrolysis experiments were conducted at different initial temperatures. The 0.1 wt.% CB ENF with sodium hydroxide concentrations of 1 wt.%, 5 wt.%, and 10 wt.% was electrolyzed. The 10 wt.% sodium hydroxide electrolytes without CB were also tested for comparison.

Finally, we performed the electrolysis experiments under different CB concentrations (0.01 wt.% ~ 0.3 wt.%). In this work, two different illuminated areas were set by using a screen to allow the lamp to only irradiate selected regions of the apparatus. The two red rectangles in Figure 2 (b) show the location and size of the illuminated areas. When the larger illuminated areas, where the area of the main radiation area was approximately 0.015 m^2, were applied, we focused on the thermal properties of ENF. Almost all nanofluids can absorb light energy and make the temperature of the entire system increase fast. Hence, the electrical properties became the main object when using a narrower illuminated area with an area of 0.005 m^2. In this situation, only the nanoparticles dispersed in the path between the two electrodes were irradiated directly. They could affect the motion of ions and currents. In addition, the smaller illuminated area could also diminish the effect of the heat absorption by the metal parts in the system.

2.3 Evaluation of hydrogen production

The amount of hydrogen produced by electrolysis of alkaline ENF is challenging to calculate, because one needs to consider many factors such as, temperature, pressure, concentrations of components, agglomeration of nanoparticles, etc. Therefore, in this study, we focused on the electrical conductivity of nanofluids and explored a simplified correlation with some assumptions on the basis of widely used electrical theories.

The theoretical total hydrogen production can be evaluated by Faraday's law of electrolysis (Godula-Jopek, 2015):

$$n = \frac{It}{zF}, \tag{4}$$

where n is moles of the produced substance at an electrode, respectively, I is current, t is time, z is the valence of the counter-ion, F is the Faraday constant.

The current I can be determined by Ohm's Law for Electromagnetics (Nie et al., 2008):

$$I = \sigma EA, \tag{5}$$

where σ is the electrical conductivity of the electrolyte, in this study, it is the electrical conductivity of the alkaline ENF, E is the electric field, and A is the area that the charge flows through.

The electrical conductivity of the ENF is determined by the electrical conductivity of the base fluid (SH solution) and the electrical conductivity of CB nanoparticles, and it can be calculated by the Maxwell model (Maxwell, 1873):

$$\sigma = \sigma_f \left[1 + \frac{3\left(\frac{\sigma_p}{\sigma_f} - 1\right)\varphi}{\frac{\sigma_p}{\sigma_f} + 2 - \left(\frac{\sigma_p}{\sigma_f} - 1\right)\varphi} \right], \tag{6}$$

where σ is the electrical conductivity of the ENF; σ_f is the electrical conductivity of the base fluid; σ_p is the electrical conductivity of the particles, and φ is the concentration of the nanofluid. Normally, the concentration of nanofluids is less than 1 wt.%, which means that term $(\frac{\sigma_p}{\sigma_f} + 2)$ is at least two orders of magnitude less than the term $\left(\frac{\sigma_p}{\sigma_f} - 1\right)\varphi$ is at least 2 orders of magnitude smaller. Therefore this small term can be ignored in equation (6).

However, many researchers reported that the Maxwell model has low accuracy as it only considers the electrical properties of nanoparticles and neglects the motion of nanoparticles in nanofluids (Said et al., 2022). Hence, Shen et al. (2012) proposed a new model that takes electrophoresis and Brownian motion into consideration on the basis of the Maxwell model. In his model, the electrical conductivity enhanced by electrophoresis can be given by:

$$\sigma_E = \frac{2\varphi {\varepsilon_d}^2 {\varepsilon_{d0}}^2 \zeta^2}{\mu r^2}, \tag{7}$$

where σ_E is the electrical conductivity due to electrophoretic mobility; ε_d is the dielectric constant of base fluid; ε_{d0} is the dielectric constant of vacuum; ζ is the zeta potential of nanoparticles that will be discussed in detailed in Section 3.1; μ is the viscosity of the nanofluid and r is the radius of nanoparticles.

Also, the electrical conductivity enhanced by Brownian motion is (Shen et al., 2012):

$$\sigma_B = \frac{3\varphi \varepsilon_d \varepsilon_{d0} \zeta \left(\frac{RT}{L} \cdot \frac{1}{3\pi\mu}\right)}{r^{\frac{3}{2}}}, \tag{8}$$

where σ_B is the electrical conductivity caused by Brownian motion, R is the thermodynamic constant, T is temperature, and L is the Avogadro constant.

Therefore, by combining equations (6) ~ (8) and implementing them into equation (5), the current I can be written as:

$$I = \left\{ \sigma_f \left[1 + \frac{3\left(\frac{\sigma_p}{\sigma_f} - 1\right)\varphi}{\frac{\sigma_p}{\sigma_f} + 2 - \left(\frac{\sigma_p}{\sigma_f} - 1\right)\varphi} \right] + \frac{2\varphi {\varepsilon_d}^2 {\varepsilon_{d0}}^2 \zeta^2}{\mu r^2} + \frac{3\varphi \varepsilon_d \varepsilon_{d0} \zeta \left(\frac{RT}{L} \cdot \frac{1}{3\pi\mu}\right)}{r^{\frac{3}{2}}} \right\} EA, \quad (9)$$

To simplify equation (9), some assumptions were adopted. First, the stability of the nanofluids must be assured, which means that no aggregation and deposition formed during the electrolysis. Hence, the radius of nanoparticles and zeta potential can be treated as constant. Second, the change of electrical conductivity due to concentration change during the electrolysis can be ignored as the process duration was rather short. Third, we evaluated the Brownian motion conductivity and electrophoretic conductivity, and found that the temperature change had less impact on the Brownian motion conductivity, as well as the overall electrical conductivity. Thus, the temperature effects on total electrical conductivity are negligible. Therefore, equation (9) can be simplified as follows:

$$I = \sigma_f EA + \left[\frac{3\left(\frac{\sigma_p}{\sigma_f} - 1\right)\sigma_f}{\frac{\sigma_p}{\sigma_f} + 2} + \frac{2{\varepsilon_d}^2 {\varepsilon_{d0}}^2 \zeta^2}{\mu r^2} + \frac{3\varepsilon_d \varepsilon_{d0} \zeta \left(\frac{RT}{L} \cdot \frac{1}{3\pi\mu}\right)}{r^{\frac{3}{2}}} \right] EA\varphi = \mathcal{A} + \mathcal{B}\varphi. \quad (10)$$

From the discussion above, $\mathcal{A}$ and $\mathcal{B}$ can be considered constant. These can be treated as fitting empirical parameters.

3. Results and discussion

3.1 Stability of the nanofluids-based electrolyte

In this study, an observation of the time-dependent sedimentation method was used to test the stability of ENF, which is considered an effective way to confirm nanofluids' stability (Li et al., 2020). In Table 1, samples 1-3 and 7-9 are set for comparison. The results are shown in Figure 3. These photos were taken after the suspensions were prepared, after three days, and after seven days.

The aqueous CB nanofluids (see the first three images in Figure 3c) showed excellent stability as expected (Ulset et al., 2018). However, both the sodium sulfate electrolyte nanofluids (SSENF) and the sodium hydroxide electrolyte nanofluids (SHENF) maintained their stability for a short time and then deteriorated, where the stability of SHENF were worse than SSENF. According to our observation, the distinguishable small clusters were formed after two days, three days, and three days in the SHENF at the CB concentration of 0.5 wt.%, 0.1 wt.%, 0.05 wt.%, respectively. The visible sedimentation that can be identified in the graphics appeared after seven days. However, there was no visible sedimentation in SSENF after three days, as seen in Figure 3(b) A possible explanation is that the particles had already agglomerated, but their sizes were still very small and the dark environment made them difficult to observe.

The existence of SH significantly increases the pH of nanofluids. Also, pH can be slightly increased by adding SS. With the increase of pH, the zeta potential decreases due to electrochemical charge neutralization on the surface of CB nanoparticles, which deteriorates the EDL (Kessler et al., 2019). When the pH reaches the isoelectric point, the zeta potential becomes zero. Some researchers found the isoelectric point of graphene to correspond to a pH of 7.5 (Zuccaro et al., 2015). It should be noted that the isoelectric point is very sensitive to the particle size, and smaller particles have higher isoelectric points

(Alnarabiji and Husein, 2020). Therefore, it is reasonable to assume the isoelectric point of CB nanofluids is higher than 7.5, which makes SHENF show worse stability than SSENF.

Zeta potential is an important parameter indicating the stability of nanofluids. Ohshima (Ohshima, 2003) suggested that when the surface charge is very high, zeta potential is equal to the critical zeta potential, where the repulsive force is equal to the maximum van Der Waals force according to Derjaguin-Landau-Verwey-Overbeek (DLVO) theory. The critical zeta potential can be calculated by (Teh et al., 2010):

$$\zeta = \frac{k_B T}{ze} ln \frac{1}{\phi}, \tag{11}$$

where, k_B is the Boltzmann constant, e is the elementary electric charge, ϕ is the volume fraction of primary particles given by (Prasher et al., 2006):

$$\phi = \phi_p \phi_{a,} \tag{12}$$

where ϕ_p is the volume fraction of the particles in the aggregates, ϕ_a is the volume fraction of the aggregates in the nanofluid.

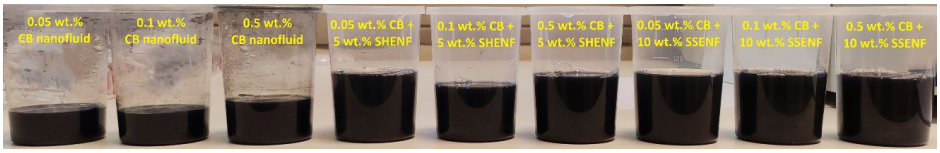

(a) 0 days

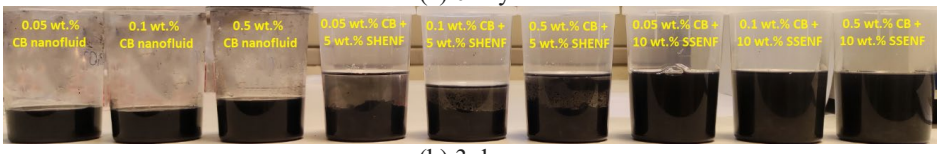

(b) 3 days

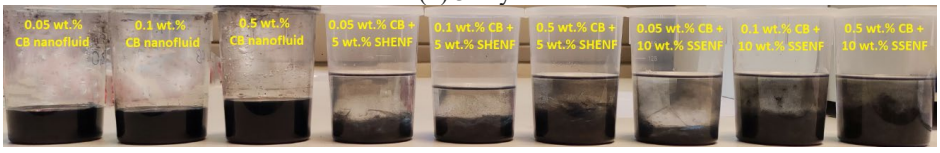

(c) 7 days

Figure 3 Photographs of the different suspensions (CB nanofluids, CB/SHENF, CB/SSENF) at different times.

The process of sedimentation in SHENF could be divided into three stages. When SHENF were prepared, almost no aggregate in the fluid exists. Hence, $\phi_p = 1$, and $\phi = \phi_a$, where the nanoparticles were also treated as aggregates in the model. First, the nanoparticles formed aggregates and grew, but they were hard to observe. In our tests, this stage occurred in the first two days. In the second stage, when the aggregates grew large enough, the deposition appeared due to gravity. During this time, ϕ increased as the volume of aggregates increased, leading to a decrease in critical zeta potential, as shown by equation (11). In the meantime, small agglomerations still existed and dispersed in the liquid. The sedimentation was mixed as shown in Figure 3 (b). In our experiments, this stage lasted for about three days until the fully sedimented stage, where $\phi_a = 1$, and $\phi = \phi_p$. In this final stage, almost all the particles were sedimented in the base fluid. However, flocculate suspensions were observed above the surface of sedimentation, as shown in Figure 3.

Ali et al. (2019) divided the sedimentation behaviour of nanofluids into three categories, namely, dispersed sedimentation, flocculated sedimentation, and mixed sedimentation. They concluded that the flocculated sedimentation in aluminum nanofluids was caused by the nanoparticle's oxidation. According to Leong and Ong (2003), when the zeta potential of a stable colloidal dispersion reached the critical zeta potential, it started to transmit to a flocculated dispersion, in which the viscosity of flocculated dispersion was several orders of magnitude larger than its stable state.

Commonly, in a stationary container without any external force except gravity, the aggregation of nanoparticles is caused by Brownian motion regardless of the thermal boundary resistance between the particles and the base fluid (Prasher et al., 2006). The aggregation in a nanofluid with time can be described as (Hanus et al., 2001):

$$\frac{R_a}{r} = \left(1 + \frac{t}{t_a}\right)^{\frac{1}{d_f}}, \tag{13}$$

where R_a is the gyration radius of the aggregates, t is the time, t_a is the aggregation time constant, d_f is the fractal dimension of the aggregates. Waite et al. (2001) suggested that d_f was in the range of 1.8~2.3. For the Brownian agglomeration, the fractal dimensions is lower than 2

The aggregation time constant t_a is given by:

$$t_a = \frac{\pi \mu r^3 W}{k_B T}, \tag{14}$$

where W is the stability ratio. When $W = 1$, there is no repulsive force as well as hydrodynamic interactions between the nanoparticles in the presence of a repulsive force, $W > 1$. According to DLVO theory, stability ratio W can be calculated by the repulsive and attractive potential energies. It is a strong function of nanoparticles radius r, as W decreases rapidly with decreasing r (Prasher et al., 2006).

Following equation (14), the aggregation time constant t_a decreases with the decrease in particle size, which indicates smaller particles are more prone to agglomerate. When SS or SH is added to CB nanofluids, the repulsive force potentially deteriorates, which induced a decrease in W. Furthermore, equation (13) indicates the growth speed of aggregates will become slower with time, which shows an agreement with our results, as seen in Figure 3.

Therefore, the stability states of SHENF make them become made-and-use instantly samples. Many researchers also confirmed this conclusion (Liu et al., 2016; Wang et al., 2016), and there is no suitable method to maintain the stability of ENF as it is possible for standard nanofluids at present.

3.2 Effect of nanoparticles on total hydrogen production

In this study, the hydrogen production from the electrolysis of a 10 wt.% SHENF with 0.1 wt.% CB was presented, and the results were compared with the hydrogen production from the electrolysis of a 10 wt.% SH solution. The light and SDS were applied in both systems. Figure 4 shows the comparison results. The hydrogen was produced in a greater amount and also faster in SHENF than in SH solution. For SHENF, it took 7 minutes to reach the maximum hydrogen volume of 57.9 ml. However, the maximum hydrogen volume of 60.2 ml was achieved at 9 minutes for SH solution. This indicates the hydrogen production rate for SHENF was about 23.61% higher than the SH solution.

Obliviously, CB particles played an essential role in the process. As discussed in Section 2.3, the enhancement of electrical conductivity caused by electrophoresis and Brownian motion has a positive impact on hydrogen production.

Another reason is the enhancement of mass transfer induced by nanoparticles. In the electrical field, the motion of nanoparticles is empowered by Brownian motion and electrophoresis as well. The velocity of Brownian motion for a single particle or cluster can be calculated from (Beiki et al., 2013):

$$v_B = \sqrt{\frac{9k_BT}{4\rho\pi r^3}}, \tag{15}$$

where v_B is the velocity of Brownian motion, ρ is the density of nanoparticles.

The velocity of a particle caused by electrophoresis can be calculated by the electrophoretic mobility formula (Huckel et al.,1924):

$$\mu_E = \frac{v_P}{E} = \frac{2\varepsilon_p\varepsilon_{p0}}{3\mu}\zeta, \tag{16}$$

where μ_E is the electrophoretic mobility, v_P is the velocity of electrophoresis, ε_p is the relative permittivity of the fluid, ε_{p0} is the permittivity of a vacuum.

The viscosity μ is a temperature-sensitive parameter, decreasing with the temperature increase. Following equations (15) and (16), v_B and v_P increase with temperature, which induces higher convective mass transfer at higher temperatures. Figure 5 shows the temperature history with and without CB. The presence of the CB improved the temperature-increasing pattern due to the enhanced thermal conductivity of the fluid. Therefore, the mass transfer was stronger in SHENF. This conclusion can be confirmed by Beiki et al. (2013). They investigated the convective mass transfer of Al_2O_3 and TiO_2 ENF in a circular tube and discovered a higher mass transfer ratio in laminar flow.

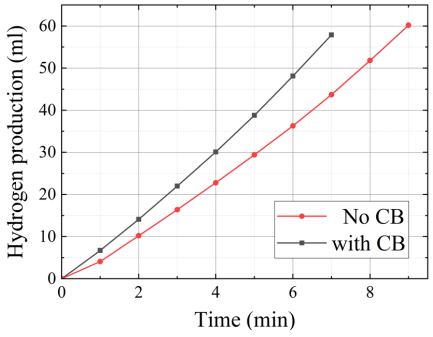

Figure 4 Hydrogen production for 10 wt.% SH electrolytes at different time with and without CB (φ = 0.1 wt.%, $T_{initial}$ = 30 ℃).

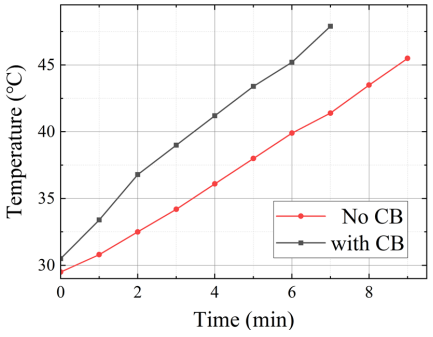

Figure 5 Temperature increases for 10 wt.% SH electrolytes at different time with and without CB (φ = 0.1 wt.%, $T_{initial}$ = 30 ℃).

Furthermore, the two explanations mentioned above are the primary reason that CB nanofluids improved hydrogen production. However, there are still some factors that can potentially affect hydrogen production. Although they have limited influence, they are still worth discussing.

The first factor is that nanoparticles adhered to the electrodes. This fact was also noticed by Choi et al. (2020), who reported the cellulose nanofluid was coated on the anode. They state this phenomenon indeed hindered the process of electrolysis and reduced gas production. Nevertheless, in our work, the CB nanoparticles did not fully cover the electrodes: we estimate that more than 50% of the electrode area was clean from the

nanoparticles. Indeed, this partial deposition by carbon nanoparticles may be beneficial for the process: the presence of the particles may enhance the electrical conductivity and expand the surface area. According to Ghosh et al. (2022), carbon nanotubes have been widely used as electrodes in microbial fuel cells and proton exchange membrane fuel cells as their high aspect ratio, low weight, and high conductivity. Therefore, it is reasonable to assume the CB nanoparticle coating on electrodes has a positive impact on electrolysis.

The second factor is the formation of bubbles. SDS was used to stabilize the ENF, however, it caused the formation of bubbles during the electrolysis. On the other hand, to diminish other chemicals to affect the properties of ENF, we did not add anti-foam in the preparation of ENF. According to Wang et al. (2014), the effect of bubbles can be divided into two types, namely bubble coverage on electrodes and bubble dispersion in an electrolyte. In our experiments, as mentioned in the previous paragraph, the presence of CB in the electrolyte resulted in the adhesion of nanoparticles, which coated the electrodes and prevented bubbles from adhering to them. Hence, the suspension of bubbles became the main behavior of the bubble effect. Correspondingly, this behavior was not obvious in the samples without CB. Bubbles can increase the void fraction which leads to large electrolyte resistance, and extra energy consumption (Matsushima et al., 2012).

The third factor is the potential caused by the sedimentation of aggregates. This interesting assumption was proposed by Ohshima (2003), who investigated the velocity of sedimentation and the potential of sedimentation using the Stokes formula. The findings revealed that the sedimentation potential is highly dependent on the aggregate's radius. Nevertheless, this factor has limited effects on a stable ENP.

3.3 Effect of initial temperature

As an essential factor in electrolysis, the temperature can affect the activity of substances and reaction rate. In this work, we tested the total hydrogen production at different initial temperatures with different SH concentrations, as shown in Figure 6. The concentration of CB nanofluids was 0.1 wt.%. As expected, the total hydrogen production increases with the growth of initial temperature and SH concentration.

This result is consistent with the findings of Hiraki et al. (2005), who investigated the reaction rates when the range of the initial temperature was 291 K~333K. Their study revealed that the initial temperature of NaOH solutions had a significant impact on the reaction rate. Specifically, when the initial temperature was set to 313 K or above, the reaction was completed within 1200 s in their experimental set-up. However, when the temperature was set to 291 K, the generation of hydrogen continued for more than 2400 s.

The reaction rate constant depends on several factors, including temperature, pressure, etc. The relationship between the reaction rate constant and temperature can be described by the Arrhenius equation (Crapse et al., 2021):

$$k_a = A_a e^{-\frac{E_a}{RT}} \tag{17}$$

where k_a is the reaction rate constant, A_a is an exponential factor that is a constant for a given chemical reaction, relating the frequency of collisions of atoms and molecules, E_a is the activation energy of the reaction.

Based on Equation (17), a higher initial temperature results in a faster reaction rate, which in turn leads to an increase in the amount of hydrogen produced. Additionally, during the electrolysis process, the nanoparticles absorb radiation, which causes the temperature of the electrolyte to rise even further, thus accelerating the reaction rate even more.

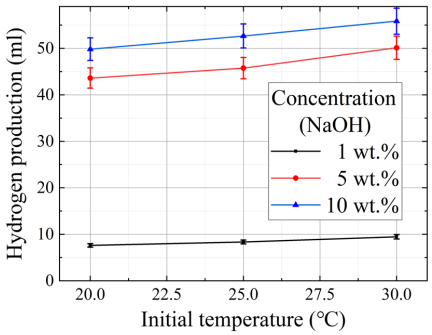

Figure 6 Total hydrogen production at different initial concentrations (φ = 0.1 wt.%).

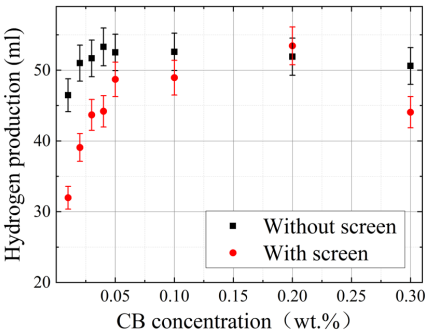

Figure 7 Total hydrogen production vs. different CB concentrations with and without the screen ($\varphi_{(NaOH)}$ = 5 wt.%, $T_{initial}$ = 30 ℃).

3.4 Effect of CB concentration

Figure 7 depicts the comparison of hydrogen production at different CB concentrations for two cases: (i) with the screen; (ii) without the screen. These experiments were conducted at the initial temperature of 30 ℃, and the concentration of sodium hydroxide was 5 wt.%. In both studied cases, the total hydrogen production shows the tendency to increase first and then decrease with the growth of the CB concentration. For no screen case, the maximum production occurred at 0.04 wt.%, while when the screen was used the maximum hydrogen production showed at a higher concentration.

The increasing tendency was caused by the following reasons. Firstly, equations (6) and (7) indicated that an increase in CB concentration φ led to an increase in electrical conductivity caused by electrophoresis σ_E and Brownian motion σ_B, respectively. Secondly, according to equation (11), zeta potential ζ was proportional to the temperature T. Hence, it could be seen from equations (15) and (16) that the particle velocity of electrophoresis v_E and Brownian motion v_B increased with the rising of temperature, which improved the mass transfer in the ENF. Thirdly, the convective heat transfer was enhanced by the applied electrical field (Sheikholeslami et al., 2017), leading to faster temperature. Additionally, CB nanoparticles might have formed a chain-shaped conducive path in the fluid, which escalated the electrical conductivity. Lastly, the strengthening of EDL was also a possible reason that was discussed in our previous study (Wei et al., 2022).

The reason for the decreasing tendency was mainly caused by the agglomerations and sedimentation of CB nanoparticles. The agglomeration meant the growth of particle size r. Hence, the electrical conductivity and mass transfer enhanced by electrophoresis and Brownian motion were diminished, according to equations (6), (7), (11), (15), and (16). In addition, the total mass transfer in the ENF is affected by the Brownian Reynolds number, which is given by (Prasher et al., 2006):

$$Re = \frac{2v_B r\rho}{\mu}, \tag{18}$$

And the thermal conductivity of ENF is given by (Prasher, 2005):

$$\frac{k}{k_0} = 1 + A \times Re^m Pr^{0.333}\phi, \tag{19}$$

where k is the thermal conductivity, k_0 is the thermal conductivity of the base fluid, A and m are constants measured by experiments, Pr is the Prandtl number.

Prasher et al. (2006) reported that aggregation can significantly decrease the Brownian Reynolds number, which also worsens the thermal conductivity, as seen in equation (19). Also, according to Beiki et al. (2013), the mass transfer coefficient for Al_2O_3 ENF increased with the concentration of nanofluids up to 0.01% and then decreased, which corresponds to our conclusions.

Secondly, the chain-shaped conductive path did not always assist the electrical conductivity. When the aggregates became large enough, the path formed a considerable resistance, which could hinder the current and reaction and reduce hydrogen production.

Lastly, the high concentration of CB was able to form a "shield", which could block the mass transfer and the penetration of light. Then, causing the deteriorated thermal performance of nanofluids.

Furthermore, the use of the screen had little effect on hydrogen production, as seen in Figure 8. The maximum hydrogen production was 52 ml at 16 minutes when the screen was applied, corresponding to the 57 ml of the case without the screen. Thus, the production was 9 % lower. However, the difference in the temperature was significant, as shown in Figure 9. The larger illuminated area allowed more heat to be absorbed, and the temperature increased faster. Whereas a higher temperature can make the formation of aggregation faster, according to equations (13) and (14). Hence, the negative impact of CB nanofluids showed at lower CB concentrations for the case without the screen, as shown in Figure 7. On the other hand, there was a temperature gradient between the illuminated area and the unilluminated area. Temperature gradient facilitated the convective heat transfer, as well as mass transfer. These convective transfers were more significant when the screen was used, leading to an increased hydrogen production.

Moreover, the better performance for the smaller illuminated case showed that the electrical properties played a more important role than thermal properties. This phenomenon indicates that the enhancement of light mainly occurred in the current path area. A concentrated light can be used in the further investigation to save energy.

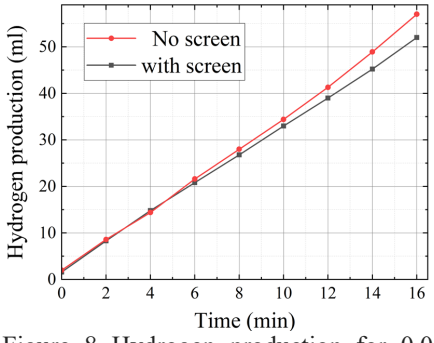

Figure 8 Hydrogen production for 0.05 wt.% CB SHENF at different times with and without the screen ($\varphi_{(NaOH)}$ = 5 wt.%, $T_{initial}$ = 30 °C).

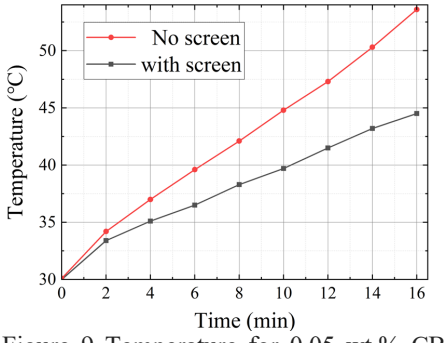

Figure 9 Temperature for 0.05 wt.% CB SHENF at different times with and without the screen ($\varphi_{(NaOH)}$ = 5 wt.%, $T_{initial}$ = 30 °C).

3.5 Relationship between the current and CB concentrations

According to the conclusions of the previous section, we decided to use the current data recorded in the electrolysis of SHENF with the screen, as they showed better stability and were potentially used in industries.

As discussed in Section 2.3, a critical parameter to evaluate the total hydrogen production for electrolysis in SHENF is current, as seen in equation (4). The black dots in Figure 10 show the average current at different CB concentrations. The average current history exhibits a similar tendency as hydrogen production. It increased first and then decreased, with the maximum current showed at the CB concentration of 0.1 wt.%. In the previous section, we analyzed that the high concentrations of CB had a negative impact on the electrical conductivity of ENF. This conclusion can be proved by Figure 10. However, when the CB concentration was higher than 0.1 wt.%, the adverse effects on the electrical conductivity caused the current to decrease. In the meantime, nanofluids' thermal properties still played an important role in promoting hydrogen production, which made the highest hydrogen production shown at the concentration of 0.2 wt.%.

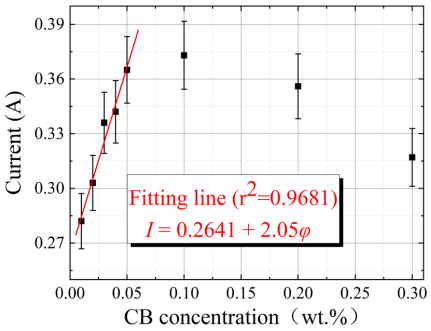

Figure 10 Current vs. CB concentration and fitting line ($\varphi_{(NaOH)}$ = 5 wt.%, $T_{initial}$ = 30 ℃, screen applied).

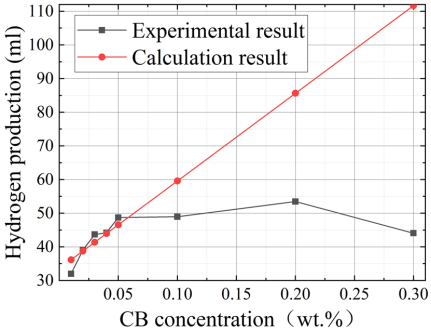

Figure 11 Comparison between experimental and calculation results ($\varphi_{(NaOH)}$ = 5 wt.%, $T_{initial}$ = 30 ℃, screen applied).

According to equation (10), the current has a linear relationship with CB concentration. However, some assumptions are not met at higher CB concentrations, such as the assumption of no agglomeration in the SHENF during the electrolysis process. Hence, we focused on the lower CB contractions, namely $\varphi < 0.05$ wt.%., which showed better stability and allow us to evaluate the hydrogen production

The fitting result is shown in the red line of Figure 10. Generally, the efficiency of hydrogen production is less than 100%. Hence, we introduced a correction factor η that indicates the different processes of electrolysis. According to our calculation, when a screen is applied in the electrolysis, η becomes 0.57. Substituting the fitting result and correction factor η into equation (4), it becomes:

$$n(\mathrm{H_2}) = 0.57\frac{(0.2641 + 2.05\varphi)t}{2F}, \tag{20}$$

Figure 11 shows the comparison of hydrogen production between the experimental results and calculation results from equation (20). The calculation results show a good agreement with the experimental results when the CB concentrations are below 0.1 wt.%. The errors are shown in Table 2.

Table 2 Error analysis of experimental results and simulation results.

CB concentration /wt.%	0.01	0.02	0.03	0.04	0.05	0.10	0.20	0.30
Hydrogen production (experiments) /ml	31.98	39.08	43.69	44.20	48.71	48.95	53.45	44.07
Hydrogen production (simulations) /ml	36.16	38.76	41.36	43.97	46.57	59.59	85.64	111.68
Error	0.115	-0.008	-0.056	-0.005	-0.0459	0.179	0.376	0.605

Equation (20) is a simplified model with considerable limitations. The most important one is that it does not take agglomeration into consideration. However, the agglomeration process is very random, similar to the Brownian motion. Some researchers have presented models that may forecast agglomeration. Equations (13) and (14) were built based on the effect of aggregate radius on repulsive force and attractive force (Prasher et al., 2006), but the impacts of the electrical field were not included. Similarly, Ohshima took the density difference between nanoparticles and base fluids into account (Ohshima, 2003), but the effect of the electrical field was absent. Therefore, the direction to optimize equation (20) is to find the agglomeration and sedimentation behavior in an electrical field.

4 Conclusions

In this study, SHENF was prepared, and its stability was investigated. The electrolysis experiments were conducted in a Hoffman voltameter at different initial temperatures, SH concentrations and CB contractions, and the results were used to build a model to evaluate the total hydrogen production. A possible technical method to assess the total hydrogen production was presented, and a simplified model was built to evaluate the total hydrogen production for electrolysis SHENF with a screen. Some of the crucial conclusions are as follows:

- The presence of salt or alkaline solution can weaken the stability of CB nanofluids, and CB nanoparticles were fully sedimented in seven days in SHENF.
- CB nanoparticles can improve the hydrogen production of electrolysis by the enhancement of electrical conductivity, mass transfer, and heat absorption. The hydrogen production rate was improved by 23.62% when 0.1 wt.% CB was applied in 10 wt.% SHENF.
- The initial temperature had an impact on the hydrogen production
- For electrolysis of SHENF, the total hydrogen production increased with the increases in CB concentration and then decreased. When employing a screen, the maximum hydrogen production showed at the concentration of 0.2 wt.%, whereas the maximum hydrogen production showed at the concentration of 0.04 wt.% without a screen.

A semi-empirical correlation was proposed to evaluate the total hydrogen production for electrolysis of SHENF with a screen, which had a higher precision when the CB concentrations were below 0.1 wt.%

According to our research, it is an interesting problem to use nanofluids for water electrolysis. This may create a new path to connect solar energy and hydrogen, which is meaningful for the energy industry. However, two important issues should be investigated in further work. The first one is finding a better method to enhance the stability of ENF. Another one is building a model that describes how the electrical field influences the aggregation and sedimentation of nanoparticles.

Acknowledgments

Shihao Wei gratefully acknowledges financial support from the China Scholarship Council. Boris Balakin thanks the Norwegian Research Council for funding (project 300286).

References

[1] European Commission, 2020. Communication on the 2030 Climate Target Plan. (COM(2020) 562 final). https://eur-lex.europa.eu/legal-content/EN/TXT/?uri=CELEX:52020DC0562

[2] The state council of the people's republic of China, 2021. Action Plan for Carbon Dioxide Peaking Before 2030. (State Council (2021) No. 23) http://english.www.gov.cn/policies/latestreleases/202110/27/content_WS6178a47ec6d0df57f98e3dfb.html

[3] Léon, A. ed., 2008. Hydrogen technology: mobile and portable applications. Springer Science & Business Media.

[4] Godula-Jopek, A., 2015. Hydrogen production: by electrolysis. John Wiley & Sons.

[5] Bellos, E., Tzivanidis, C. and Antonopoulos, K.A., 2017. A detailed working fluid investigation for solar parabolic trough collectors. Applied Thermal Engineering, 114, pp.374-386.

[6] Kumar, V., Tiwari, A.K. and Ghosh, S.K., 2015. Application of nanofluids in plate heat exchanger: a review. Energy conversion and management, 105, pp.1017-1036.

[7] Struchalin, P.G., Yunin, V.S., Kutsenko, K.V., Nikolaev, O.V., Vologzhannikova, A.A., Shevelyova, M.P., Gorbacheva, O.S. and Balakin, B.V., 2021. Performance of a tubular direct absorption solar collector with a carbon-based nanofluid. International Journal of Heat and Mass Transfer, 179, p.121717.

[8] Kosinska, A., Balakin, B.V. and Kosinski, P., 2022. Photothermal conversion of biodegradable fluids and carbon black nanofluids. Scientific Reports, 12(1), p.3398.

[9] Balakin, B.V., Zhdaneev, O.V., Kosinska, A. and Kutsenko, K.V., 2019. Direct absorption solar collector with magnetic nanofluid: CFD model and parametric analysis. Renewable Energy, 136, pp.23-32.

[10] Balakin, B.V., Stava, M. and Kosinska, A., 2022. Photothermal convection of a magnetic nanofluid in a direct absorption solar collector. Solar Energy, 239, pp.33-39.

[11] Sheikholeslami, M. and Bhatti, M.M., 2017. Active method for nanofluid heat transfer enhancement by means of EHD. International Journal of Heat and Mass Transfer, 109, pp.115-122.

[12] Wang, G., Zhang, Z., Wang, R. and Zhu, Z., 2020. A review on heat transfer of nanofluids by applied electric field or magnetic field. Nanomaterials, 10(12), p.2386.

[13] Khan, U., Ahmed, N., Mohyud-Din, S.T. and Bin-Mohsin, B., 2016. A bioconvection model for MHD flow and heat transfer over a porous wedge containing both nanoparticles and gyrotatic microorganisms. Journal of Biological Systems, 24(04), pp.409-429.

[14] Khan, U., Ahmed, N. and Mohyud-Din, S.T., 2016. Influence of viscous dissipation and Joule heating on MHD bio-convection flow over a porous wedge in the presence of nanoparticles and gyrotactic microorganisms. SpringerPlus, 5, pp.1-18.

[15] Zawrah, M.F., Khattab, R.M., Girgis, L.G., El Daidamony, H. and Abdel Aziz, R.E., 2016. Stability and electrical conductivity of water-base Al2O3 nanofluids for different applications. HBRC journal, 12(3), pp.227-234.

[16] Bagheli, S., Fadafan, H.K., Orimi, R.L. and Ghaemi, M., 2015. Synthesis and experimental investigation of the electrical conductivity of water based magnetite nanofluids. Powder Technology, 274, pp.426-430.
[17] Minea, A.A., 2019. A review on electrical conductivity of nanoparticle-enhanced fluids. Nanomaterials, 9(11), p.1592.
[18] Liu, C., Lee, H., Chang, Y.H. and Feng, S.P., 2016. The study of electrical conductivity and diffusion behavior of water-based and ferro/ferricyanide-electrolyte-based alumina nanofluids. Journal of colloid and interface science, 469, pp.17-24.
[19] Wang, R.T. and Wang, J.C., 2016. Alumina nanofluids as electrolytes comparisons to various neutral aqueous solutions inside battery. Journal of Mechanics, 32(3), pp.369-379.
[20] Sheikholeslami, M., Farshad, S.A., Ebrahimpour, Z. and Said, Z., 2021. Recent progress on flat plate solar collectors and photovoltaic systems in the presence of nanofluid: a review. Journal of Cleaner Production, 293, p.126119.
[21] Manikandan, E., Mayandi, K., Sivasubramanian, M., Rajini, N., Rajesh, S., Muthulakshmi, L. and Rashedi, A., 2022. A comprehensive review on the impact of nanofluid in solar photovoltaic/thermal system. Proceedings of the Institution of Mechanical Engineers, Part C: Journal of Mechanical Engineering Science, 236(9), pp.5078-5096.
[22] Hiraki, T., Takeuchi, M., Hisa, M. and Akiyama, T., 2005. Hydrogen production from waste aluminum at different temperatures, with LCA. Materials transactions, 46(5), pp.1052-1057.
[23] Choi, D. and Lee, K.Y., 2020. Experimental study on water electrolysis using cellulose nanofluid. Fluids, 5(4), p.166.
[24] Wei, S., Hikmati, J., Balakin, B.V. and Kosinski, P., 2022. Experimental study of hydrogen production using electrolyte nanofluids with a simulated light source. international journal of hydrogen energy, 47(12), pp.7522-7534.
[25] Ulset, E.T., Kosinski, P., Zabednova, Y., Zhdaneev, O.V., Struchalin, P.G. and Balakin, B.V., 2018. Photothermal boiling in aqueous nanofluids. Nano Energy, 50, pp.339-346.
[26] Taylor, R., Coulombe, S., Otanicar, T., Phelan, P., Gunawan, A., Lv, W., Rosengarten, G., Prasher, R. and Tyagi, H., 2013. Small particles, big impacts: A review of the diverse applications of nanofluids. Journal of applied physics, 113(1), p.1.
[27] Chung, S.J., Leonard, J.P., Nettleship, I., Lee, J.K., Soong, Y., Martello, D.V. and Chyu, M.K., 2009. Characterization of ZnO nanoparticle suspension in water: Effectiveness of ultrasonic dispersion. Powder Technology, 194(1-2), pp.75-80.
[28] Timofeeva, E.V., Moravek, M.R. and Singh, D., 2011. Improving the heat transfer efficiency of synthetic oil with silica nanoparticles. Journal of colloid and interface science, 364(1), pp.71-79.
[29] Ezzahra Chakik, F., Kaddami, M. and Mikou, M., 2017. Effect of operating parameters on hydrogen production by electrolysis of water. International Journal of Hydrogen Energy, 42(40), pp.25550-25557.
[30] Schalenbach, M., Tjarks, G., Carmo, M., Lueke, W., Mueller, M. and Stolten, D., 2016. Acidic or alkaline? Towards a new perspective on the efficiency of water electrolysis. Journal of The Electrochemical Society, 163(11), p.F3197.
[31] Sharaf, O.Z., Taylor, R.A. and Abu-Nada, E., 2020. On the colloidal and chemical stability of solar nanofluids: From nanoscale interactions to recent advances. Physics Reports, 867, pp.1-84.

[32] Nie, J., Chen, Y., Boehm, R.F. and Katukota, S., 2008. A photoelectrochemical model of proton exchange water electrolysis for hydrogen production. Journal of Heat Transfer, 130(4).
[33] Maxwell, J.C., 1873. A treatise on electricity and magnetism (Vol. 1). Oxford: Clarendon Press.
[34] Said, Z., Sundar, L.S., Tiwari, A.K., Ali, H.M., Sheikholeslami, M., Bellos, E. and Babar, H., 2022. Recent advances on the fundamental physical phenomena behind stability, dynamic motion, thermophysical properties, heat transport, applications, and challenges of nanofluids. Physics Reports, 946, pp.1-94.
[35] Shen, L.P., Wang, H., Dong, M., Ma, Z.C. and Wang, H.B., 2012. Solvothermal synthesis and electrical conductivity model for the zinc oxide-insulated oil nanofluid. Physics Letters A, 376(10-11), pp.1053-1057.
[36] Li, X., Chen, W. and Zou, C., 2020. An experimental study on β-cyclodextrin modified carbon nanotubes nanofluids for the direct absorption solar collector (DASC): Specific heat capacity and photo-thermal conversion performance. Solar Energy Materials and Solar Cells, 204, p.110240.
[37] Kessler, J.C., Padoin, N., Hotza, D. and Soares, C., 2019. Rheological behavior of a silver aqueous nanofluid stabilized with aminosilane-based surfactant under confined flow. Brazilian Journal of Chemical Engineering, 36, pp.229-237.
[38] Zuccaro, L., Krieg, J., Desideri, A., Kern, K. and Balasubramanian, K., 2015. Tuning the isoelectric point of graphene by electrochemical functionalization. Scientific reports, 5(1), pp.1-13.
[39] Alnarabiji, M.S. and Husein, M.M., 2020. Application of bare nanoparticle-based nanofluids in enhanced oil recovery. Fuel, 267, p.117262.
[40] Ohshima, H., 2003. Electrokinetic phenomena in a dilute suspension of spherical colloidal particles in a salt-free medium. Colloids and Surfaces A: Physicochemical and Engineering Aspects, 222(1-3), pp.207-211.
[41] Teh, E.J., Leong, Y.K., Liu, Y., Ong, B.C., Berndt, C.C. and Chen, S.B., 2010. Yield stress and zeta potential of washed and highly spherical oxide dispersions—critical zeta potential and Hamaker constant. Powder Technology, 198(1), pp.114-119.
[42] Prasher, R., Phelan, P.E. and Bhattacharya, P., 2006. Effect of aggregation kinetics on the thermal conductivity of nanoscale colloidal solutions (nanofluid). Nano letters, 6(7), pp.1529-1534.
[43] Ali, N., Teixeira, J.A. and Addali, A., 2019. Aluminium nanofluids stability: A comparison between the conventional two-step fabrication approach and the controlled sonication bath temperature method. Journal of Nanomaterials, 2019, pp.1-9.
[44] Leong, Y.K. and Ong, B.C., 2003. Critical zeta potential and the Hamaker constant of oxides in water. Powder Technology, 134(3), pp.249-254.
[45] Hanus, L.H., Hartzler, R.U. and Wagner, N.J., 2001. Electrolyte-induced aggregation of acrylic latex. 1. Dilute particle concentrations. Langmuir, 17(11), pp.3136-3147.
[46] Waite, T.D., Cleaver, J.K. and Beattie, J.K., 2001. Aggregation kinetics and fractal structure of γ-alumina assemblages. Journal of Colloid and Interface science, 241(2), pp.333-339.
[47] Beiki, H., Esfahany, M.N. and Etesami, N., 2013. Turbulent mass transfer of Al_2O_3 and TiO_2 electrolyte nanofluids in circular tube. Microfluidics and nanofluidics, 15, pp.501-508.
[48] Huckel, E., 1924. Die kataphorese der kugel. Physikalische Zeitschrift, 25, pp.204-210.
[49] Ghosh, S. and Subudhi, S., 2022. Developments in fuel cells and electrochemical batteries using nanoparticles and nanofluids. Energy Storage, 4(3), p.e288.

[50] Wang, M., Wang, Z., Gong, X. and Guo, Z., 2014. The intensification technologies to water electrolysis for hydrogen production–A review. Renewable and sustainable energy reviews, 29, pp.573-588.

[51] Matsushima, H., Iida, T. and Fukunaka, Y., 2012. Observation of bubble layer formed on hydrogen and oxygen gas-evolving electrode in a magnetic field. Journal of Solid State Electrochemistry, 16, pp.617-623.

[52] Crapse, J., Pappireddi, N., Gupta, M., Shvartsman, S.Y., Wieschaus, E. and Wühr, M., 2021. Evaluating the Arrhenius equation for developmental processes. Molecular systems biology, 17(8), p.e9895. Doi: 10.15252/msb.20209895.

[53] Prasher, R., 2005, January. Brownian-motion-based convective-conductive model for the thermal conductivity of nanofluids. In Heat Transfer Summer Conference (Vol. 47314, pp. 343-353).

[54] Beiki, H., Esfahany, M.N. and Etesami, N., 2013. Laminar forced convective mass transfer of γ-Al_2O_3/electrolyte nanofluid in a circular tube. International journal of thermal sciences, 64, pp.251-256.

Graphic design: Communication Division, UiB / Print: Skipnes Kommunikasjon AS

uib.no

ISBN: 9788230863275 (print)
9788230846049 (PDF)